QATAR UNIVERSITY

COLLEGE OF ENGINEERING

EXPERIMENTAL AND THEORETICAL INVESTIGATION ON BOND BEHAVIOUR OF TENSILE LAP SPLICED BASALT FIBER REINFORCED POLYMER BARS IN HIGH STRENGTH CONCRETE BEAMS

BY

ISLAM REDA MOHAMED ELTANTAWI

A Thesis Submitted to

the College of Engineering

in Partial Fulfillment of the Requirements for the Degree of

Masters of Science in Civil Engineering

January 2020

COMMITTEE PAGE

The members of the Committee approve the Thesis of
Islam Reda Mohamed Eltantawi defended on 03/12/2019.

_____
Dr. Wael Alnahhal
Thesis/Dissertation Supervisor

_____
Dr. Moncef Nehdi
Committee Member

_____
Dr. Mohammed Arafa
Committee Member

_____
Dr. Jamil Renno
Committee Member

_____

Approved:

_____
Khalid Kamal Naji, Dean, College of Engineering

ABSTRACT

Eltantawi, Islam, R, Masters : January : 2020, Masters of Science in Civil Engineering

Title:EXPERIMENTAL and THEORETICAL INVESTIGATION of BASALT FIBER REINFORCED POLYMER TENSION LAP SPLICES BARS USED to REINFORCE HIGH STRENGTH CONCRETE BEAMS

Supervisor of Thesis: Dr. Wael, I, Alnahhal.

Basalt fiber reinforced polymer (BFRP) reinforcements are a possible replacement for corroding conventional steel bars. BFRP bars tension lap splices are necessary due to construction stoppages and limitations on rebar lengths. They also provide means to facilitate many forms of precast construction. Splices are used in joints to transfer forces from one reinforcing bar to the next enabling structural continuity within a member. The most widely used form of splicing is the lap splice where forces are transferred across adjacent discontinuous bars by means of the concrete in between them.

The objective of this study is to investigate the factors that affect the strength of the bond behavior of the high strength concrete's tensile lap-spliced FRP basalt bars and to determine the appropriate recommendation for the high strength concrete's (HSC) lap-splices of FRP basalt bars in design codes.

The number of the tested beams was 11 large-scale beams which were reinforced with basalt FRP bars with two surface textures, sand-coated and helically wrapped. The beams had different splice lengths depending on the bar size. Three bar diameters were used in this study i.e. (10, 12 and 16 mm). The bars were tested to obtain their tensile strength, ultimate strain, and modulus of elasticity. The investigation of the critical splice length was done theoretically and experimentally and was compared. The

theoretical part was obtained by three design codes which are: CSA-S806, CSA-S6, and ACI 440.1. The three codes were evaluated and compared to the experimental results and a conclusion was drawn.

The outcomes of this study are that the prediction of the strain at the end of the splice of basalt FRP bars can be done using the ultimate strength analysis, the performance of at least one beam test leads to an appropriate prediction of the critical splice length for basalt FRP bars used for reinforcing high strength concrete beams, and the Canadian code (CSA-S806) is the best suitable code to be used in the determination of the splice length for the basalt FRP bars used to reinforce high strength concrete beams. Moreover, the bond strength decreases as the splice length increases. Additionally, the sand-coated bars showed a higher bond strength than the helically wrapped bars.

Keywords: fiber reinforced polymer (FRP), basalt, high strength concrete (HSC), large-scale beams, lap-spliced, splice length, bond strength, sand coated, helically wrapped.

DEDICATION

“To my grandparents, parents, and beloved sisters”

ACKNOWLEDGMENTS

I would like to express my utmost appreciation and gratitude towards my supervisor, Dr. Wael Alnahhal, Department of Civil Engineering, Qatar University, for his invaluable guidance, knowledge and experience which have played a significant role in the success of this project, if it were not for him; this research was not going to be accomplished in this marvelous way.

I also wish to thank the technical staff for their support and help during the experimental works.

Most of all, I would like to thank my parents for their encouragement and support which are greatly appreciated. I would like to thank them for providing me with this incredible learning opportunity.

TABLE OF CONTENTS

LIST OF TABLES

LIST OF FIGURES

NOMENCLATURE

Abbreviations

FRP	Fiber Reinforced Polymer
BFRP	Basalt Fiber Reinforced Polymer
HSC	High Strength Concrete
SBFRP	Sand-Coated Basalt Fiber Reinforced Polymer
HWBFRP	Helically Wrapped Basalt Fiber Reinforced Polymer
LVDT	Liner Variable Differential Transducer
W/C	Water to Cement ratio
HPC	High performance concreter

SYMBOLS

μ	Bond stress
V	Shearing force
Ab	Bar's nominal cross-sectional area
ld	Development length
ls	Splice length
k_1	Bar location factor
k_2	Coating factor
k_3	Concrete density factor
k_4	Bar size factor
f_y	Yield stress in reinforcement bar
$f'c$	Compressive strength of concrete
Atr	Nominal area of the rebar stirrups
fyt	Yield stress in the rebar stirrups
ψe	Coating factor
ψs	Reinforcement size factor
λ	Density of the concrete,
fu	Ultimate tensile strength
Fu	Ultimate tensile load
E	Modulus of elasticity
εu	Ultimate strain of reinforcement
ρFb	Balanced reinforcement ratio
b	Width of the beam
d	Depth of the beam
εcu	Ultimate strain of concrete
Ma	Applied moment
Mr	Resistant moment
Mu	Ultimate moment

CHAPTER 1: INTRODUCTION

The unfavorable environmental conditions remain the main reason concrete structures become weak to a point of exposing reinforcing steel bars to corrosion. In the State of Qatar, the issue of corrosion is hastened in residential buildings, bridges, and multi-story parking garages due to significantly high temperature that prevails almost all the year in addition to severe humidity and coastal conditions. A combination of moisture, temperature, and chlorides has the ability to reduce concrete alkalinity to an extent of exposing steel bars to corrosion. In order to protect the steel reinforcement from the corrosion, various methods have been developed such as the cathodic protection of the steel, synthetic membranes, coating the steel bars with a corrosion protection material (metallic or nonmetallic coating) such as epoxy coating, improving the quality of concrete by admixtures, and increasing the thickness of the concrete cover. Following the need to contain corrosion, recent research seems to have yielded the positive results after fiber reinforced polymer proved to be the best alternative for steel bars in relation to reinforcement for concrete structures. One promising solution to the problem caused by the deterioration of the steel reinforcement is the use of FRP bars, which are corrosion-free type of materials. Since the steel protection from corrosion has shown to be uncertain (Michaluk et al. 1998 and ACI 440.1R-15). Therefore, extensive research has been undertaken to use FRP bars in structural applications. FRP bars have many advantages. Some of such benefits include ease of handling, nonconductivity, high tensile strength, better strength to weight ratio and high corrosion resistance. There are 4 main types of FRP composites which are aramid, glass, carbon and basalt fiber reinforced polymer, all of them are easily available.

It emerges that the bonding behavior of the FRP with concrete makes it the best alternative to combating corrosion, making it possible for being the main reinforcement

of various concrete structures design. It is clear that the bond characteristics are responsible for transferring the load from concrete to reinforcement and vice versa. Therefore, one of the fundamental aspects of the structural behavior is the bond development phenomenon. What is more, bond features of the reinforcement can directly affect the deflection of concrete member and the crack width (serviceability limit states). However, there has not been enough research on the bond existing between the concrete and FRP bars. The mention of spliced bars deems essential as they define limitation of manufactured length. In addition, it is required at construction joints. Hence, it has been the main impetus to carry out this study to investigate the behavior of the bond of FRP bars within the concrete. Moreover, the research discusses the influence of several important parameters to obtain a better knowledge of FRP bars and their bond behavior. The outcomes of the research project will serve as recommendations key to determining concrete design to work with FRP bars. Surface configuration and several mechanical features remain the main areas of focus since they facilitate FRP bars into developing various bond characteristics. Surface configuration as well as material properties of the reinforcing bars are from the most important parameters that effect the bond behavior between the concrete and the reinforcement (ACI 318R-14 and ACI 408R-03). FRP bars often have a deformed shape (helical wrap) or a surface modification (often with sand coating or lugs). The study used helically wrapped and sand-coated BFRP bars. The research consists of laboratory investigations and data collection of 11 tested beams in order to accomplish the objective of this study.

In the following sections, the fundamentals and basic studies on the bond of traditional reinforcement in concrete are briefly presented.

1.1 Bond Stress

The reinforcing bars and the concrete cannot yield the reinforcement required without acknowledging forces involved across the interface. It is on such grounds the definition of bond stress comes in which entails that shear stress acting between concrete and reinforcing bars. As a result, there is a change in axial force along the length of reinforcing bars. It is worth recognizing that changing the axial stress of the reinforcing bar is the genesis for having bond stress. It is on that note it becomes clear that bond stress is entirely shear force per unit area of the bar surface.

1.2 Flexural Bond

Figure 1 shows the flexural stresses in a part dx along the bar by taking two adjacent sections at a distance dx and in the part l in the bar (Pillai and Kirk, 1988). By assuming a uniformly distributed bond stress over the surface, the following equilibrium equation is applied:

$$\mu \, \pi \, \phi \, dx = dT \tag{1}$$

then,

$$\mu = \frac{1}{\pi \, \phi} \, \frac{dT}{dx} \tag{2}$$

or,

$$\mu = \frac{1}{\pi \, \phi} \, \frac{V}{y_{ct}} \tag{3}$$

where μ is the bond stress (MPa), ϕ is the diameter of the bar (mm), dT is the change of the forces in the reinforcing bars within a distance dx (N), V = shearing force (N), and y_{ct} = distance between the resultants of the compressive stress and the resultant of the tensile stress (mm).

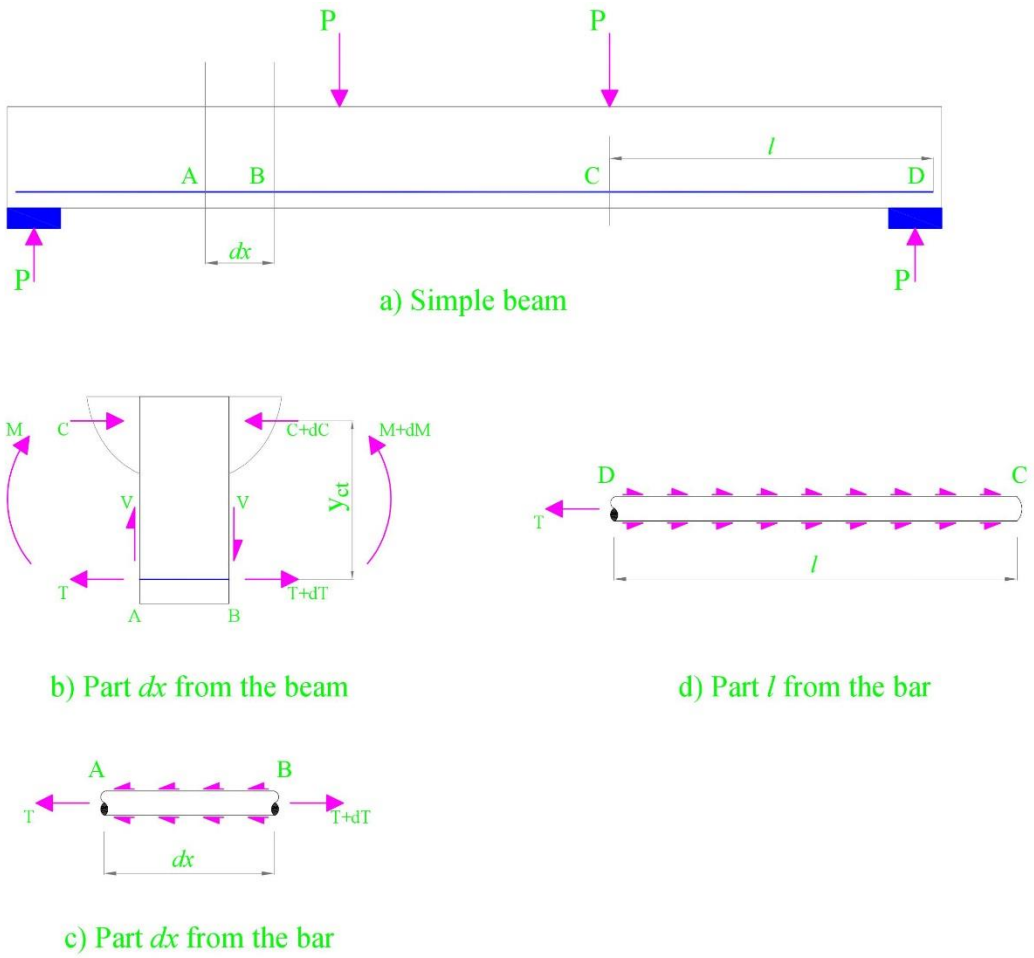

Figure 1: Bond stress in a beam

Hence, the bond stress is given by:

$$\mu\ (\pi\ \phi\ l\ ) = A_b\ f_b \tag{4}$$

or,

$$\mu\ = \frac{A_b\ f_b}{\pi\ \phi\ l} = \frac{\phi\ f_b}{4\ \ l} \tag{5}$$

where μ is the bond stress (MPa), ϕ =bar diameter (mm), l = embedment length (mm). A_b = bar's nominal cross-sectional area (mm), and f_b = stress in the reinforcing bar (MPa).

The stresses within the cracked beam, reinforcing bars, concrete, and bond stresses in

between are shown in Figure 2.

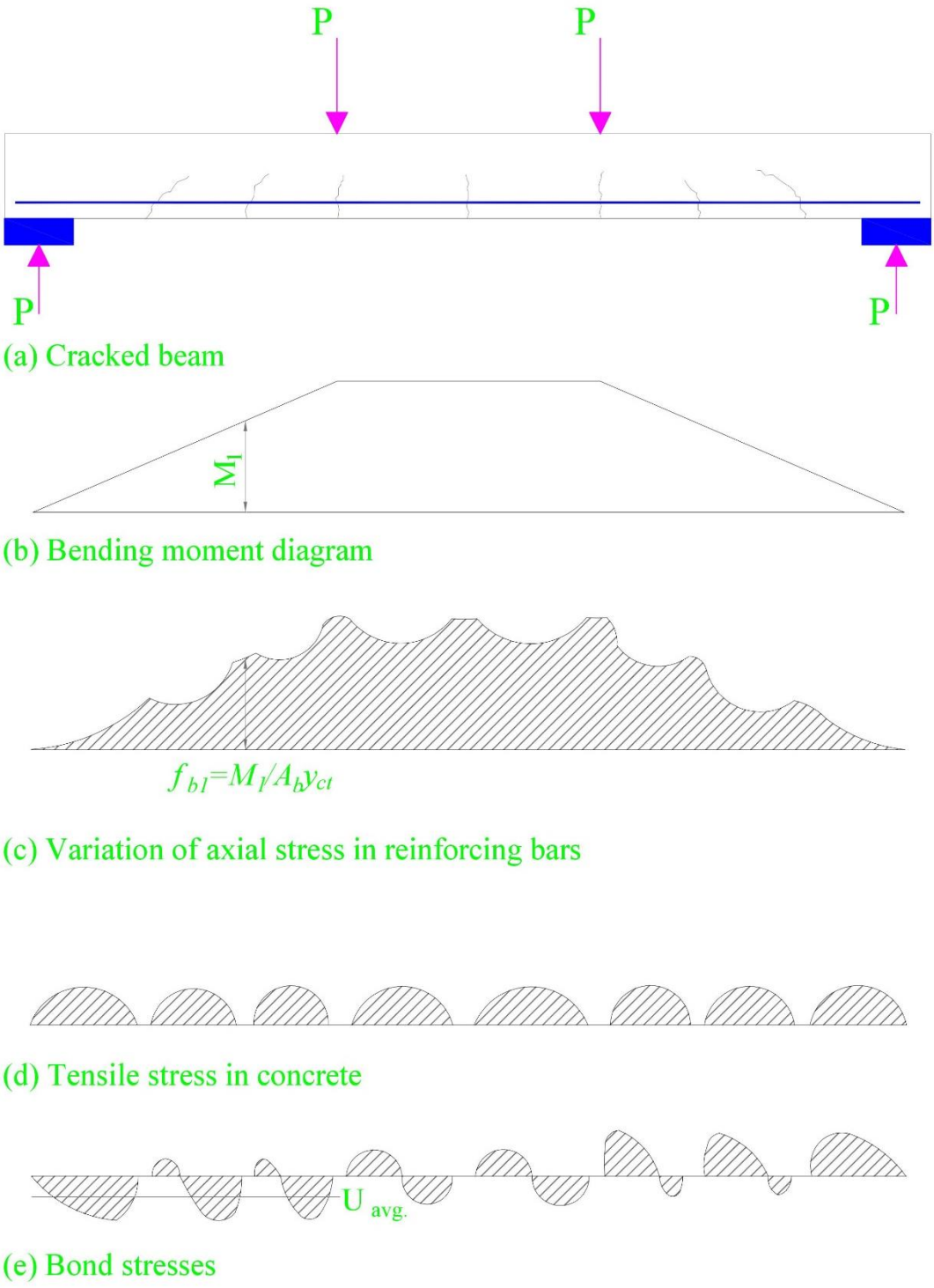

Figure 2: Bond stresses in a cracked beam

1.3 Bond Failure Modes

Pull out and splitting failure are modes of bond failure. The failure may occur when the bar pulls out without splitting of concrete. A small bar is embedded in a large concrete cube or cylinder means that such a particular bar is bound to pull out of the concrete. This may happen in the case of a good confinement by the concrete. As such, the inclined forces tend to move from the reinforcing bar to the concrete leading to bond failure as depicted in Figure 3. There is balancing of the circumferential tensile stress of the concrete with radial components of the compressive inclined forces. The splitting of the ring of tension is a definite connotation that the potential to transfer load to the concrete by the bar will be limited to the failure of the ring. Surface deformation is the major reason longitudinal splitting of the concrete occurs. Radial Forces of the rib also form part of the longitudinal splitting of the concrete. The circumferential tensile stresses are caused by radial forces and these stresses occur in the concrete surrounding the bar. It is for that reason cracks occur at the less concrete cover around the bars. Typical splitting failure surfaces are shown in Figure 4. Side split occurs when the side concrete cover and half of the bar spacing are less than the bottom concrete cover as shown in Figure 4a. V split occurs when the bottom concrete cover is less than the side concrete cover and 50% of the bar spacing as indicated in Figure 4b. However, the face and side split occur when the side concrete cover equates the bottom cover of the concrete as indicated in Figure 4c.

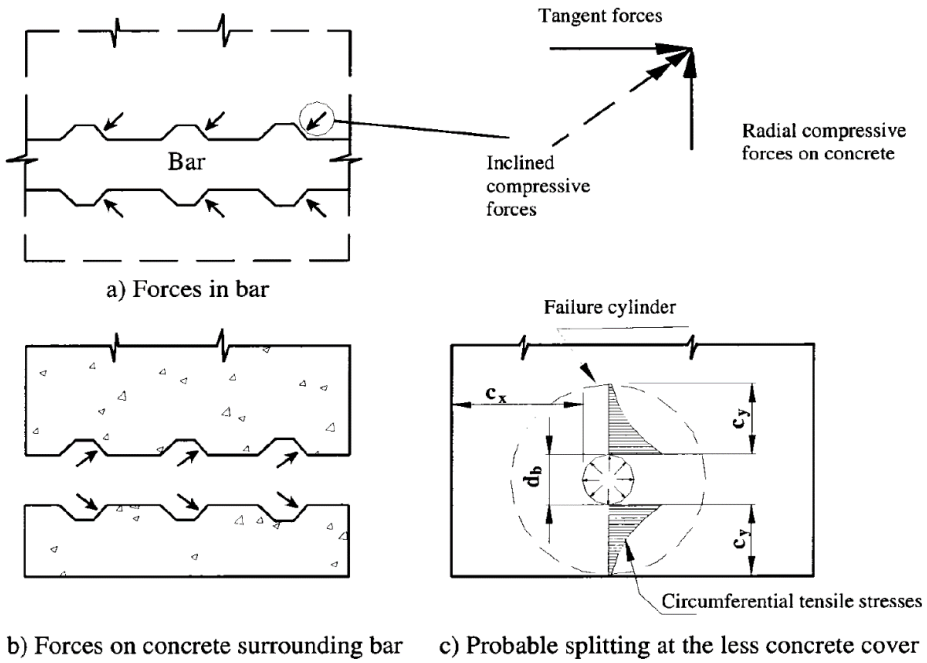

Figure 3: Splitting forces with deformed bars. From (Canaby & Frosch, 2005)

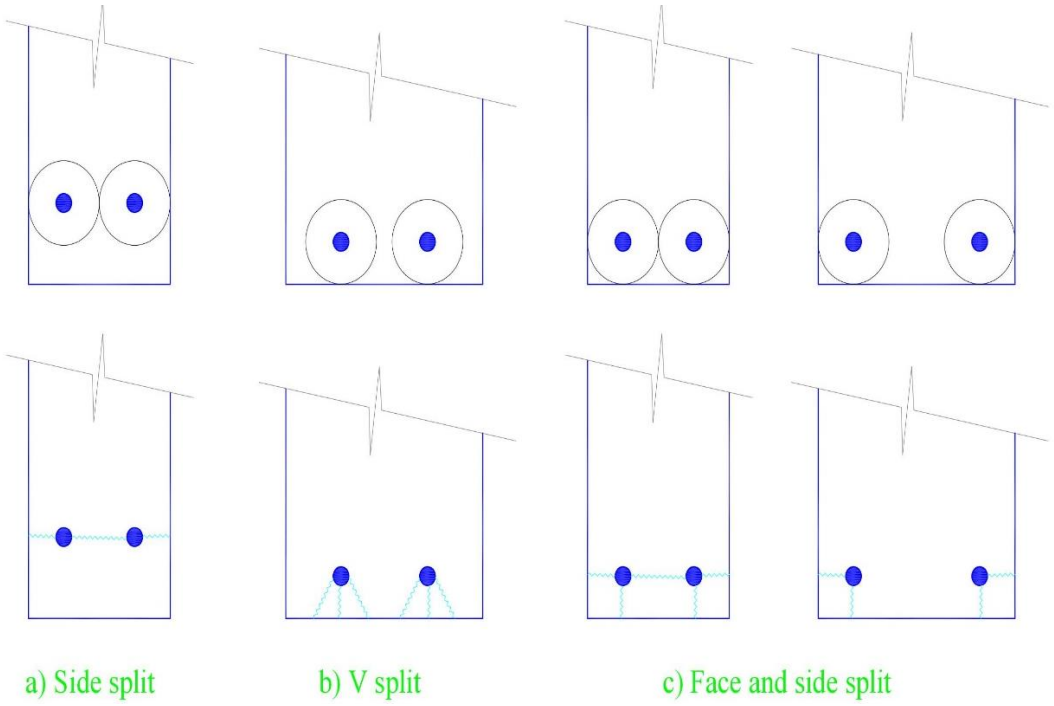

Figure 4: Typical splitting failure surfaces

1.4 Influencing Factors on Bond Strength

There are several factors that determine the bond strength of the reinforcing bars. It is not possible to mention bond strength of the reinforcing bars without highlighting such elements as loading condition, environmental condition, concrete strength, stirrups, spacing, concrete cover, bar diameter and embedment length (Mains 1951; Thompson et al. 1979; Hamad et al. 1996; Harajli et al. 1997; Tighiouart 1997; Sener et al. 1999; Esfahani et al. 2000, and ACI408R-03). The bar diameter and the embedded length are the most important parameters, which should be investigated for all the reinforcing bars. The strength of the bond is directly proportional to the degree of confinement (Ferguson et al. 1954; Lutz et al. 1993; Plizzari et al. 1996; and Hamad et al. 2002). The average strength of the bond in the reinforcing bars represents inverse proportionality to the bar diameter and the embedment length. Bond strength is also influenced by the depth of the fresh concrete below the bar during casting and the bar position. Figure 5 shows the effect of the stirrups to reduce the crack width and to improve directly the bond strength.

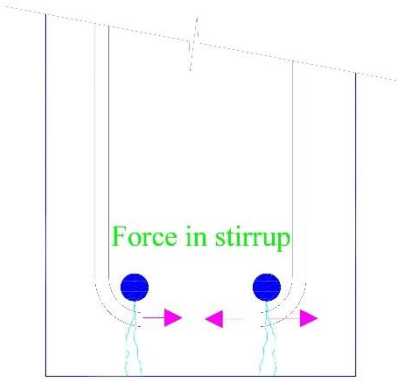

Figure 5: Stirrups forces due to bond splitting

It is vital to understand that it is possible to reduce the chances of splitting if the bar can be properly confined to the concrete as the bond strength tends to increase (Tepfers 1982; Sakurada et al. 1995; Rezansoff et al. 1997; and Tabata et al. 1998).

Stirrups cross potential longitudinal splitting cracks at right angles and hence can resist, partially, the tensile force, which causes the splitting thereby delaying the initiation of the splitting. They can also restrain the width and propagation of the splitting cracks, once formed. On the same note, Transverse reinforcement is critical in that it weakens the tensile force responsible for splitting thus ensuring the structure remains strong. There is also restraining of the width of cracks once formed to prevent further cracks that might intensify to a point of bringing the structure down.

1.5 Bond Tests

Beam and pullout tests are the roots for both the bond stress and bond strength distributions. The pullout tests happen when a bar is embedded in a cylindrical or cube concrete block while taking care of the measurements required to pull it out. A schema that illustrates the pullout test is given in Figure 6. The case of beam test seems to differ with that of pullout test in that the pullout test fails to feature those in the flexural members. In addition, pullout test does not consider such factors as shear forces, diagonal cracks and flexural cracks. The concrete within a pullout specimen is in compression, and the friction at the bearing on the concrete offers some restraint against splitting. More data on bond strength is available from pullout tests than from beam tests. In pullout tests, the bond stress distribution is not uniform. It is imperative to underline that a small load has a potential of developing high bond stress but the upper bar side of the bar (without the load) remains unstressed. The specimen is also bound to experience slip and bond stress as the pullout load increase. The maximum bond stress moves from the loaded end to the free end at failure or close to failure.

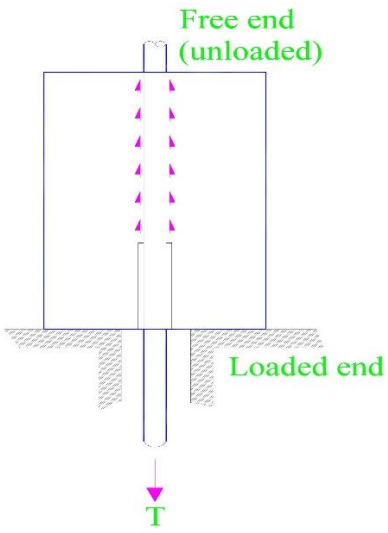

Figure 6: Pullout test

A hinged beam test is shown in Figure 7 according to RILEM specifications (RILEM/CEB/FIP), *Test of the bond strength of reinforcement of concrete: test by bending*, Recommendation RC.5, 1978). This test engages laboratory used in Europe for bond evaluation. The advantage of the test compared with pullout test is that there is no direct application of the external load to the bar. In addition, stress situation regarding concrete can easily be simulated by the test while the concrete element is subjected to bending.

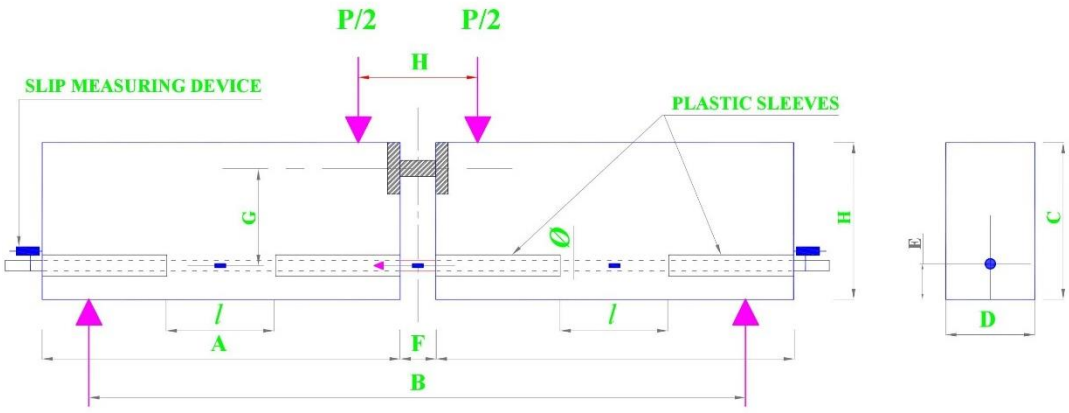

Figure 7: Hinged beam test

Various types of methods of testing are available for the determination of

different bond characteristics of reinforcing bars in concrete, as shown in Fig. 8 (ACI 408R-03 and ACI 440.3R-04).

In inverted half-beam tests, one half of the beam is tested, and the bar is subjected to an applied axial load while the remainder of the beam is supported, as shown in Figure 8a.

In the notched beam test, a beam is cast with notches at the bottom. Then, a load is applied to the top of the beam, directly over the notches and the beam is supported on each end, as shown in Figure 8b.

In splice tests, a large-scale beam is simply supported with two applied point loads and two bars are spliced in the constant bending moment zone, as shown in Figure 8c.

In the cantilever beam test, a beam is cast with a notch at the top. Then, the load is applied to the top of the beam and the beam is supported on one end and directly under the notch as shown in Figure 8d.

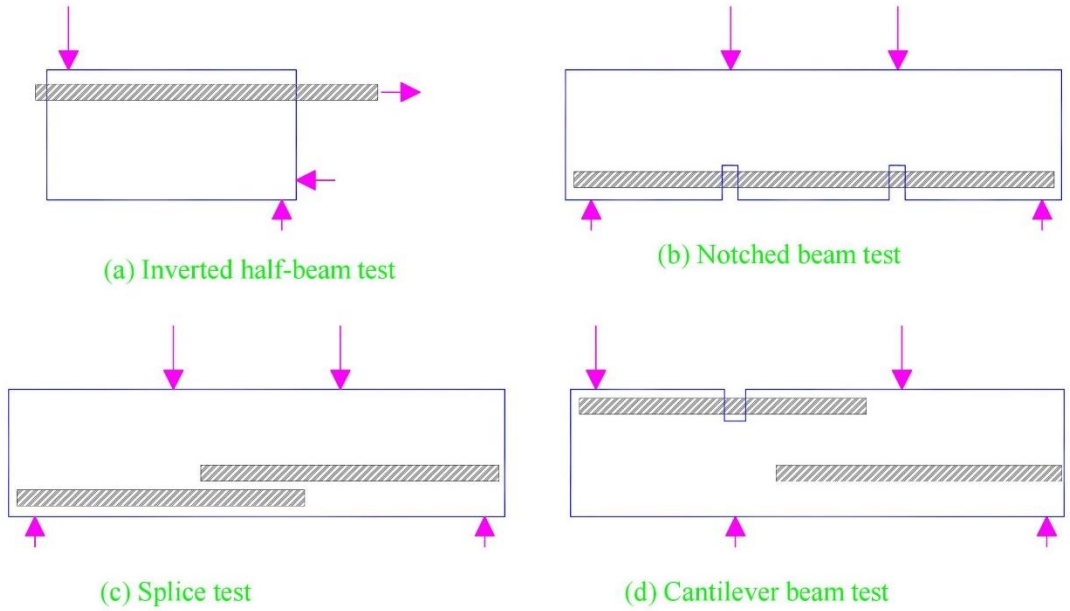

Figure 8: Types of test methods for bond values by beam testing

1.6 Development Length for Steel Reinforcing Bars

The development length is the length that is for developing a maximum stress into a bar through a bond. Because of the unpredictable and extreme non-uniformity in the actual bond stress distribution, the basic development length was specified in different codes and recommendations as a maximum permissible average bond stress over the embedment length.

The development length for steel bars specified in the CSA A23.3-04 is the following:

$$l_d = 1.15 \frac{k_1 k_2 k_3 k_4}{(d_{cs} + K_{tr})} \frac{f_y}{\sqrt{f_c'}} A_b \quad (6)$$

Where l_d = development length in mm, k_1 = bar location factor, k_2 = coating factor, k_3 = concrete density factor, k_4= bar size factor, f_y = yield stress in reinforcement bar in MPa, f_c' = concrete's compressive strength in MPa, A_b = nominal area of the reinforcing bar in mm^2, d_{cs} = smaller for:

a) the length from the nearest concrete surface to the centre of the bar or

b) 2/3 the bar's spacing from centre to centre, and K_{tr} is the rebar stirrups index.

$$K_{tr} = \frac{A_{tr} f_{yt}}{10.5\, sn} \quad (7)$$

Where A_{tr} = nominal area of the rebar stirrups in mm, f_{yt} is the yield stress in the rebar stirrups in MPa, s = maximum spacing from centre to centre of rebar stirrups in l_d, and n = bars along the potential plane of bond splitting.

The term $(d_{cs} + K_{tr})$ will not be used above $2.5d_b$. The development length l_d might be multiplied by the factors (A_s required) / (A_s provided) where reinforcement is in excess in a flexure member required in the analysis.

Recommendations for using spliced bars are for Class A is that $l_s = 1.0l_d$ and for Class B is that $l_s = 1.3l_d$, where l_s is the splice length (mm). Class A can be applied to the reinforcing bars which are stressed 50% below their overall strength and about half of

the bars are spliced. Class B applies to all other cases.

Based on ACI Building Code (ACI 318R-14), the development length is specified as:

$$l_d = \frac{3}{40}\frac{f_y}{\lambda\sqrt{f_c'}}\frac{\psi_t\psi_e\psi_s}{\left(\frac{c_b + K_{tr}}{d_b}\right)}d_b \tag{8}$$

Where l_d = development distance of deformed bars (mm), f_y = yield stress in the reinforcing bar (MPa), f_c' = concrete's compressive strength (MPa), ψ_t = reinforcement location factor, ψ_e = coating factor, ψ_s = reinforcement size factor, λ = density of the concrete, d_b = diameter of the reinforcing bar in mm, c_b = smaller of:

a) the length from centre of the bar to the nearest concrete surface in mm or

b) half the centre-to-centre bars' spacing in mm, and K_{tr} is the transverse reinforcement index.

$$K_{tr} = \frac{40A_{tr}}{sn} \tag{9}$$

The term $\frac{c_b+K_{tr}}{d_b}$ will not be above 2.5. K_{tr} can be taken as 0 to simplify the design even if transverse reinforcement exists.

1.7 Research Significance

There is inadequate literature or evidence about the bond of spliced FRP reinforcement bars. The spliced bars are critical in limiting the bar lengths thus suitable for use at the joints during construction. The standards or codes for steel reinforcement, such as ACI318 and CSA A23.3, might not be used for FRP bars because of the inherent differences in surface configurations and their mechanical properties. The current design guidelines related to FRP reinforcing bars (such as ACI 440.1-15 and CSA-S806-12) do not include the basalt fiber reinforced polymer in their standards. The findings of this study will address this gap. From the previous discussion, more investigation is required on the behavior of the bond of tensile lap-splices of the

concrete's FRP bars, especially basalt fiber reinforced polymer.

1.8 Research Objectives

The objectives of this study are to:

1. Explore the factors that impact on the strength of bond of the high strength concrete's tensile lap-spliced basalt FRP bars.

2. Study the bond cracking performance and the bond stress distribution along the embedment length of spliced basalt FRP bars.

3. Determine the appropriate recommendation for the high strength concrete's lap-splices of basalt FRP bars in design codes.

This context termed as the four-point flexural test was undertaken on 11 large-scale reinforcement FRP bars for concrete beams up to a point of failing. The context utilized FRP bars used in collaboration with two different coatings, namely basalt FRP. The investigation went on to evaluating the coating of the FRP bars, splice length and bar diameter.

1.9 Thesis Organization

This dissertation consists of five chapters.

Chapter 1

In this chapter, an introduction of this current research is presented including the fundamentals and basic studies on bond of traditional reinforcement in concrete. In addition, the objectives of this research are briefly discussed.

Chapter 2

This chapter includes a brief description of the available research in the literature.

Chapter 3

This chapter presents the information about the experimental program.

Chapter 4

The results of the tested beams are discussed in this chapter.

Chapter 5

Conclusions and recommendations and aspects to address in the future work are presented in this chapter.

CHAPTER 2: LITERATURE REVIEW

This chapter describes some theoretical and practical researches on bonding behavior of FRP reinforcement bars in concrete found in the literature.

The application of FRP bars also referred to as fiber reinforced polymers as a strengthening alternative to traditional steel bars is a promising approach that can contribute to reduce the very costly corrosion crisis in the Qatari infrastructure. Several obstacles hinder the acceptance of the FRP reinforcing bars in the industry sector to date. Technical issues that need to be resolved include the bond of the reinforcement bars to concrete. The earlier generation of these bars had serious bond problems, which severely slowed down the adoption of the products by the construction sector. The newer generation has seen under major improvement in the fabrication to enhance the surface conditions for a better bond with concrete and to have much higher inter-laminar shear strengths.

Unlike conventional steel reinforcing bars, FRP bars can be produced with a wide range of surface conditions. These include sand-coated, ribbed, indented, helical wrapped, and more. The bond between these bars and concrete varies greatly and is also dependent on the material of the bars (fiber type and binding matrix) (Benmokrane et al. 1996; Achillides et al. 1997; Hattori et al. 1997; Tepfers 1998; Bakis et al. 1998; ISISM03- 01; and ACI 440.1R-15). In addition, the technique used to cure the FRP bars affects significantly the surface properties. In the past, there have been strategies made to make an extension of the well-established strategy laws developed for concrete reinforced with steel to FRP materials (Cosenza et al. 2002). This was mainly done to save valuable time needed to promote the FRP materials in construction. However, this approach is deemed unrealistic because of the inherent variances in the physical and mechanical features between the steel and FRP. The main differences between the two

materials are the non-yielding, the low elasticity modulus, and the wide variety of surface conditions of the FRP bars.

In the last few years, the manufacturing processing technology of the FRP bars has been dramatically improved; this was associated with a higher demand for the material. These two facts called for more modeling and experimental investigations of the behavior of the reinforcing (FRP) bars in concrete elements. The need to introduce rational analytical expressions for the bonding style of FRP bars within the concrete materials was identified by several authors to be one of several critical issues in a need of an immediate address (Harris et al. 2003). In addition, the bonding among the two material, concrete and FRP is an essential factor in reducing the crack width as well as the crack spacing in concrete elements reinforced with FRP, which is an issue of large debate (Newhook et al. 2002).

The bonding between the two major elements, the FRP and Concrete has attracted numerous researches, especially in reference to the type of bars with different qualities and quantities of fibers. In addition, they are studied in reference to the shapes, as well as their outer surface structures. From the results of the experimental studies, it was concluded that the bonding between concrete and the FRP reinforced concrete is determined by more than one factor, and they are friction because of the surface roughness of the FRP bars, the chemical adhesion, as well as the hydrostatic pressure against the bars. Additionally, the other major factors are like the interlocking of the FRP materials against the concrete as well as the swelling of the bars due to the changes in temperature and the absorption of the moisture (Achillides et al. 1997; Hattori et al. 1997; Bakis et al. 1998; and Tepfers 1998).

The strength of the bonding between FRP and concrete reinforcement is a significant parameter in the strength and serviceability of concrete structures reinforced

with the FRP. The surface configuration and material characteristics of the bars (FRP) control the bond strength between the concrete and reinforcement (Bakis et al. 1988). FRP bars usually have deformed shapes (helical wrap) or surface structure (often with sand coating or lugs). Helical wrap and sand coating often give a better improvement in the bond strength than other types of reinforcement.

Studies have found out that the performance of the bonding of the FRP bar is dependent on many factors such as the design, mechanical features as well as the production process (Achillides et al. 1997; Hattori et al. 1997; Bakis et al. 1998; and Tepfers 1998). During the anchoring of the reinforcing bar on the concrete, the bonding force is transferred through adhesion resistance within the interface, the mechanical interlock as well as the friction against the slip. In addition to that, the bonding force may also be transferred through the resin and directly to the FRP. A failure in the resin may mean a scenario where the adhesion breakdown and the irregularities on the surface of the FRP bars that may result to the inclining of the contact forces between concrete and the bar.The force over the surface area, which is the stress, when applied in the direction of the bar it can be considered as the bond stress. The mechanism of transferring the stress between concrete and the bars has been identified by several researchers (Achillides et al. 1997; Bakis et al. 1998; Tighiouart et al. 1999; and Mesbah and Benmokrane 2002) to be the combined effect of three following factors: 1) chemical bond, 2) friction bond, and 3) mechanical interlock. The chemical bonding between concrete the FRP bar is initially responsible for stress transfer until slip between the two occurs then resistance (caused by friction) and a mechanical interlock take over (Bakis et al. 1998 and Tighiouart et al. 1999).

Over the past few years, the research group at the Department of Civil and Architectural Engineering at Qatar University has conducted extensive research on the

use of FRP bars in concrete structures.

2.1 The Theoretical and Experimental Studies on Bond of FRP Bars

Faza and Gangarao (1990) studied the bending and the bonding behavior of beams of concrete that are reinforced with FRP bars. The experimental program contained twenty-two rectangular beams subjected to flexural tests and twelve specimens submitted to bond forces by pullout testing. It was established that the crack widths of concrete reinforced with the FRP beams were larger than the crack widths of equivalent steel reinforced concrete beams. It was also found that the crack widths were reduced when using sand-coated FRP bars.

Chaallal et al. (1992) conducted a study to evaluate the development length of GFRP coated with sand such, E-glass fibers were used and polyester resin. Some tests such as the pullout tests were carried out with both normal and high strength concrete and cement grout. Different bars, three of them were utilized where the anchored length was made dissimilar by making them varied from about five to ten times the diameter of the bar. A development length of about 20 d_b where d_b is the bar diameter was recommended.

Brown and Bartholomew (1993) investigated for bending capacity and the bond strength of concrete specimens reinforced with FRP bars. They studied the flexural behavior by testing six simply supported reinforced beams to failure under three-point loading test, while bond strength was investigated by conducting twenty-four pullout tests. Although the results for flexural strength indicated that the FRP reinforced concrete beams in many aspects behaved in the same manner as would be expected in beams supported with steel bars; however, the beams reinforced with FRP exhibited much larger deflections than their steel counterparts, because of their low elasticity modulus. The pullout test results appeared to suggest that the bond strength of FRP bars

is approximately two-thirds the one for steel bars.

Chaallal and Benmokrane (1993) examined the bonding strength of GFRP bars in concrete. The GFRP bars were composed of unbroken longitudinal glass-fiber and polyester resin by the pultrusion process. Glass-fiber strands were wrapped, and sand coating was placed on the superficial layer of the bars for an improved bonding strength. The modulus of elasticity of the bars was found to be 45 Gpa while that of the tensile strength was discovered to be about 700 MPa. Eighteen series were tested (four tests per each series) to investigate the anchored length, bar diameter, concrete strength and top-cast modification factor. Bar diameters were 12.7, 15.9, and 19.1 mm. All pullout assessments were performed based on the ASTM C234-86. It was established that the bond strength of a glass-fiber bar to concrete is 12 MPa. The development length is 20 d_b (d_b is the bar diameter) to achieve the ultimate tensile load capacity of the GFRP rod. The top-cast modification factor was found to be equal to 1.23. In addition, it was found that the bond strength of the tested GFRP bars does not differ linearly with the compressive strength of concrete.

Cosenza et al. (1995) examined the bond behavior between the FRP reinforcing bars and concrete. The analytical modeling and experimental results of the bonding strength of FRP reinforcing bar to concrete were discussed. It was concluded that the bonding capacity of the FRP reinforcing bars is determined by the outer surface and bar's industrial process of manufacturing.

Malvar (1995) investigated the bonding behavior of the FRP bars in concrete. He used four various GFRP reinforcing bars with varied surface features. The data from the experiment involved bond stress slip and bond stress radial deformation for the different levels of confinement. The specimens included GFRP bar of 19.1 mm diameter fixed in a cracked cylinder with a measurement of 75 by 100 millimeters. The

material was subjected to a controlled pressure (axisymmetric radial pressure). The length of the GFRP reinforcing bars was 3.5 times the diameter of the bar. The observation was that the small surface indentations was enough to attain a powerful bond. On top of that, the bonding strength of the steel bar is about 1.2 to 1.5 more than that of the GFRP.

Benmokrane et al. (1996) carried out a study on the strength of the bond and the load distribution of the GFRP reinforcing bars in concrete. A longitudinal type E glass fiber and the polyester resin were used to make the GFRP reinforcing bars. Helically winding were applied on the surface of the reinforcing bars in order to deform it. On top of that, sand coating was applied on the GFRP bars. The characteristics of the bars were that the mean tensile strength of the GFRP bars was 683 MPa while that of the modulus of elasticity was found to be 42 Gpa. The whole study utilized a normal strength concrete. Five laboratory pullout tests were used for 19.1 mm diameter bars. The five specimens were three instrumented GFRP bars and two instrumented steel bars for comparison purposes. The instrumented reinforcing bars were fixed and cast at the center of the concrete cylinders. The molds were 254 mm x 400 mm. Additionally, 20 beams of concrete reinforced with 4 diameters between 12.7 and 25.4 of GFRP and steel bars, the beams were tested based on the specifications by the RILEM. The specifications are for testing bond strength of materials such as concrete reinforced with FRP bars. The testing was under four-point loading. Out of the 20 beams, 3 beams were reinforced or each diameter (12.7, 15.9, 19.1, and 25.4 mm), with GFRP bars and 2 of the beams with steel reinforcing bars for a comparison. It was found that the bond stress and tensile stress distributions of reinforcing bars which are steel and GFRP was typical. The bond stress distribution was non-linear. The average bond strength of the GFRP bars varied from 0.73 to 0.96 times that of steel reinforcing bars. The friction, as

well as, the adhesion were the most significant features of the bonding stress mechanisms in the GFRP reinforcing bars. The bond strength obtained from pullout tests was greater than bond strength for beam assessments. The beam specimen test recommended by RILEM (RILEM/CEB/FIB, 1978) is more realistic in simulating bond behavior conditions and is preferred over the pullout test.

Ehsani et al. (1996) conducted 48 inverted half-beam tests and 18 pullout tests. The tested factors included the diameter of the bar, the depth of the cast of the concrete, the concrete cover, the compressive strength and the embedded length of the bars. The bars used for the reinforcement, the GFRP, was made of 72% type E-glass which also had a volume of 28 per cent polyester resin. The surface was wrapped in a helical pattern to improve the bond strength. The 18 pullout tests resulted in 15 pullout and 3 tensile failures. The 48 beam tests resulted in 25 pullouts, 4 splitting, and 19 tensile failures. It was found that at 0.0025 in (0.064 mm) free-end slip or 0.015 in (0.38 mm) loaded-end slip, the embedment length has a slight influence on the load-slip relationship. Therefore, this value is recommended of allowable slips of the GFRP bars. For the calculation of the developmental length, an equation was recommended. The development length could be computed from this equation: $l_{db} = 0.022(A_b f_y / \sqrt{f_c{}'})$ and not less than that $l_{db} = 0.0508\, d_b f_y$. Where l_{db} is the basic development length (mm), A_b is the nominal cross-sectional area of the FRP bars (mm^2), f_y is the yield stress in the steel reinforcing bar or the tensile strength of GFRP rebars (MPa), d_b being the bar diameter, and $f_c{}'$ being the compressive strength of concrete. A minimum development length of 381 mm was also recommended. Furthermore, they calculated a confinement factors to show the impact of the cover of concrete and the casting point. The findings were the modification factors of 1.5 for the concrete cover and 1.25 for the top bars, the concert cover factor is used when it is less than or equal to the diameter

of the bar.

Achillides et al. (1997) carried out an independent study on the bond strength of the FRP bars in concrete. The study was basically on the testing of about 100 specimens in a direct pullout as well as another 30 concrete beams on a 4-point bending element. The used bars in the pull-out specimens were composed of aramid, carbon and a mix of glass and carbon which called hybrid. The bars were embedded in the concrete cubes in a distance of 150 mm. The two sides of the bar in the concrete cube were debonded to reduce the end effects. It was concluded that the diameter, type, and shape of the FRP bar, and the strength of the concrete influence the bond strength. Bond strength was also found to be influenced by the location of the members under testing. Members subjected to flexure and shear could have different bond strengths than reinforcing members subjected to tension and compression. CFRP and GFRP exhibited similar bond behavior compared to that of steel bonding in pullout tests. The average bond stress drops as the embedment length increases as the surface area increases. The decrease in bond strength with embedding distance is attributed through to non-linear bond stress distribution.

Cosenza et al. (1997) carried out a literature review, especially experimental studies on the bond behavior of the FRP bars in the concrete. The study presented an in-depth report on the bond strength of FRP bars in the concrete material. The study expounded on the ways in which the bond stress is transmitted from the FRP to the concrete material. The investigations included a study on the major parameters such as confining pressure and the bar diameter, as well as the influence of fiber and surface texture on the bond performance. Other major parameters included environmental conditions, concrete strength and temperature changes. The studies included straight FRP reinforcing bars such as smooth, sand-covered and altered FRP reinforcing bars

such as the spiral glued-type bars, ribbed-type and braided as well as the twisted ones. It was found from several experimental studies that FRP smooth bars are not adequate for the use in reinforced concrete structures. The sand coating shows a good bond but inelastic bonding failure. The bond strength is provided by a friction mechanism. An altered smooth bar surface by pasting spiral on it did not make any improvement in the bond strength. Twisted strands improve slightly the bond strength. The greatest results in terms of the stiffness and the bond strength are gained for both the altered bars and the ones that are sand-coated. Additionally, the study included the relationships in terms of analytical models of bond-slip.

Joh et al. (1997) investigated the bond cracking performance of concrete that has been reinforced with FRP bars. 12 sorts of FRP reinforcing bars were used. They used tension testing and flexural testing of concrete beams reinforced with FRP reinforcing bars. The results were that the width of the cracks in concrete reinforced with FRP might be evaluated via the substitution of the modulus of elasticity of FRP in the calculations for concrete reinforced with conventional steel. Additionally, the cracks which occurred in the beams reinforced with fiber bars had equal spaces to those occurring in concrete beams reinforced with steel. Thus, the used formula to calculate the crack spaces for beams reinforced with steel reinforcement can be used to calculate the crack spaces for the ones reinforced with FRP bars. The propagation of cracks (flexural) of concrete beams reinforced with FRP bars was similar to the ones for beams reinforced with steel. Furthermore, testing the tension for FRP bars in the concrete confirmed that the initial cracking loads became small when there was an increase in the elastic modulus or the FRP reinforcing bar's bond strength.

Tepfers et al. (1998) conducted a study on the tensile reinforcement splice tests and the pullout test using the GFRP bars. The GFRP bars were tested using pullout tests

with central placement in a block of concrete having measurements of 200 mm by 200 mm by 200 mm. Bond stress-slip relations were measured at the end of the bar. The diameters of the GFRP reinforcing bars were 15 and 25 mm. The lengths of the bond were equivalent to 45, 75, and 105 mm and three different concrete strengths corresponding to 25, 40, and 55 MPa were considered in the experimental study. Also, pullout tests with eccentric placement of bar were used with different concrete covers (d, 1.5 d and 2 d). Three beams were tested with two over-lapped GFRP bars. The diameter of the bars was 25 mm and splice lengths were 400, 600, and 800 mm. It was concluded that at slips ranging from 6 to 20 mm, the loads were about 50% of the maximum load. By raising the thickness of the cover of concrete, the bond power was increased. Moreover, the GFRP bar has low concrete splitting tendency.

Tighiouart et al. (1998) carried out an analysis on the bond of FRP bars in the concrete. An overall number of 64 beams made of concrete and also reinforced with FRP bars were investigated. The study utilized two types of the GFRP bars which were also manufactured via the pultrusion procedure. The bars were composed of polyester resin as well as the continuous longitudinal sort E-glass fiber. The surface textures of the bars were helical winding and sand coated. To include the bar diameter parameter, four bar diameters were used (12.7, 15.9, 19.1, and 25.4 mm). Also, 3 embedded lengths were tested (6 d_b, 10 d_b, and 16 d_b). Bond strength from beam tests was performed in line to the specifications of RILEM (RILEM/CEB/FIP. 1978). Eighteen specimens were tested as pullout tests to examine the influence of the top bar. Three concretes of depths, 1000, 600, and 200 mm were examined. The direct pullout specimen consisted of a concrete wall and the GFRP bars placed at the upper part, middle and lowest part. Two diameters of GFRP bars (12.7 and 19.1 mm) were examined. The authors found the GFRP reinforcing bars have less bond strength than steel, which was attributed to

the lack of mechanical interlock between the GFRP bars and concrete. The average maximum bond strength decreases for the GFRP reinforcing bars when the diameter of the bar increased. The modification factor, which represents the proportion of the bond power for bottom bar to that of upper bar, is recommended to be 1.30. A different model was projected for the ascending branch of the bond stress-slip relationship.

Cosenza et al. (1999) carried out a study to examine the bond between GFRP bars and the concrete. Ribbed GFRP bars were utilized in the investigation. The specimens were prismatic concrete with cross-section of 150 x 150 mm^2 and the bar was centered in it. The embedment lengths extended from 5 to about 30 times the diameter of the bar. It was found that the mode of failure of bond tests was one of the two modes (pullout failure and tensile failure). The bond mechanisms of the tested ribbed GFRP bar depends on the bar ribs and concrete strength. Moreover, the slips that were tested at the loaded end were expressively greater than the ones at the free end.

Katz (1999) investigated a bonding mechanism of FRP bars in concrete. Five kinds of surface texture for the reinforcing bars (FRP) were tested, including sand-coated, deformed, and helically wrapped FRP bars. The specimen consisted of concrete block of measurements 150 mm x 150 mm x 420 mm. A 1000 mm long bar was embedded in the center of the block horizontally. The samples were segmented at a spacing of 120 mm from all the sides to get two samples from each specimen. Furthermore, additional specimens were cast vertically. The bars were embedded vertically at 150 mm diameter concrete cylinder. It was found that the physical and mechanical characteristics of the external coating of the FRP reinforcing bars have a significant consequence on the bonding strength of the FRP bars. When the pull out test was performed for the steel bars, the failure was in the surrounding concrete to the steel bars. Unlike the FRP bars where the damage was located in either the surrounding

concrete or both the surrounding concrete and the FRP bars itself.

Taly and Gangarao (2001) analyzed outcomes from numerous experimental studies that examined the bonding behavior of the FRP reinforcing bars in concrete. A report about the bond of the FRP bars in concrete was presented. The authors reported that most of the bond examinations found in the studies were pullout tests. The majority of the assessments were conducted in a way that only a very few tests included cyclic loading. Also, the authors reported that very limited research was done by using FRP bundled bars. The bond strength tests of the beam were lesser than that from the other tests. However, the beam test is more realistic in a way that it takes considers the actual behavior of reinforced concrete members. The results also found that the chemical bond is too low. However, the mechanical interlock and friction are the main ways of stress transfer. Finally, the authors reported that there is no effect of the compressive strength of concrete on the bond strength of FRP bars.

Okelo and Yuan (2005) conducted 151 pullout tests using the three major FRP bar types along with steel rebar. It was found that the strength of the bond of an FRP bar can be more by 40 to 100 per cent that of steel rebar when failure is by pullout. It was also found that the change in bar modulus due to the various fiber types of glass, carbon, and aramid can also influence the bond properties.

Okelo (2007) conducted RILEM beam tests which showed that CFRP provides 85% the bond strength of steel. Additionally, the GFRP bars which had lower modulus of elasticity than CFRP showed lower bond strength.

Moon et al. (2008) used a mixture of milled glass fibers and epoxy resin to formulate a ribbed surface structure for GFRP fiber cores and obtained 56-90% the bond strength of steel rebar with a similar diameter.

2.2 Behavior of Splice Steel and FRP Bars in Bond

David (1976) established an efficient experimental technique to evaluate the critical splice length. The author indicated that it is possible to determine the critical splice length from the knowledge of the mechanical properties of steel bars and some splice test results. In addition, it was found that the ultimate strength analysis could predict the strain measurements along the spliced length.

Tepfers (1980) evaluated the bond strength of spliced steel reinforcing bars in concrete through the utilization of the modulus of displacement model. The theory is grounded on the actual displacement of the reinforcement. In addition, the author investigated simpler equations disregarding the effective concrete area around the steel bars. A match between the model and the test results was found.

Cynthia et al. (1993) investigated the bond of epoxy-coated steel reinforcement. The influences of coating (epoxy) and transverse reinforcement within the splices of the strengthening bars were investigated. Two bars sizes, 19.1 and 25.4 mm-diameters, were tested. Also, three deformation patterns of bars were tested. The experimental program contained 65 beams and a slab specimen. All the beams measured 3960 mm in length. The splices were in the constant bending zone. The cross section of the beams was 406 mm in wide by 381 or 406 mm in deep. It is concluded that the bond strength of the epoxy-coated bars is smaller than the one for the uncoated bars. Confined splices are better than unconfined splices (without transverse reinforcement). The specimens with stirrups behaved in a ductile manner. Moreover, the specimens without stirrups failed in a brittle manner. The development length can be reduced by the use of transverse reinforcement.

Einea et al. (1999) studied the behavior of lap splices which is spirally confined by deformed steel bars in concrete. The studied factors included in the study are the strength of the concrete, the spirals count and the length of the splice. The findings of

the study were that, spiral confinement of spliced steel reinforcing bars can end in a massive decrease in the essential length needed for the splice. Furthermore, a formula was proposed to be used in the prediction of spirally confined lap splices length.

Tighiouart et al. (1999) studied the bond strength of GFRP bar in concrete through the means of lap-splices in beams under a static loading. Sixteen reinforced concrete beams were loaded in 4-points loading test. The length of the beam was three meters. The effect of the splice length and diameter of the GFRP reinforcing bars were investigated. The diameters of the bars, which were used in this study, were 12.7 and 15.9 mm. The lap-splices were tested from 0.6 l_d to 1.6 l_d. The type of GFRP reinforcing bar contained E-glass fibers which are bonded using polyester resin. A helicoidally glass fiber (strand windings) and sand coating were used to add more strength to the bond of the bars. The lap-splices were located in the pure bending moment zone. The clear cover was 30 mm. Normal mild steel was used for compression reinforcement and stirrups. Hydraulic jacks applied loading incrementally until failure. The development length was taken as $l_d = 60.47\ d_b$. It was found that a modification factor of 1.3 ought to be taken into account for the development length of GFRP bars. In addition, when the splice length was 1.6 l_d , the ultimate capacity of GFRP reinforcing bar was achieved.

Aly (2006) conducted spliced beam tests on sand coated bars (CFRP, GFRP). The strength of concrete was 40 MPa. The diameters of the bar were 15.9 and 19.1 mm for GFRP and 9.5 and 12.7 mm for CFRP. The dimensions of the beam were 250 mm width and 400 mm depth while the shear span was 1000 mm with a 1600 mm constant moment region. Shear reinforcement was provided throughout the shear span at a spacing of 100 mm and an increased spacing of 150 mm within the constant moment region. Splice lengths for the study ranged from 500 mm to 1400 mm. An additional

full bar beam was cast for comparison using GFRP rebar. The concrete cover was 40 mm. There was also the mounting of strain gauges at various locations along the splice for verification. The strain behavior showed that little force is carried by the bar prior to cracking of concrete followed by a steady increase in load afterwards until failure. The strain distribution of the bar showed that bond stress is not constant but rather more concentrated at the loaded end. Just prior to failure, however, the bar strain distribution becomes more linear. This was due to the splitting failure mode which predominately occurred for the larger bar diameters. Larger diameter bars typically showed weaker bond stress. Theoretical predictions of the neutral axis depth using the ultimate strength method were very similar to that obtained from strain compatibility from the concrete and bar stain measurements. Similarly, the strain measurements matched with those obtained from theoretical calculations. Cracks typically occurred at the ends of the splice and then propagated towards the center. Results also showed that a linear variation exists between the maximum developed bar force at the end of the splice and along the splice. It was concluded that only a couple of spliced beam tests were necessary to form a relationship for predicting the critical splice length. Critical splice length predictions ranged from 40 d_b for 15.9 mm bar diameter and 50 d_b for 19.1 bar diameter of GFRP bars, while critical bond stresses within the splice were predicted to be 4.1 and 3.0 MPa in that order. Due to the consistent splitting failure mode of the splice, the concrete tensile strength was deemed essential in enhancing the bond strength of splices.

Aly (2007) conducted further theoretical analysis using the MD theory (modulus of displacement) to forecast the bond stress distribution and bar force distribution for some of the tests in the previous study. The previous research showed that the contribution of the confining reinforcement allowed a constant bond stress

alongside the measurement of the bar while for unconfined splices the bond stress was non-uniform. The modulus of displacement theory was adopted from Tepfers (1980) for analysis. Additional pullout tests conducted using the free end slip showed that the modulus of displacement for 19.1 mm GFRP rebar was in the range of 300 N/mm^2 and 30 N/mm^2 for tangent and secant modulus, respectively. Theoretical predictions were compared with values from the strain gauges using three stages. The first stage prior to cracking includes the contribution of concrete in the tensile region. The second stage ignores this due to the presence of cracking. While the third stage, to the failure, uses a reduced MD model due to the plastification of concrete ring surrounding the rebar. The reduced MD ranged from 5 to 30 N/mm^2. The results from strain gauges showed a good agreement with the theory.

Choi et al. (2008) tested one-way slabs using four-point loading and spirally wound GFRP rebar. The two concrete strengths used were 26.5 and 33.2 MPa with 30- or 50-mm cover. Steel shear reinforcement was used only in the shear region. The bars surface condition was spirally wound, and the nominal diameter was 13 mm. Gauges to measure the strain were used at the ends of the splice. The slab dimensions were 750 mm x 250 mm (width and height) with 5 or 9 spliced bars in the tension region. The clear span length was 3600 mm with a shear span of 1200 mm. The main failure mode for all spliced slabs was by splitting of the bottom and side cover. The bond strength reached around 2.1 to 4.8 MPa with the smaller bond strength occurring with smaller bar spacing. Similarly, reductions in cover and increases in embedment length reduced the average bond strength

Harajli and Abouniaj (2010) conducted splice tests using beams of 1800 mm span under four-point loading. Each beam had two spliced bars and steel stirrups as shear reinforcement in the shear region. Two types of surface conditions were used

namely helically wrapped and ribbed. Additional steel specimens were cast for comparison. The three splice lengths ranged from 15 to 30 bar diameters. Concrete cover ranged from 1.25 to 2.0 times the bar diameter. Some specimens also had additional transverse reinforcement in the pure bending region. The applied loads were spaced in such a way that the entire splice length would be in the pure bending region. The concrete strength was between 48 and 52 MPa. Strain gauges were also applied just outside the spliced region to verify the maximum bar force. The mode of failure for ribbed rebar including steel was by splitting with a complete loss of load capacity immediately after the maximum capacity was attained. On the other hand, threaded bars got a more ductile failure with a gradual pullout of the rebar. This also had the effect of increasing crack widths to more than 20 mm at the end of the splice. Furthermore, due to the friction between the bars and concrete after initial bond loss, a substantial load capacity still remained even through large deflections until failure. Threaded GFRP bars developed a capacity between 27 and 36% of the ultimate tensile strength while the ribbed GFRP bars developed 42 – 67%. A reduction in the bond strength was noticed, even more so for thread wrapped bars versus ribbed bars, with an increase in the splice length however an increase in the bar force was still achieved. An increase in the cover showed little improvement on the strength of bond for ribbed GFRP bars with no increase shown for thread wrapped bars. However, a considerable increase in the strength of the bond was observed with the presence of confining reinforcement for both types of GFRP.

Choi et al. (2012) conducted unconfined splice tests using a surface coated GFRP lap spliced at the center span of 4 m long normal strength concrete beams. The strength of concrete was 23.0 MPa and the GFRP bars had a modulus of elasticity and tensile strength of 37.2 Gpa and 690 MPa respectively. The bar diameter was 12

millimeters which were tested in splice lengths ranging from 15 – 60 times d_b. Effective cover thickness ranged from 19.1 to 36.4 mm with the number of spliced bars ranging from 3 to 5. The cross section was constant for all specimens, 300 x 400 mm (width x height), but the reinforcement ratio ranged from 0.31% to 0.51% while the calculated balanced ratio was 0.34%. Application of strain gauges was carried out at the ends of the splice for verification. An additional beam was cast using three full-length bars for comparison. A 4-point loading was used to test the beams with a clear span length of 3600 mm and a shear span length of 1000 mm. Shear reinforcement was provided just in the shear region so as to give the most conservative bond behavior in regards to splitting failure, which was the only mode of failure exhibited by the spliced beams. The beam with continuous bars failed because of rupture in the GFRP bars. Beams with splice lengths of 30 and 60 bar diameters had a load capacity of only 48.5% and 66.4% of a similar beam with continuous reinforcement. Cracking typically began at the ends of the splice then continued increasing in length and number while also accompanied with stiffness degradation. Longitudinal cracks along the bar height signified the onset of splitting failure. Typical load deflection behavior showed a stiff climb up to the cracking load followed by a loss of stiffness but linear increase in load until the point of failure.

Esfahani et al. (2013) tested 13 beams which had dimensions of 150 × 200 mm and two spliced glass fiber reinforced polymer bars, the bars had two surface configurations the sand coated and the ribbed, the conducted test was a four-point loading test, normal strength and high strength concretes were used. It was concluded that concrete compressive strength does not significantly influence the bond strength of GFRP bars in spliced beams. Increasing the bar diameter decreases the bond strength of GFRP bars.

Hossain et al. (2017) conducted RILEM beam test for a total of 144 RILEM beam specimens, the beams were sorted into two types based on their dimensions. Two concrete types were used, the high strength concrete and the ultra-high strength concrete as well as two glass fiber reinforced polymer bars, the low modulus and high modulus. It was found that increasing the compressive strength increases the bond strength, and the increase of the embedment length leads to the decrease of the bond strength.

Köroğlu (2018) developed a prediction for the flexural bond strength of FRP bars in concrete using artificial neural network (ANN). Eight input parameters were used for the model, these parameters were confinement, type of FRP, compressive strength of concrete, bar diameter d_b, ratio between the cover and bar diameter $\frac{c}{d_b}$, surface texture of bar, ration between the development length and bar diameter $\frac{l_d}{d_b}$, and the ratio between the area of transverse reinforcement and the product of transverse reinforcement spacing, the number of developed bar and bar diameter $\frac{A_{tr}}{s*n*d_b}$. The results of this study stated the effect of the bar's surface texture on bond strength, in addition to the effect of concrete compressive strength on the bond strength. The results showed that the sand-coated bars had a higher bond strength than the helical ribbed and spiral wrapped bars. Also, if the concrete compressive strength rise, the bond strength escalates.

Zemour et al. (2018) performed a splice test to eleven full-scale beams. The beams investigated the effect of the casting height on the bond strength by have 2 dimensions of 250 × 400 mm and 250 × 600 mm. Additionally, the study focused on the effect of the concrete type (normal and self-consolidating), and splice length on the bond strength of lap-spliced glass FRP bars in beams. The influence of the splice length was clear, and it showed that increasing the splice length decreases the bond strength.

Although, previous studies have suggested that bearing forces and subsequently radial splitting forces were much lower with FRP bars (Larralde and Silva-Rodriguez 1993; Tighiouart et al. 1998), splitting failure is still the dominant failure type of spliced Fiber Reinforced Polymer bars. Additional research in the area of tensile lap splicing of FRPs in high-strength concreter (HSC) would be beneficial since the use of a higher tensile strength concrete will reduce the occurrence of splitting failure and improve the bond conditions of splices.

CHAPTER 3: EXPERIMENTAL PROGRAM

11 large scale beams cast tested in two Groups. Group 1 contained 9 concrete beams and group 2 had 2 beams. All of the beams were reinforced with BFRP bars. The groups investigated the effects of three parameters on the bond strength of the BFRP bars in concrete. One type of FRP bars was used as well as three diameters of BFRP bars. The bar diameter, splice length, and surface texture were the tested parameters. Figure 9 shows a flow-chart that summarizes the experimental program.

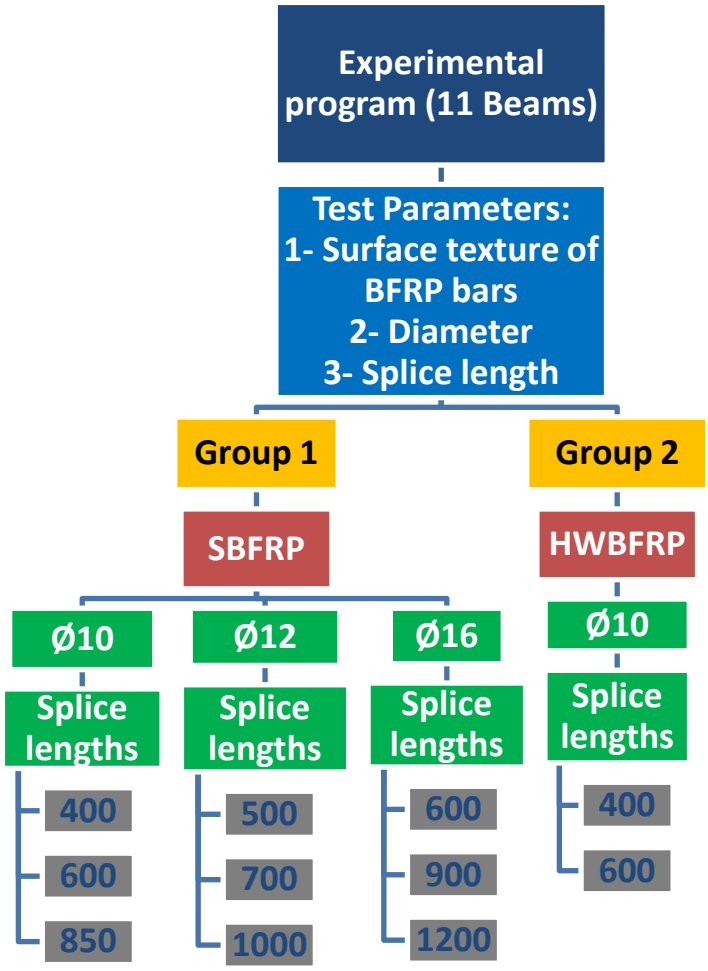

Figure 9: Flow-chart explains the methodology of the experimental program

The beams had two tension BFRP bars spliced within the constant bending moment section. Five beams were reinforced with 10 mm-diameter BFRP bars, three of them were sand coated BFRP while the other two were helically wrapped BFRP. Additionally, three beams were reinforced with 12 mm-diameter sand coated BFRP bars. Lastly, three beams were reinforced with 16 mm-diameter sand coated BFRP bars. The 11 beams were subjected to a four-point flexural test under dynamic load until rupture. A typical test took about 60-70 minutes and when some other observations were made, the test may last for 2 to 3 hours.

3.1 Test Specimens

The tested beams were categorized into two groups. Group 1 contained nine reinforced concrete beams. The beam dimensions were 300 mm X 450 mm X 3900 mm for width, depth, and length, respectively. The beams were tested under a four-point loading test. The tension reinforcement was BFRP and there were two bars spliced in each side with the region of the constant moment. The lengths for the constant moment zone, shear spans were 1700 mm and 900 mm, respectively. For the stirrups, steel reinforcement of 10 mm was used with a spacing of 150 mm in the whole beams. Two 8 mm diameter steel bars were used for compression reinforcement. Group 2 contained two reinforced concrete beams with the same exact dimensions, detailing and shear and compression reinforcement. The difference between the two groups was the surface texture of the tension reinforcement bars. Group 1 had sand coated texture while group 2 had helically wrapped outer. Figure 10 shows the details of the tested beams and their testing setup.

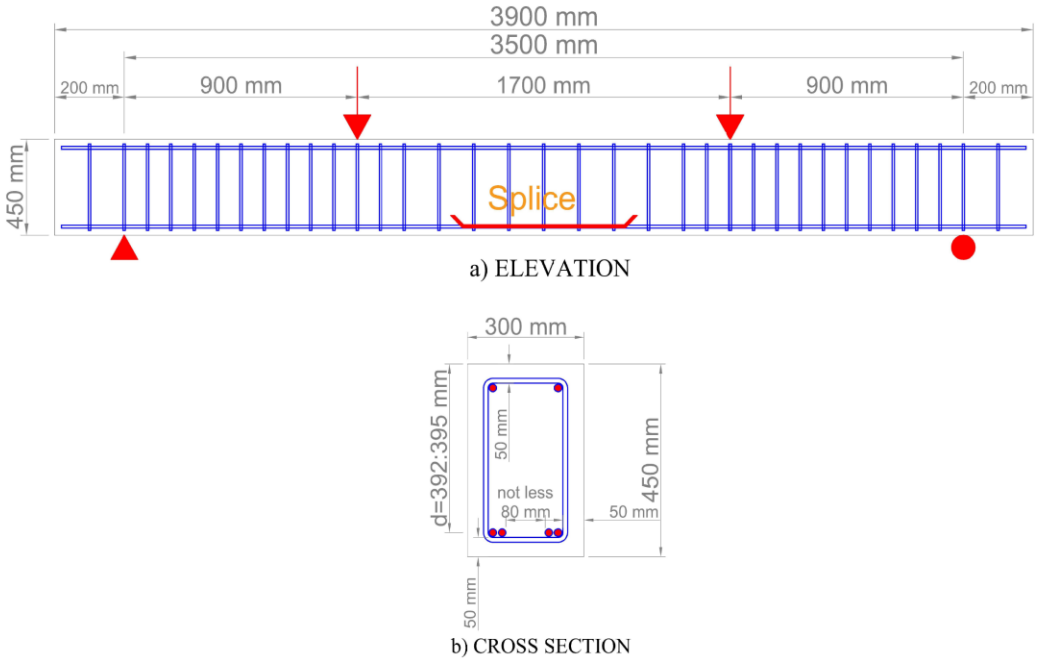

Figure 10: Cross section and information about the beams of Groups 1 and 2

The parameters investigated between the two groups were the splice length, bar outer texture, and bar size. The 10 mm diameter bars were used for 5 beams, 12 mm diameter bars were used for 3 beams and other 3 beams reinforced with 16 mm diameter bars. Amongst the 5 beams of 10 mm diameter, 3 were reinforced with sand coated BFRP with three splice lengths corresponding to 400, 600, and 850 mm while the other 2 beams were reinforced with helically wrapped BFRP with two splice lengths corresponding to 400 and 600 mm. The 3 beams of 12 mm were sand-coated with 3 splice lengths corresponding to 500, 700, and 1000 mm. The last 3 beams of 16 mm bar size were sand-coated with three splice lengths corresponding to 600, 900, and 1200 mm.

3.2 Materials Properties: FRP and Concrete

FRP bars: This research targeted the Basalt FRP reinforcing bars. The FRP bars had two different surface textures which were sand-coated and helically wrapped as shown in Figure 11 and Figure 12, respectively.

Figure 11: Sand-coated basalt FRP bars

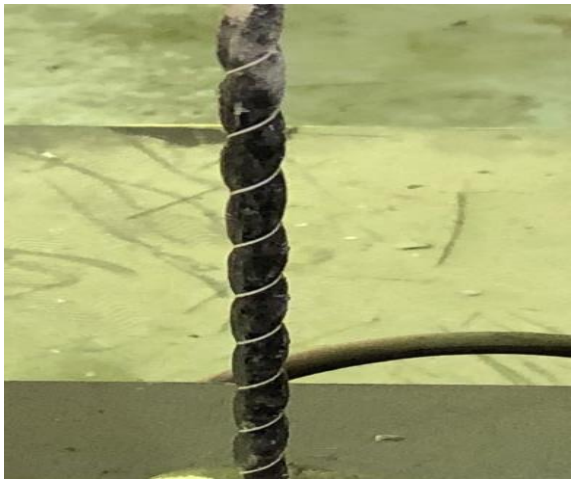

Figure 12: Helically wrapped basalt FRP bars

Three different bar diameters were used for sand-coated texture and one bar diameter for helically wrapped texture: 10, 12 and 16 mm-diameters for SBFRP bars and 10 mm-diameter for HWBFRP bars. Twenty basalt FRP bars (15 bars sand-coated of diameters:

10, 12 and 16 mm and 5 bars helically wrapped of diameter 10 mm) were subjected to tensile tests according to ASTM D7205. The obtained results are reported in the following chapter.

Table 1 provides the properties of the FRP bars used in this study. The direct tensile test results were the modulus of elasticity, and ultimate strain, and ultimate tensile strength.

Table 1: Properties of FRP bars

Type of fiber	Basalt Sand-coated	Basalt Sand-coated	Basalt Sand-coated	Basalt Helically wrapped
Nominal diameter (mm)	10	12	16	10
Nominal area (mm2)	78.54	113.1	201.06	78.54
Ultimate tensile strength (MPa)	1202.34±59.44	1177.55±164.4	1110.67±83.74	756.6±19.41
Elastic modulus (Gpa)	47.25±0.2	49.48±0.24	46.51±0.27	35.41±1.12
Ultimate strain (%)	2.14±0.08	2.55±0.13	2.38±0.34	2.39±0.19

Concrete: ready-mix high-strength concrete was used. The mix contained ordinary 40ortland cement (OPC), 20 mm and 10 mm gabbro. The target compressive strength at 28-day was 85 MPa. The concrete mix composition and concrete characteristics are given in Table 2.

Table 2: Concrete mix constituents

Water (kg/m^3)	Cement (kg/m^3)	Water-cementratio (W/C)	Sand (kg/m^3)	Gabbro 20 mm (kg/m^3)	Gabbro 10 mm (kg/m^3)
130	437	0.3	700	840	360

3.3 Concrete placement procedure and storage of beams

The plywood was used to construct the formworks with dimensions of (3900 mm length, 300 mm width and 450 mm depth). The concrete was poured in the formworks and vibrated. Standard 100 mm x 200 mm concrete cylinders were cast for mechanical testing. The beams were removed from the formworks after three days from the time of the concrete cast. The curing lasted for three weeks by covering the beams with a plastic sheet and storing them. The beams were removed from the curing seven days before testing. The beams were stored three days in the laboratory at room temperature before testing. All the beams were tested after 28 days from the time the concrete was cast. Figures 13 and 14 show typical spliced FRP bars before the concrete casting, and Figure 15 shows the casting of the concrete beams, also, Figure 16 illustrates the curing procedure for the beams.

Figure 13: Typical spliced FRP bars before casting

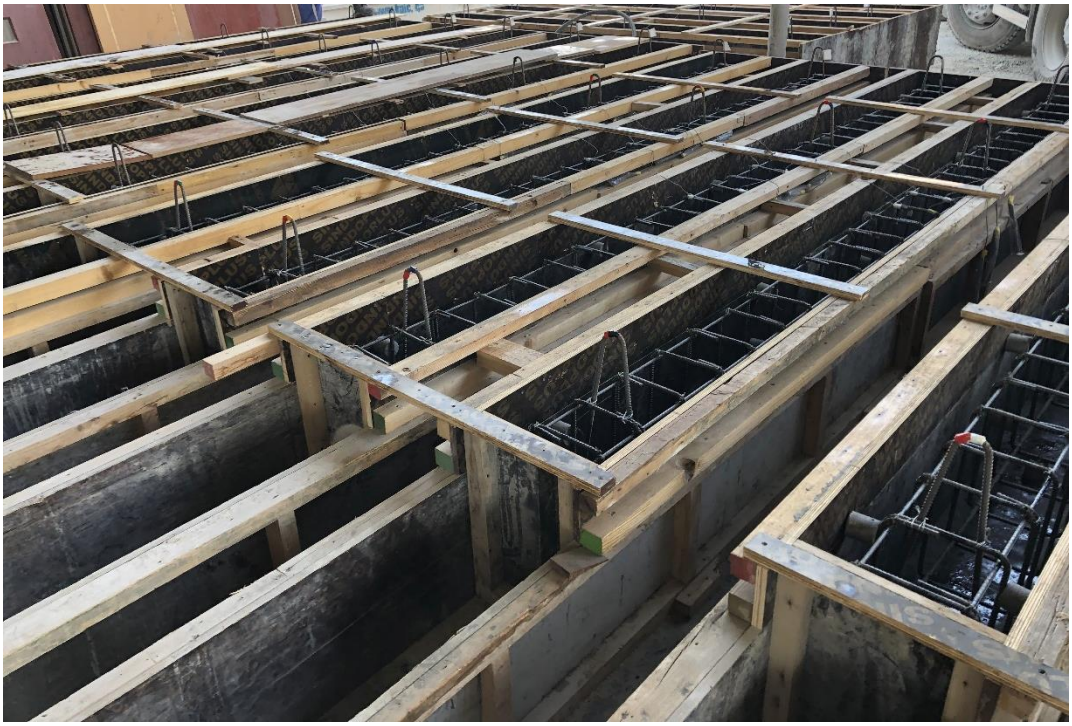

Figure 14: Spliced beams before casting

Figure 15: Casted concrete beams

Figure 16: Curing of the beams

3.4 Compressive strength

The used ready-mix concrete was tested to obtain its compressive strength. Five cylinders of 100 mm diameter and 200 mm length were casted from the same mix as the beams. The cylinders were cured by moist for 28 days. The test carried on the five cylinders was in accordance with ASTM C39 2018. The test was done in Qatar university laboratory where an automatic compression machine which has 250 kN as a maximum load capacity was used. Figure 17 shows the test setup, as can be seen the cylinders had cappers from top and bottom to ensure that the cylinders are centered in order to avoid any eccentric loading and to smoothen the surface. The calculation of the strength was done by dividing the maximum reached load by the cylinder before failure over the area of the cylinder. The average of the 5 compressive strengths of the cylinder is the compressive strength of the concrete mix.

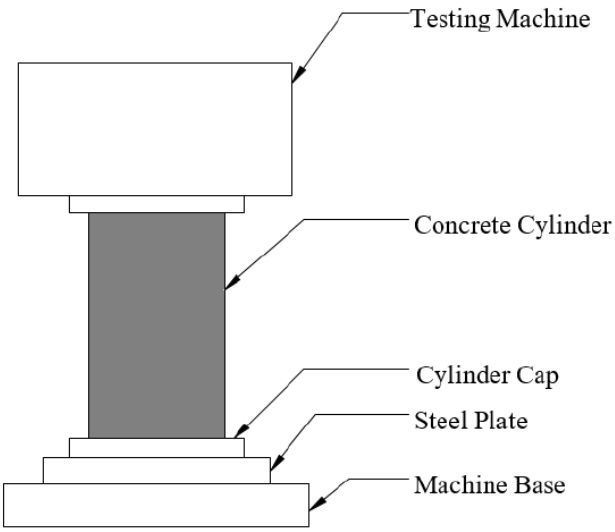

Figure 17: Setup for cylinder compression test

3.5 Flexural tensile strength (modulus of rapture)

To obtain the tensile strength of the concrete, three prisms were casted from the same mix which was used for the beams. The prisms had dimensions of 100 mm by 100 mm by 500 mm for width, depth and length. The prisms were tested in accordance with ASTM C78 2018. Figure 18 show the test set up. The flexural testing machine had a hydraulic jack and it was attached to a steel frame. The load was transferred using two loading cylinders (point loads). The distance from each point load to its nearest support was 100 mm. Also, the distance from one-point load to the other point load was 100 mm.

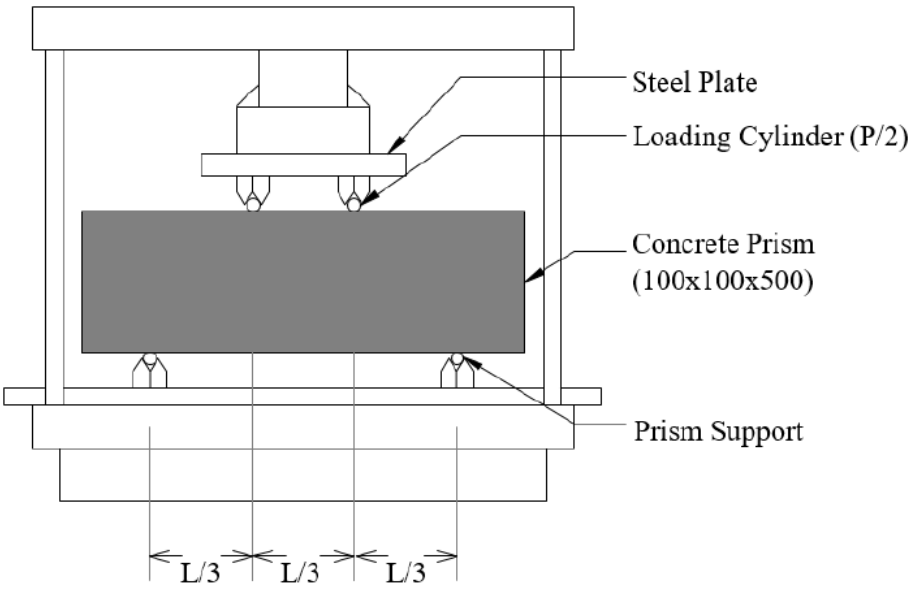

Figure 18: Tensile strength test setup

3.6 Test for beams procedure and Instrumentation

The tests were carried out at Qatar University structural laboratory. The load, deflection and strain in FRP bar and concrete data was gathered by automatic acquisition system. TML strain gauges were used to obtain the strain in basalt FRP bars and in concrete. For the FRP the gauges type was BFLA-5-8 while for the concrete the type was PL-60-11. For the former the gauges were installed along the splice in different locations as shown in Figures 20 and 22, and for the later the gauges were installed at three locations and they are two and both ends of the splice and at the middle of the beam at the top surface. The deflection was measure at one location which is the middle of the beam where the max deflection occurs in a simply supported beam, it was measured using linear variable differential transformers (LVDT), and two of them were used on the two sides of the beam. The beams were tested in four-points load testing setup as shown in Fig. 19. The data were collected using a data acquisition system from TML as depicted in Figure 21. Typical instrumented beam is shown in Figure 22. Details of all specimens of Groups 1 and 2 are given in Tables 3 and 4, respectively.

Figure 19: Test set up of all specimens

Figure 20: Installation of strain gauges

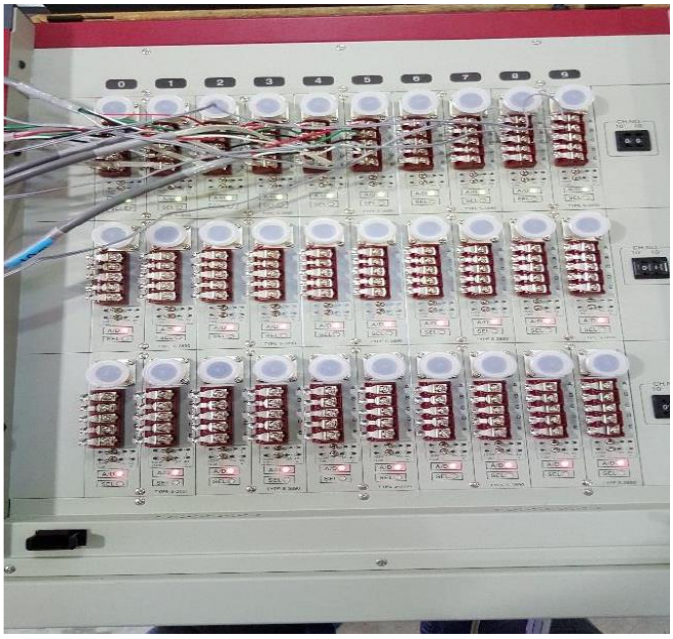

Figure 21: Data logger

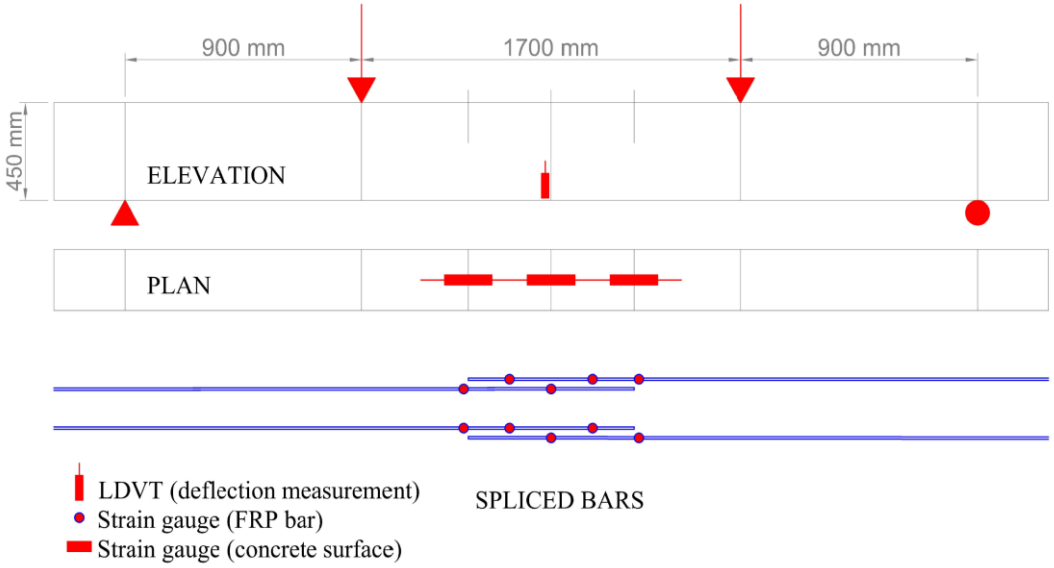

Figure 22: Details of the instrumented specimens

Table 3: Details of specimens of group 1

Identification	Type of bar	Bar diameter (mm)	Splice length (mm)	Width (mm)	Depth (mm)	Height (mm)	Total length (mm)
SBFRP-10-400	Sand-coated basalt FRP	10	400	300	395	450	3900
SBFRP-10-600			600				
SBFRP-10-850			850				
SBFRP-12-500	Sand-coated basalt FRP	12	500	300	394	450	
SBFRP-12-700			700				
SBFRP-12-1000			1000				
SBFRP-16-600	Sand-coated basalt FRP	16	600	300	392	450	
SBFRP-16-900			900				
SBFRP-16-1200			1200				

Table 4: Details of specimens of group 2

Identification	Type of bar	Bar diameter (mm)	Splice length (mm)	Width (mm)	Depth (mm)	Height (mm)	Total length (mm)
HWBFRP-10-400	Helically wrapped basalt FRP	10	400	300	395	450	3900
HWBFRP-10-600			600				

Specimen label: 1st letter S stands for sand-coated while HW for helically wrapped, 1st number = bar diameter, 2nd number = splice length.

As example: (HWBFRP-10-600) means the used bars are helically wrapped basalt FRP with a diameter of 10 mm and splice length = 600 mm.

CHAPTER 4: RESULTS AND DISCUSSION

4.1 Introduction

The eleven beams reinforced with basalt FRP bars were tested to obtain the critical splice length and the bond behavior. The outcomes of the experimental testing were expressed in the strain in both the basalt FRP bars and the concrete, the maximum load capacity, failure modes, prediction of critical splice length, and the corresponding bond strength. Additionally, the research presented herein evaluates the existing recommendations (CSA-S6-14, CSA-S806-12, and ACI440-1R-15) for spliced FRP bars.

4.2 Concrete's compressive strength results

Three concrete cylinders for the concrete mixture as shown in Figure 23 were tested after 28 days. The test complied with ASTM C39-2018 standards. The average of three concrete cylinders is the average compressive strength. The results are shown in Table 5.

(1) Before (2) After

Figure 23: Before and after testing the cylinder specimen

Table 5: Compressive strength result

Cylinders	Compressive strength (MPa)
C1	83.37
C2	85.12
C3	85.31
Mean Compressive strength (MPa)	84.6 ≈ 85

4.3 Results of Flexural tensile strength testing (modulus of rapture)

Three concrete prisms for the concrete mixture as shown in Figure 24 were tested in a four-point loading test after 28 days to obtain the tensile strength, the average of the flexural tensile strength of the three prisms is the average flexural strength of the mixture. The test followed the guidance of ASTM C78-2018. The test results are stated in Table 6.

(1) Before (2) After

Figure 24: Failure mode of typical concrete prism

Table 6: Tensile strength result

Prisms	Tensile strength (MPa)
P1	7.01
P2	7.24
P3	7.88
Mean Tensile strength (MPa)	7.38 ≈ 7.4

4.4 Tensile test for FRP bars

Tensile test specimen preparation and procedure of their testing followed the ACI Committee 440.R-15 and ASTM D7205. Twenty specimens were prepared for testing. One type of FRP bars which is basalt FRP with two different surface textures, sand-coated and helically wrapped. Three diameters were used for sand-coated bars while one bar diameter tested for helically wrapped. The length of each specimen was determined and was cut based on it, and all the specimens were anchored at both ends. The anchoring section was filled with a high-performance resin grout and it was a steel sleeve. Figure 25 shows the proper length for each type, the length depends on the diameter of the bar. The tested bar length equaled the summation of two anchoring section lengths and the testing section length. The specimen total length was 120 times the basalt FRP bar diameter. Five specimens were tested for each diameter from each surface texture of FRP bars.

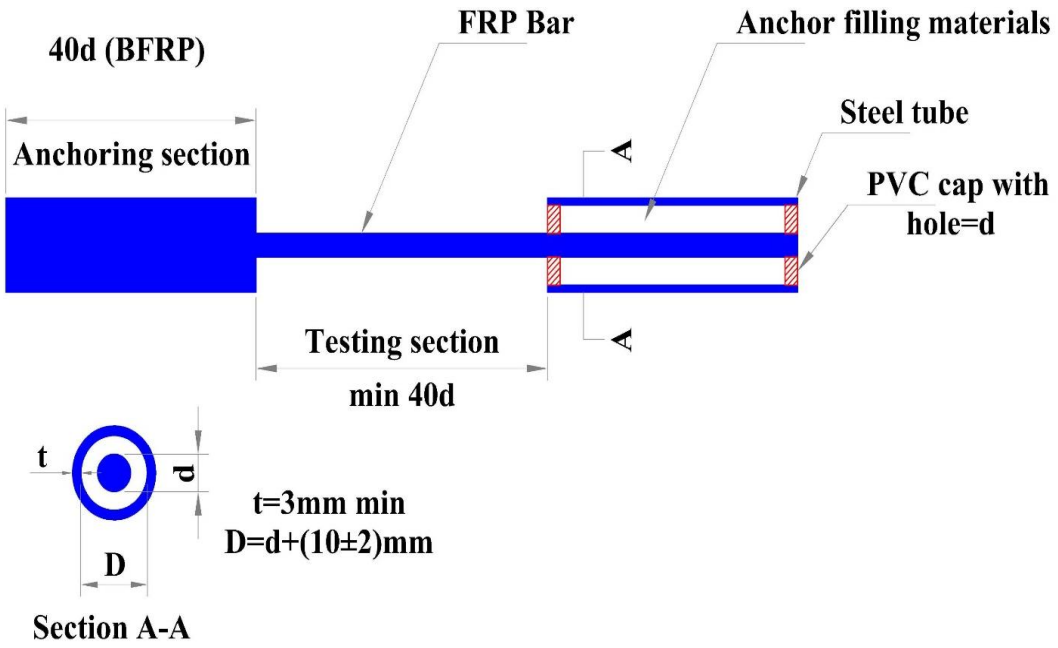

Figure 25: Sketch for tensile test specimens of basalt bars

Tensile tests were carried out using standard universal testing machine. The rate of loading was approximately 1 mm/min. Figures 26 and 27 show the setup of tensile test for sand-coated and helically wrapper bars, respectively. An LVDT with a gauge length of 200 mm and strain gauges to measure the longitudinal and transverse deformations of the specimen were used. The test was continued until failure occurred. A computer with acquisition data system was used to monitor LVDT and strain in FRP bars. The LVDT was removed when the load reached 75% of the predicted maximum load, in order to avoid damaging it.

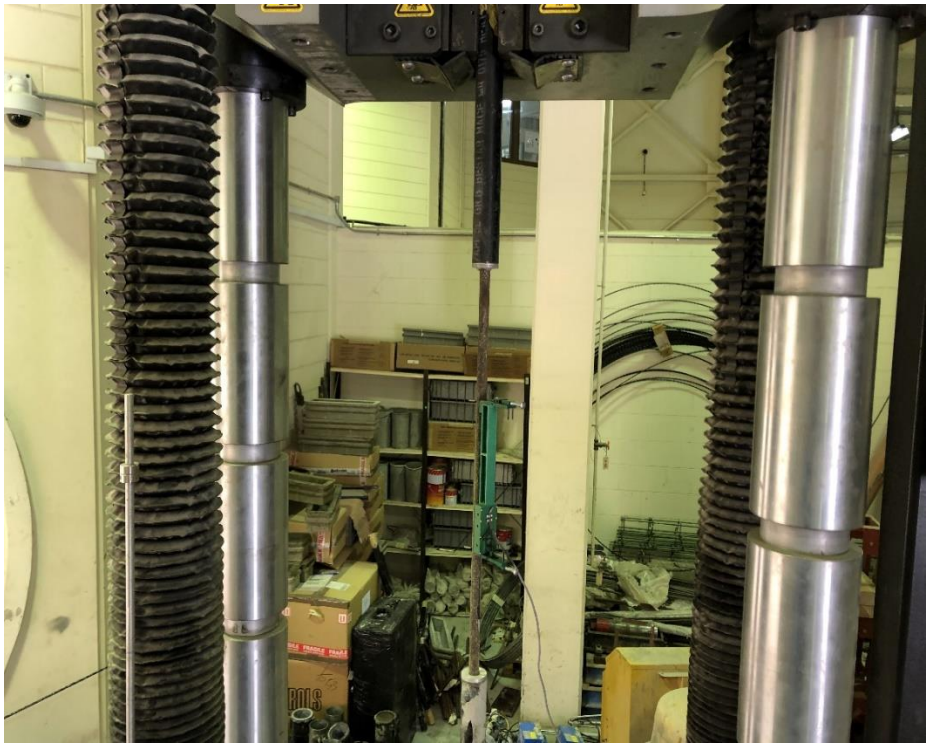

Figure 26: Tensile test setup of sand-coated BFRP bars

Figure 27: Tensile test setup of helically wrapped BFRP bars

Tensile test results:

The modes of FRP bars failure are shown in Figures 28 and 29.

Figure 28: Failure of sand-coated BFRP

Figure 29: Failure of helically wrapped BFRP

The calculations of the tensile strength are done according to this equation:

$$f_u = \frac{F_u}{A_b} \tag{10}$$

Where:

$f_u = ultimate\ tensile\ strength\ (MPa)$

$F_u = ultimate\ tensile\ capacity\ (N)$

$A_b = nominal\ cross\ section\ of\ the\ tested\ bar\ (mm^2)$

The difference between the stress-strain curve values at 25% and 50% of the tensile capacity was used to calculate the modulus of elasticity (as instructed in ASTM D7205) as shown in the equation below:

$$E = \frac{\Delta F}{\Delta \varepsilon * A_b} = \alpha * \frac{l}{A_b} \quad (11)$$

Where:

$E = modulus\ of\ elasticity\ (MPa)$

$\Delta F = difference\ between\ the\ loads\ at\ 25\%\ and\ 50\%\ of\ the\ ultimate\ tensile\ capaity\ (N)$

$\Delta \varepsilon = difference\ between\ the\ strains\ at\ 25\%\ and\ 50\%\ of\ the\ ultimate\ strain\ capacity$

$\alpha = slope\ of\ the\ load\ displacement\ curve\ between\ 25\%\ and\ 50\%\ of\ the\ ultimate\ tensile\ capacity\ (N/mm)$

$l = original\ gauge\ length\ (mm)$

To calculate the ultimate strain the equation below was used:

$$\varepsilon_u = \frac{F_u}{E * A_b} \quad (12)$$

Where:

$\varepsilon_u = ultimate\ strain.\ All\ the\ rustles\ of\ tensile\ tests\ of\ twenty\ specimens\ (five\ specimens\ for\ each\ diameter)\ with\ FRP\ bars\ are\ shown\ in\ Table\ 7.$

Table 7: Tensile test results of FRP bars

Type of fiber	Basalt Sand-coated	Basalt Sand-coated	Basalt Sand-coated	Basalt Helically wrapped
Nominal diameter (mm)	10	12	16	10
Nominal-area (mm^2)	78.54	113.1	201.06	78.54
Ultimate tensile strength (MPa)	1202.34±59.44	1177.55±164.4	1110.67±83.74	756.6±19.41
Elastic modulus (GPa)	47.25±0.2	49.48±0.24	46.51±0.27	35.41±1.12
Ultimate strain (%)	2.14±0.08	2.55±0.13	2.38±0.34	2.39±0.19

4.5 Large scale beams testing results

4.5.1 Strains in FRP bars and concrete

4.5.1.1 Beam 1 (SBFRP-10-400)

Beam specimen 1 (SBFRP-10-400) has bottom reinforcement of 10 mm diameter sand-coated basalt FRP which has a lap splice of 400 mm. The specimen was tested in flexure as shown in Figure 30. The initial crack occurred at a load of 89 kN within the constant moment region near the middle of the beam after the static load been applied gradually. More flexural cracks spread along the beams. All of the cracks were vertical ones and were initiated at the bottom and moved upward, at the same time the deflection of the beam was becoming more visible. With the increment of the applied load, the concrete split in the tension zone and beam 1 failed as illustrated in Figure 31.

Figure 32 indicates to the measured strains along spliced FRP bars versus applied load. The strain values were very low at the beginning till the first crack occurred then a

massive increase in the strain values took place which indicates that upon the occurrence of the initial crack the load was transferred rapidly to the bar. The beam failed at a maximum load of 144.675 kN and a maximum strain at the end of the splice of 16395.21 με.

Figure 33 depicts the strain of the concrete at the top surface (compression zone) against the applied load.

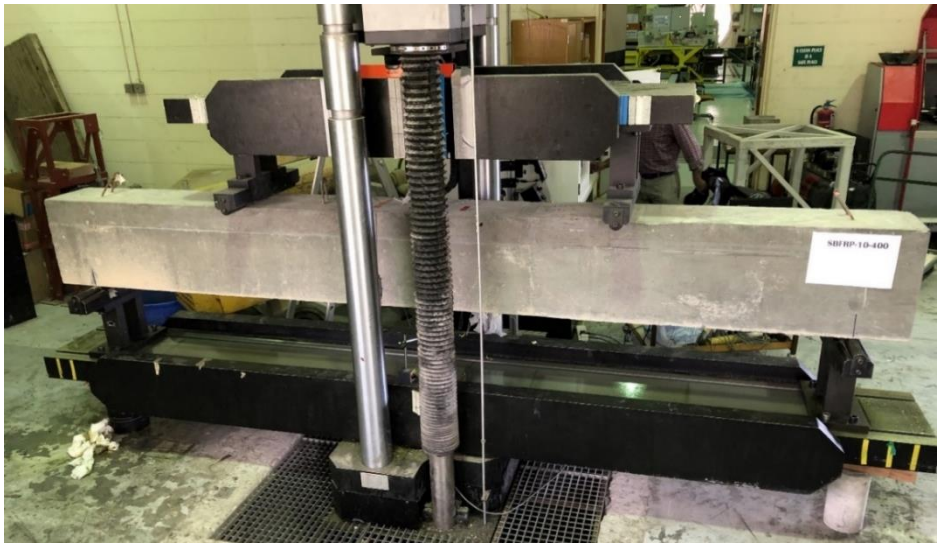

Figure 30: Beam 1 (SBFRP-10-400) testing setup

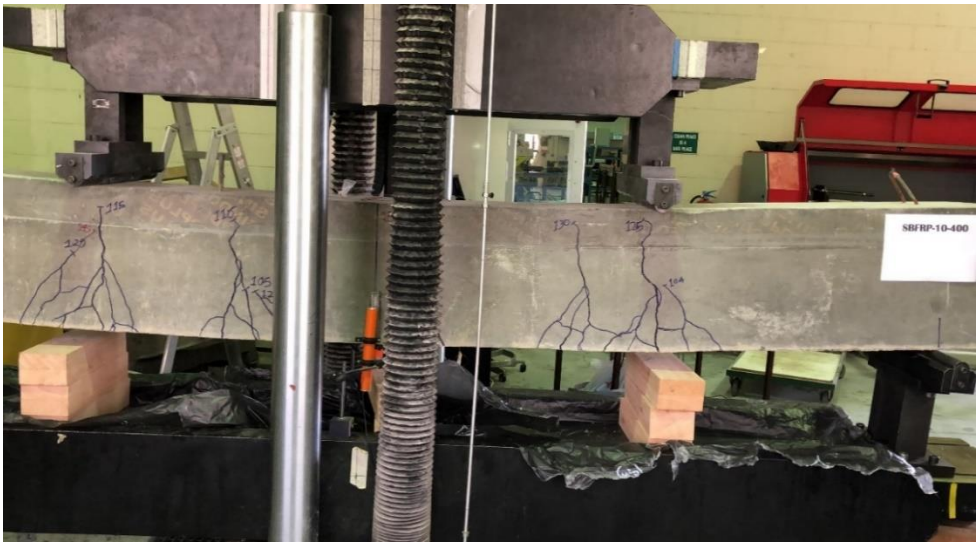

Figure 31: Cracking pattern of beam 1 (SBFRP-10-400)

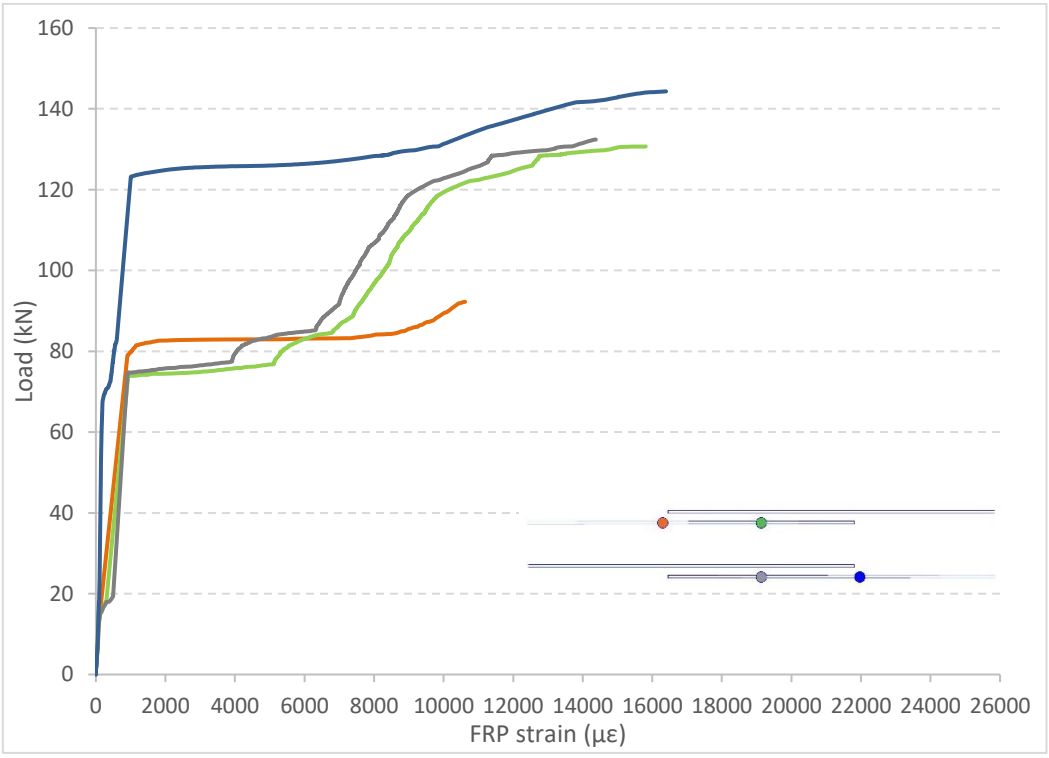

Figure 32: Variation of FRP strains of beam 1 with load along the SBFRP splice

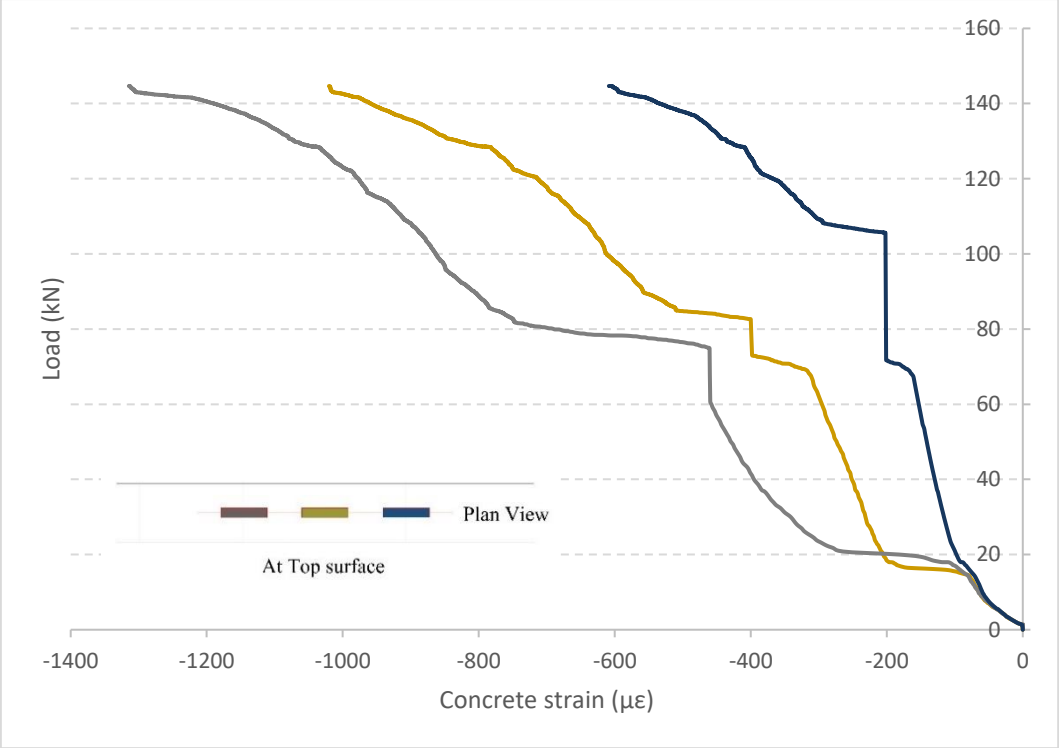

Figure 33: Concrete strains versus load in compression zone of beam 1 at the top surface of the beam

4.5.1.2 Beam 2 (SBFRP-10-600)

Beam specimen 2 (SBFRP-10-600) reinforced with 10 mm diameter sand-coated basalt FRP which has a lap splice of 400 mm. The specimen was tested in flexure as shown in Figure 34. The initial crack occurred at a load of 59 kN within the constant moment region near the right applied point load on the beam after the static load been applied gradually. More flexural cracks spread along the beams. All of the cracks were vertical ones and were initiated at the bottom and moved upward, at the same time the deflection of the beam was becoming more visible. With the increment of the applied load, the concrete split in the tension zone and beam 2 failed as illustrated in Figure 35.

Figure 36 indicates the measured strains along spliced FRP bars versus applied load. The strain values were very low at the beginning till the first crack occurred then a

massive increase in the strain values took place which indicates that upon the occurrence of the initial crack the load was transferred rapidly to the bar. The beam failed at a maximum load of 149.504 kN and a maximum strain at the end of the splice of 20924.4 με.

Figure 37 depicts the strain of the concrete at the top surface (compression zone) against the applied load, the concrete strain at the location of the end of the splice was higher than the middle and this happened because the cracks initiated at the location of the splice end and were much wider than the cracks at the middle as can be seen in Figure 35.

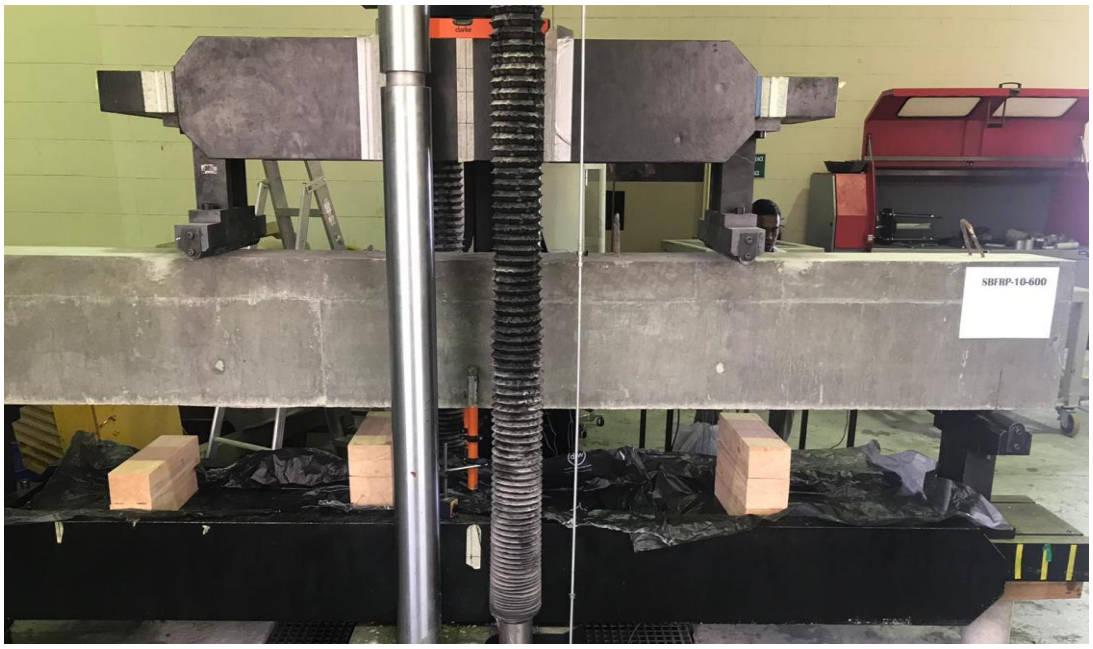

Figure 34: Beam 2 (SBFRP-10-600) testing setup

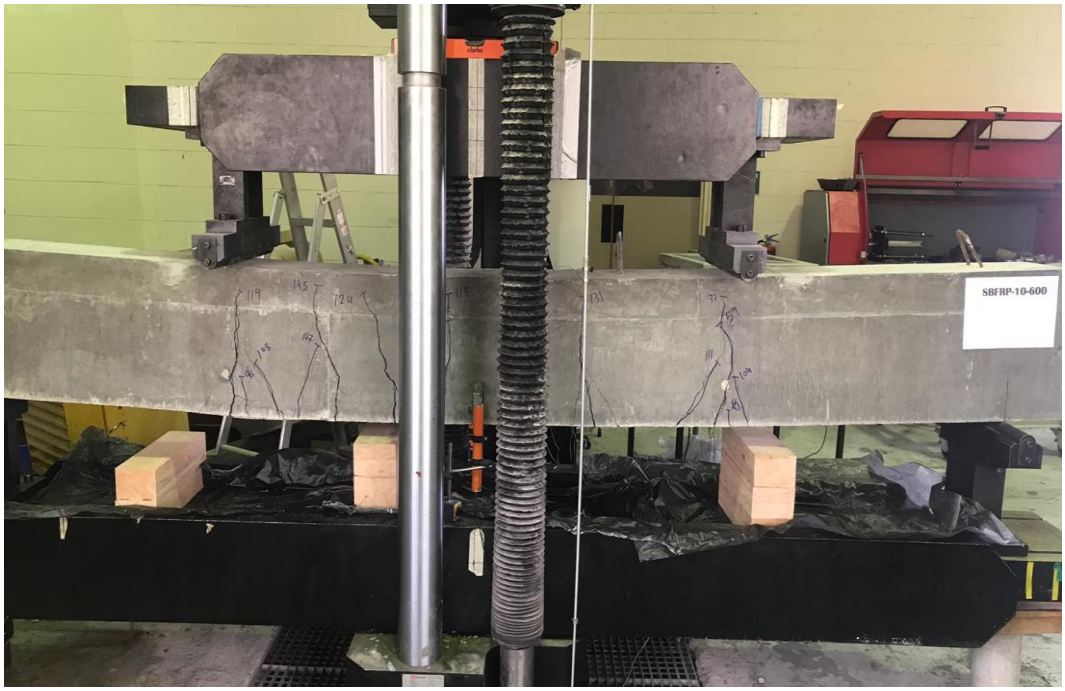

Figure 35: Cracking pattern of beam 2 (SBFRP-10-600)

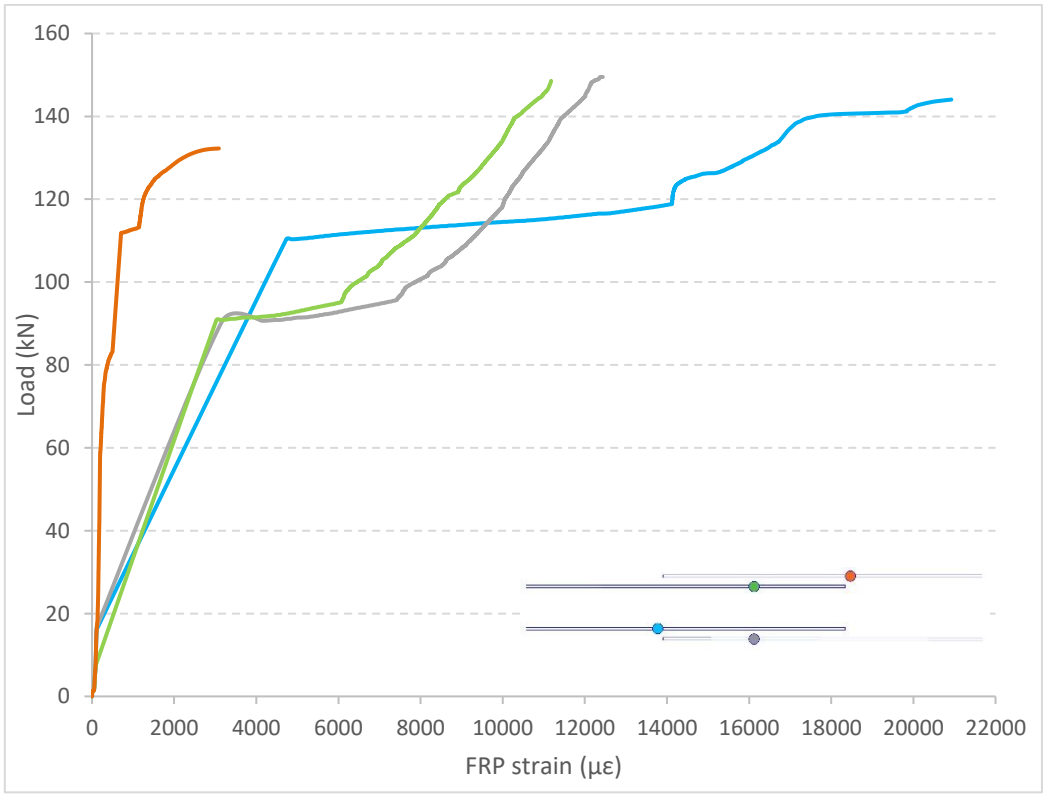

Figure 36: Variation of FRP strains of beam 2 with load along the SBFRP splice

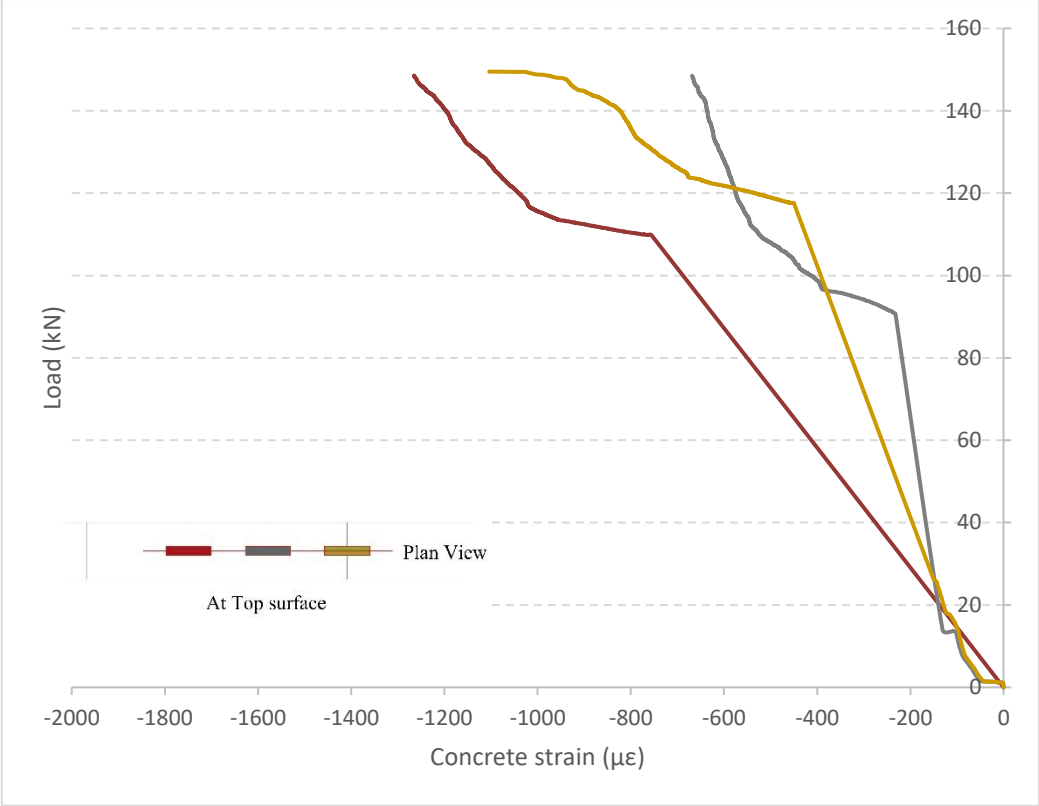

Figure 37: Concrete strains versus load in compression zone of beam 2

4.5.1.3 Beam 3 (SBFRP-10-850)

Beam specimen 3 (SBFRP-10-850) reinforced with 10 mm diameter sand-coated basalt FRP which has a lap splice of 850 mm. The specimen was tested in flexure as shown in Figure 38. The initial crack occurred at a load of 87 kN within the constant moment region near the right applied point load on the beam after the static load been applied gradually. More flexural cracks spread along the beams. All of the cracks were vertical ones and were initiated at the bottom and moved upward, at the same time the deflection of the beam was becoming more visible. With the increment of the applied load, the FRP bars have ruptured in the tension zone and beam 3 failed as illustrated in Figure 39.

Figure 40 indicates the measured strains along spliced FRP bars versus applied load.

The strain values were very low at the beginning till the first crack occurred then a massive increase in the strain values took place which indicates that upon the occurrence of the initial crack the load was transferred rapidly to the bar. The beam failed at a maximum load of 170.592 kN and a maximum strain at the end of the splice of 21353.11 με.

Figure 41 depicts the strain of the concrete at the top surface (compression zone) against the applied load.

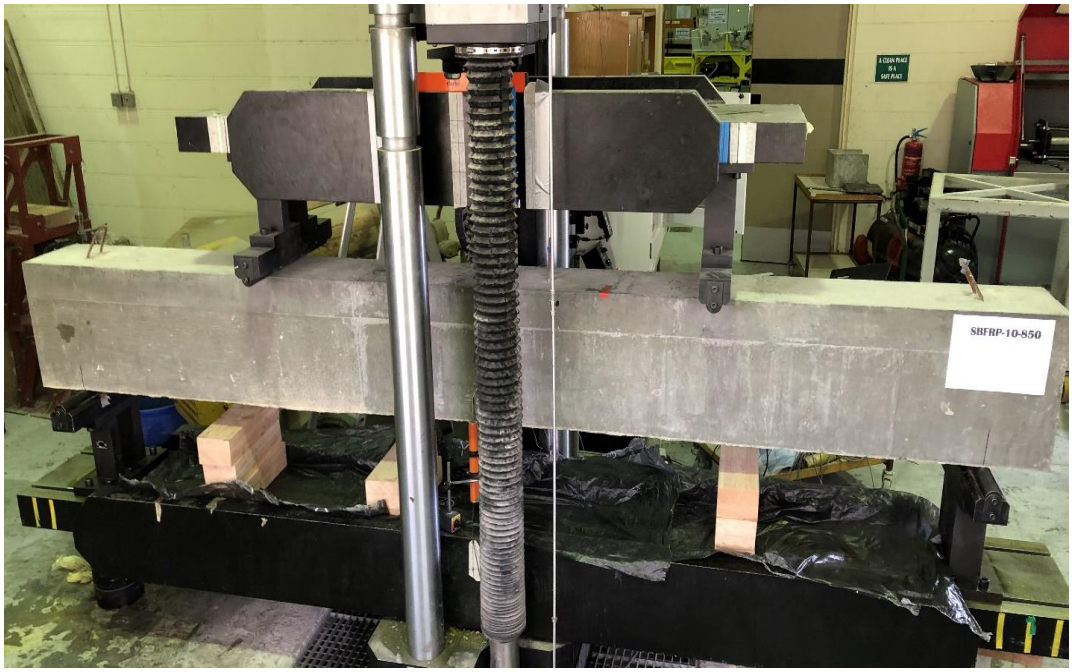

Figure 38: Beam 3 (SBFRP-10-850) testing setup

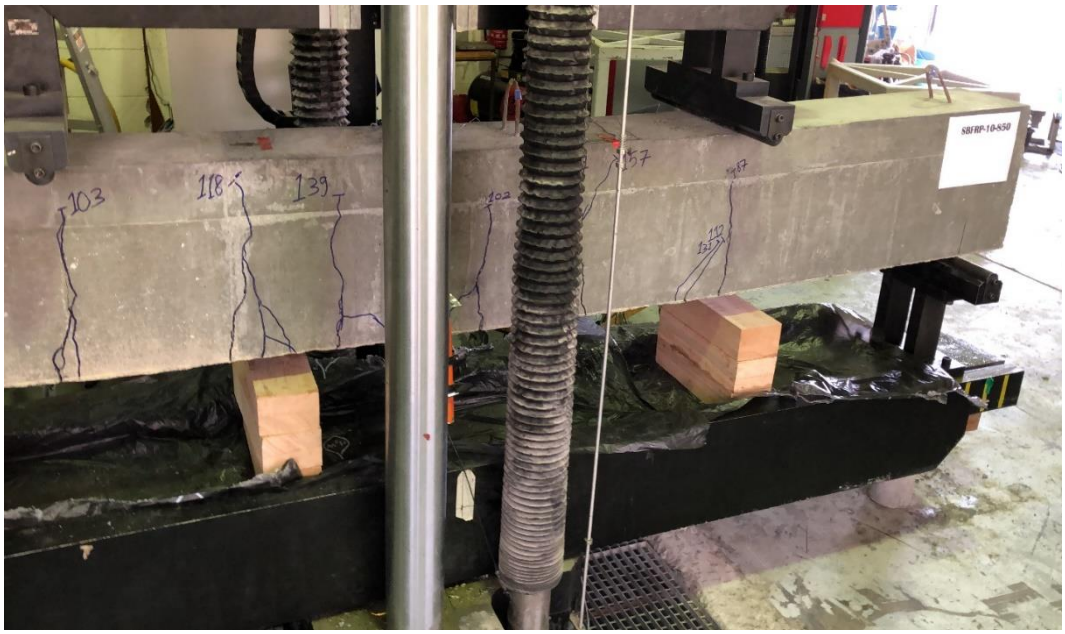

Figure 39: Cracking pattern of beam 3 (SBFRP-10-850)

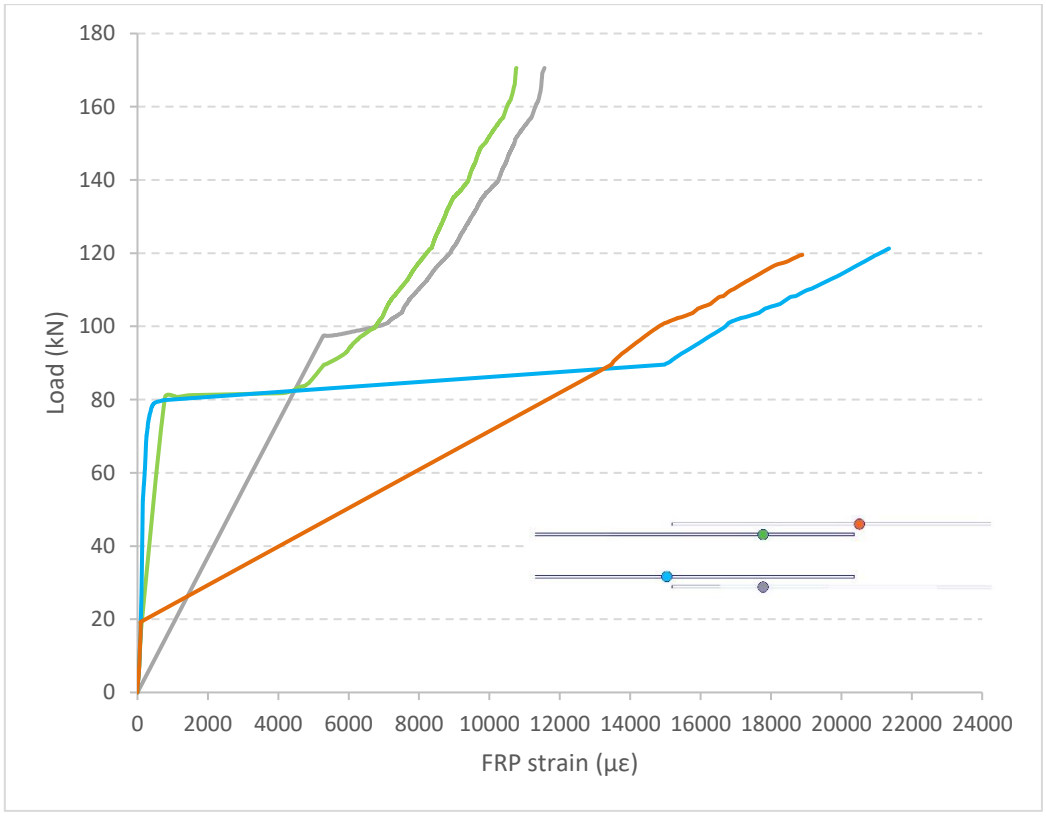

Figure 40: Variation of FRP strains of beam 3 with load along the SBFRP splice

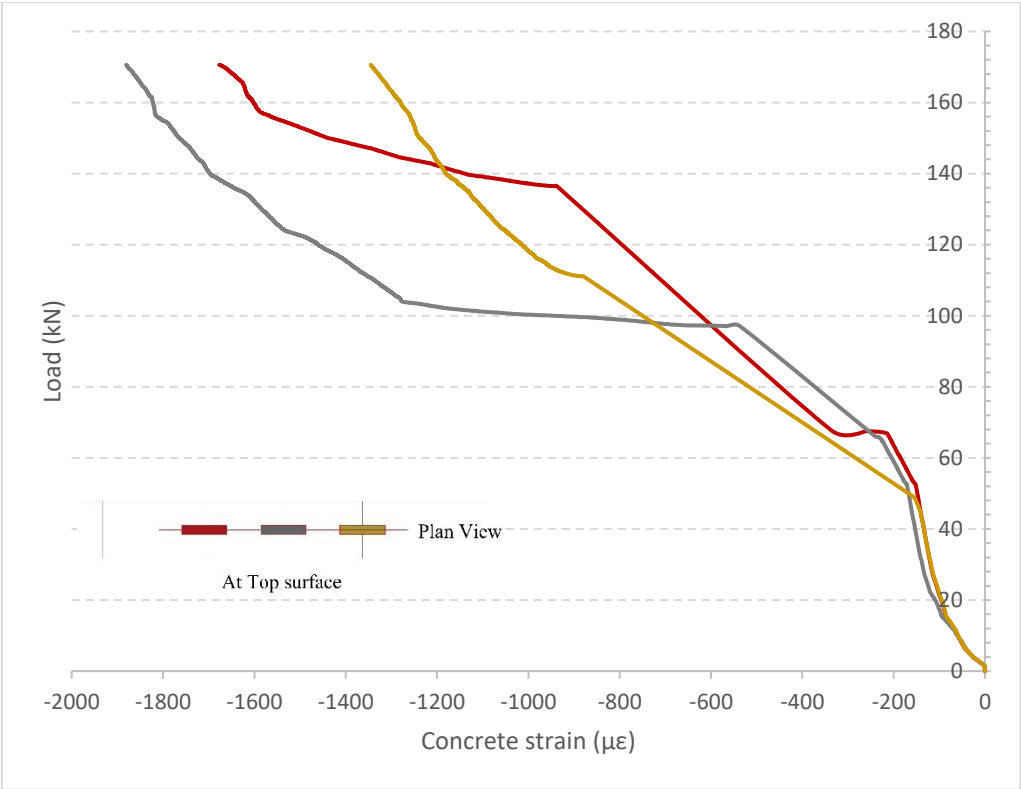

Figure 41: Concrete strains versus load in compression zone of beam 3

4.5.1.4 Beam 4 (SBFRP-12-500)

Beam specimen 4 (SBFRP-12-500) reinforced with 12 mm diameter sand-coated basalt FRP which has a lap splice of 500 mm. The specimen was tested in flexure as shown in Figure 42. The initial crack occurred at a load of 137 kN within the constant moment region near the right applied point load on the beam after the static load been applied gradually. More flexural cracks spread along the beams. All of the cracks were vertical ones and were initiated at the bottom and moved upward, at the same time the deflection of the beam was becoming more visible. With the increment of the applied load, the concrete split in the tension zone which unveiled the FRP bars and made the overlap visible and beam 4 failed as illustrated in Figure 43.

Figure 44 indicates the measured strains along spliced FRP bars versus applied load. The strain values were very low at the beginning till the first crack occurred then a

massive increase in the strain values took place which indicates that upon the occurrence of the initial crack the load was transferred rapidly to the bar. The beam failed at a maximum load of 220.63 kN and a maximum strain at the end of the splice of 16585.65 με.

Figure 45 depicts the strain of the concrete at the top surface (compression zone) against the applied load.

Figure 42: Beam 4 (SBFRP-12-500) testing setup

Figure 43: Cracking pattern of beam 4 (SBFRP-12-500)

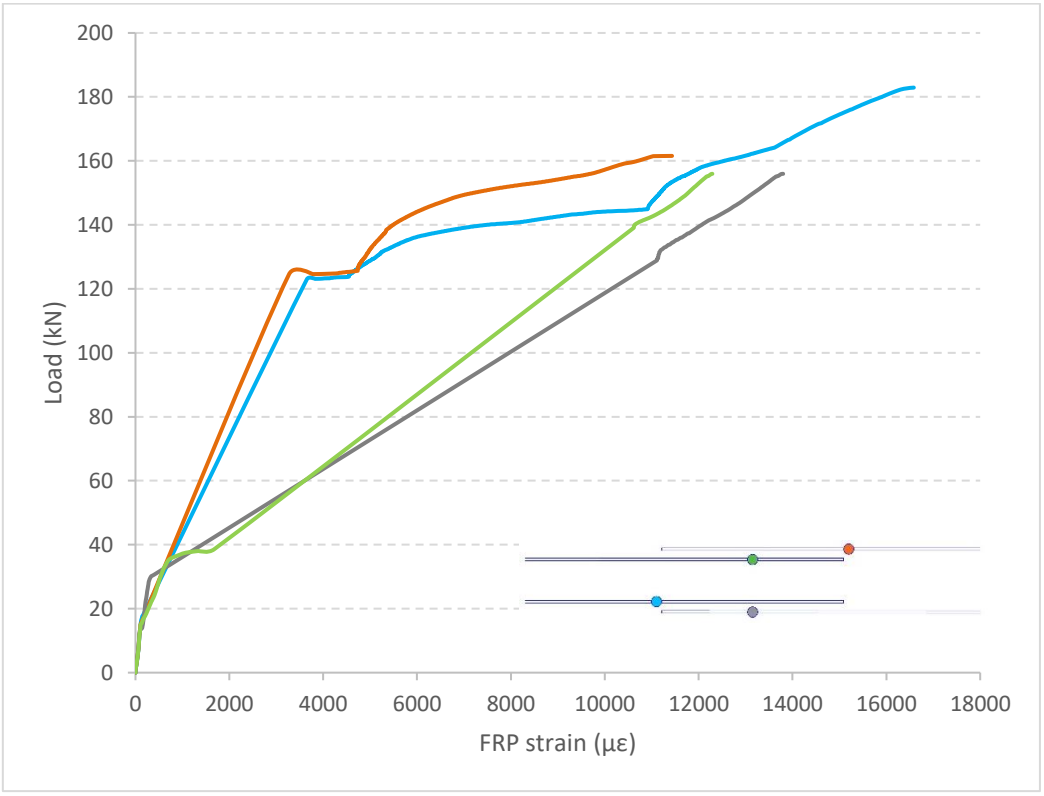

Figure 44: Variation of FRP strains of beam 4 with load along the SBFRP splice

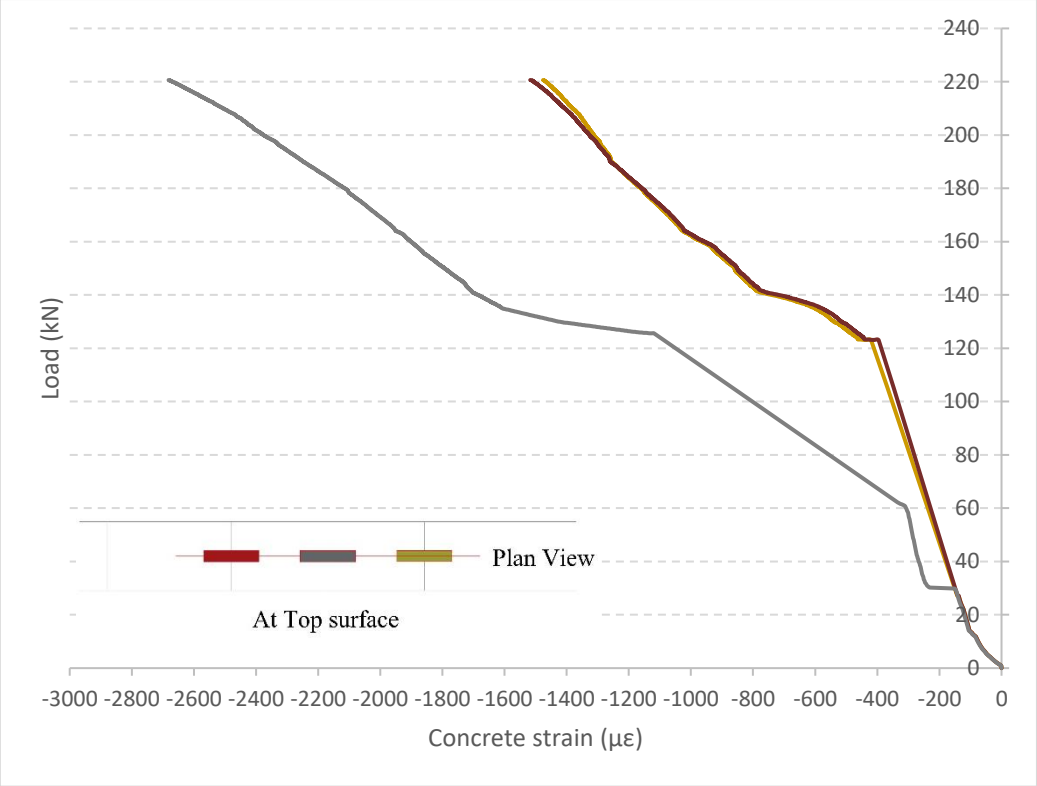

Figure 45: Concrete strains versus load in compression zone of beam 4

4.5.1.5 Beam 5 (SBFRP-12-700)

Beam specimen 5 (SBFRP-12-700) reinforced with 12 mm diameter sand-coated basalt FRP which has a lap splice of 700 mm. The specimen was tested in flexure as shown in Figure 46. The initial crack occurred at a load of 138 kN within the constant moment region near the right applied point load on the beam after the static load been applied gradually. More flexural cracks spread along the beams. All of the cracks were vertical ones and were initiated at the bottom and moved upward, at the same time the deflection of the beam was becoming more visible. With the increment of the applied load, the FRP bars have ruptured in the tension zone and beam 5 failed as illustrated in Figure 47.

Figure 48 indicates the measured strains along spliced FRP bars versus applied load.

The strain values were very low at the beginning till the first crack occurred then a massive increase in the strain values took place which indicates that upon the occurrence of the initial crack the load was transferred rapidly to the bar. The beam failed at a maximum load of 258.529 kN and a maximum strain at the end of the splice of 23807.66 με.

Figure 49 depicts the strain of the concrete at the top surface (compression zone) against the applied load.

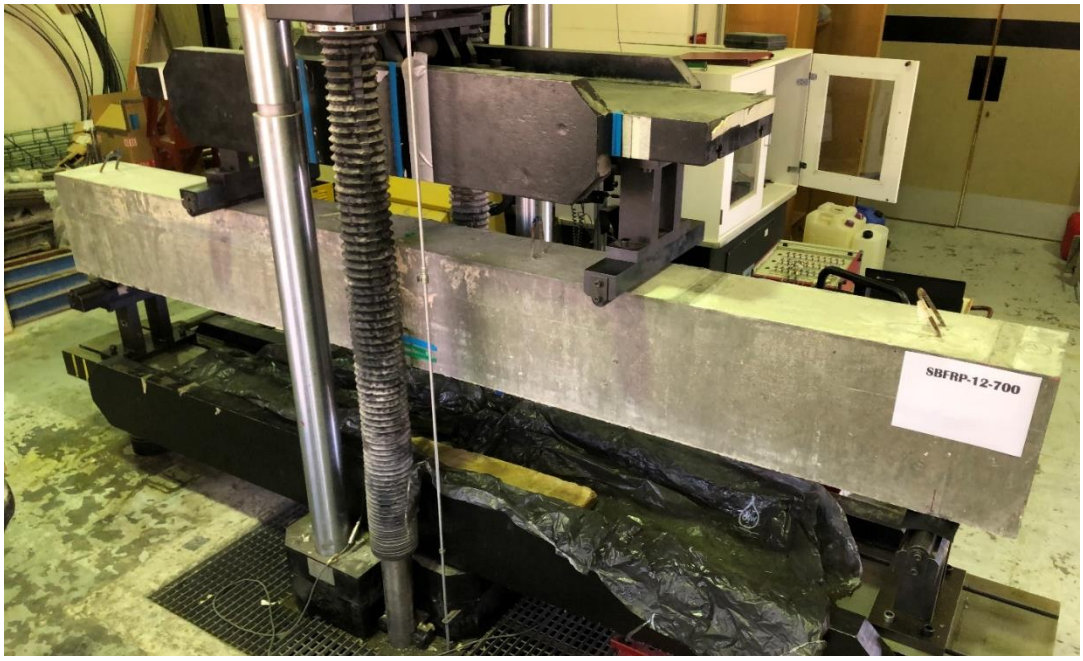

Figure 46: Beam 5 (SBFRP-12-700) testing setup

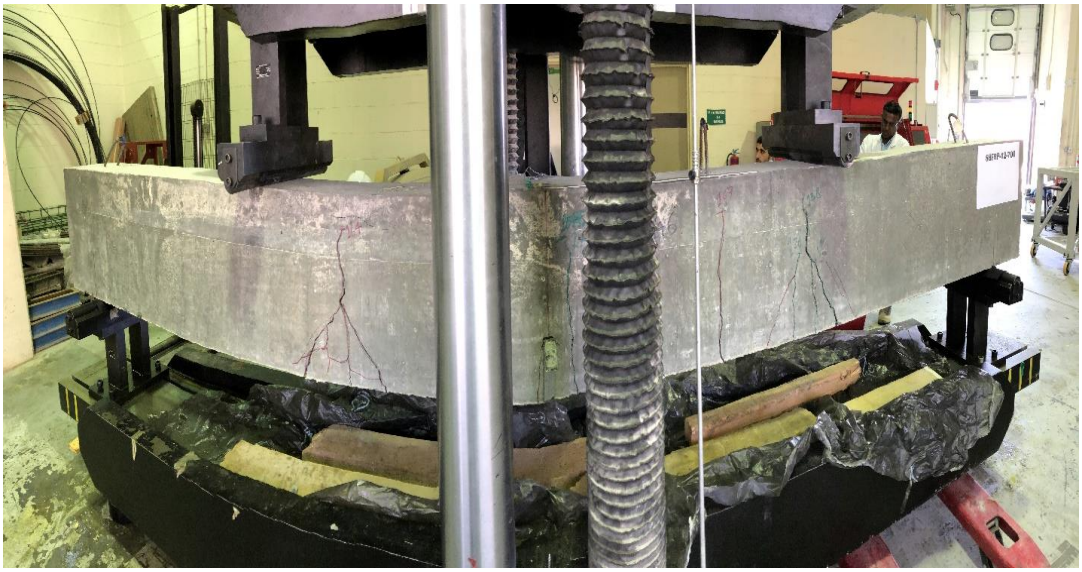

Figure 47: Cracking pattern of beam 5 (SBFRP-12-700)

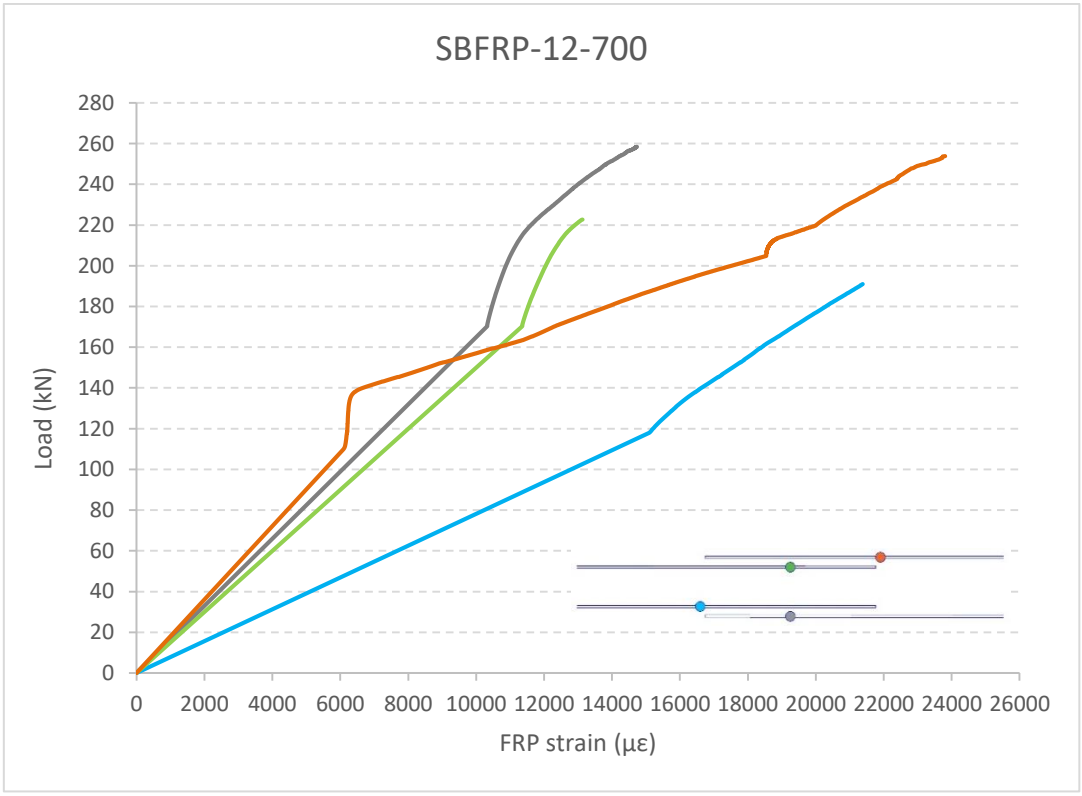

Figure 48: Variation of FRP strains of beam 5 with load along the SBFRP splice

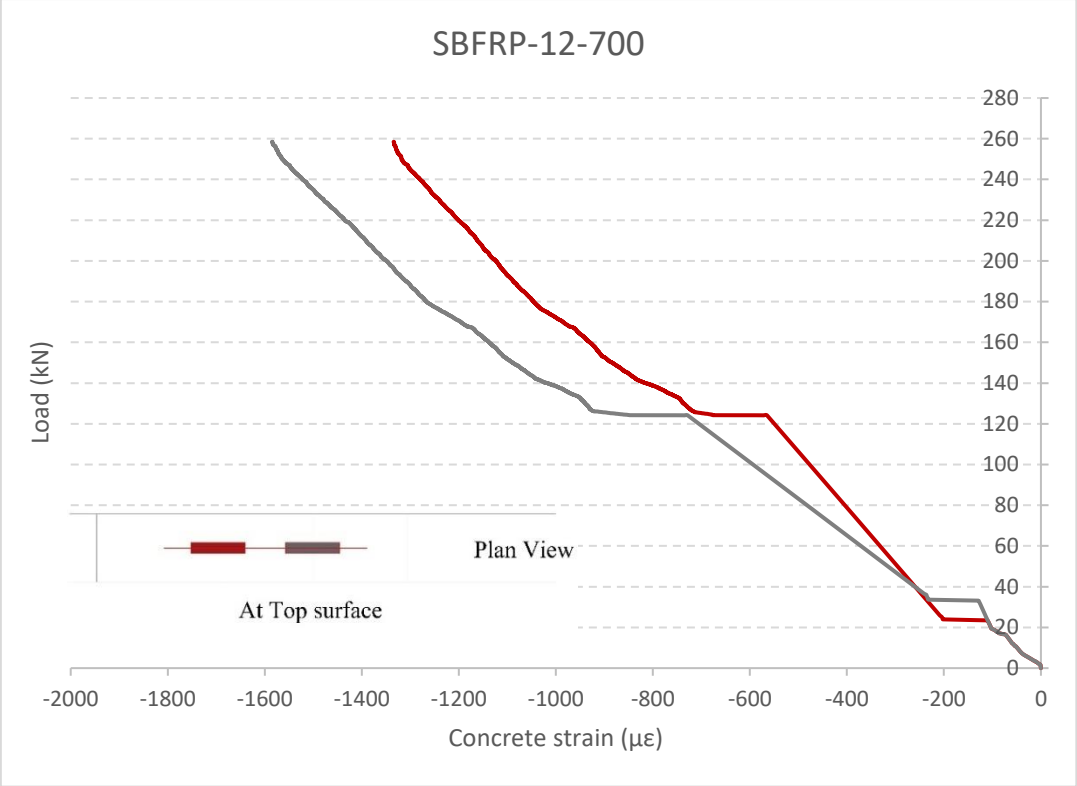

Figure 49: Concrete strains versus load in compression zone of beam 5

4.5.1.6 Beam 6 (SBFRP-12-1000)

Beam specimen 6 (SBFRP-12-1000) reinforced with 12 mm diameter sand-coated basalt FRP which has a lap splice of 1000 mm. The specimen was tested in flexure as shown in Figure 50. The initial crack occurred at a load of 102 kN within the constant moment region near the right applied point load on the beam after the static load been applied gradually. More flexural cracks spread along the beams. All of the cracks were vertical ones and were initiated at the bottom and moved upward, at the same time the deflection of the beam was becoming more visible. With the increment of the applied load, the FRP bars have ruptured in the tension zone and beam 6 failed as illustrated in Figure 51.

Figure 52 indicates the measured strains along spliced FRP bars versus applied load. The strain values were very low at the beginning till the first crack occurred then a

massive increase in the strain values took place which indicates that upon the occurrence of the initial crack the load was transferred rapidly to the bar. The beam failed at a maximum load of 187.93 kN and a maximum strain at the end of the splice of 23316.75 με. The maximum load of this beam is less than the maximum load of beams 4 and 5 which have shorter splice length, this happened because we had a technical issue with the testing machine and the test was stopped.

Figure 53 depicts the strain of the concrete at the top surface (compression zone) against the applied load, the concrete strain at the location of the end of the splice was higher than the middle and this happened because the cracks initiated at the location of the splice end and were much wider than the cracks at the middle as can be seen in Figure 51.

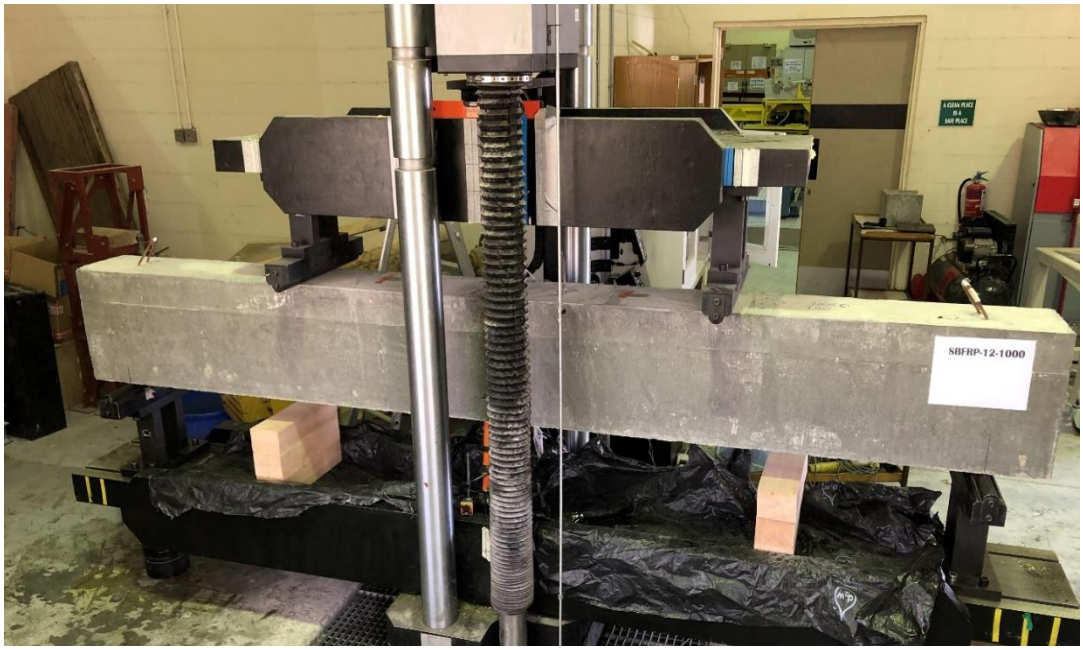

Figure 50: Beam 6 (SBFRP-12-1000) testing setup

Figure 51: Cracking pattern of beam 6 (SBFRP-12-1000)

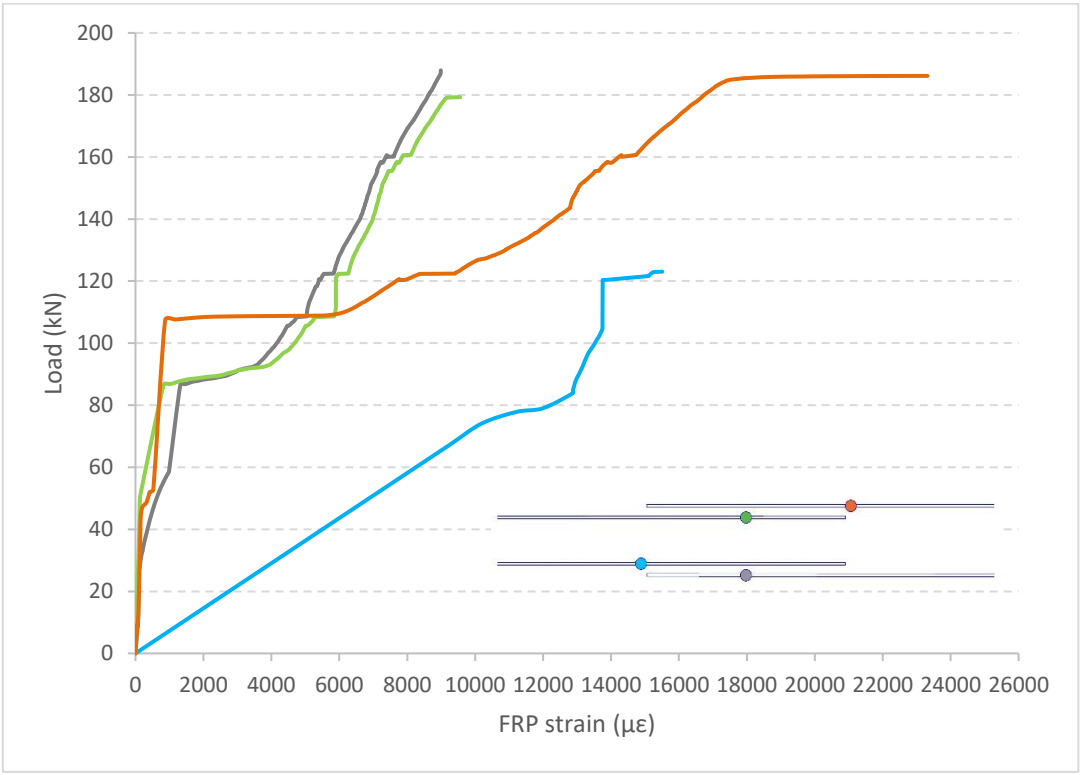

Figure 52: Variation of FRP strains of beam 6 with load along the SBFRP splice

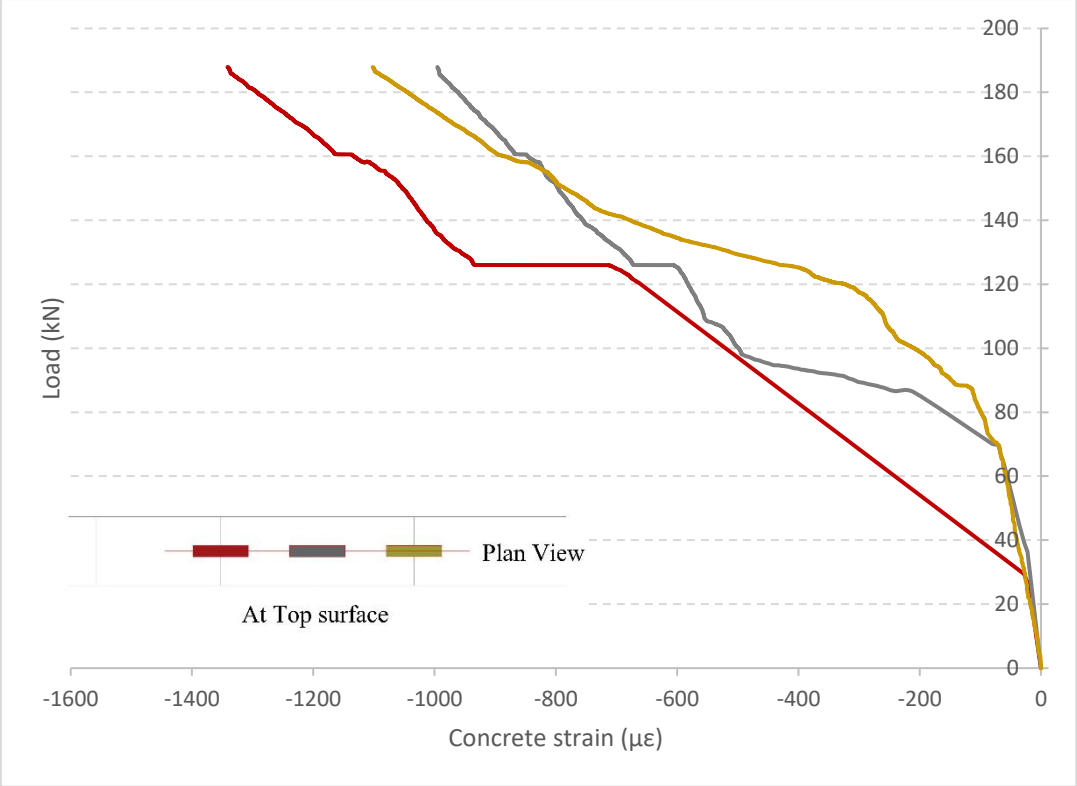

Figure 53: Concrete strains versus load in compression zone of beam 6

4.5.1.7 Beam 7 (SBFRP-16-600)

Beam specimen 7 (SBFRP-12-600) reinforced with 16 mm diameter sand-coated basalt FRP which has a lap splice of 600 mm. The specimen was tested in flexure as shown in Figure 54. The initial crack occurred at a load of 102 kN within the constant moment region near the left applied point load on the beam after the static load been applied gradually. More flexural cracks spread along the beams. All of the cracks were vertical ones and were initiated at the bottom and moved upward, at the same time the deflection of the beam was becoming more visible. With the increment of the applied load, the concrete split in the tension zone which unveiled the FRP bars and made the overlap visible and beam 7 failed as illustrated in Figure 55.

Figure 56 indicates the measured strains along spliced FRP bars versus applied load. The strain values were very low at the beginning till the first crack occurred then a

massive increase in the strain values took place which indicates that upon the occurrence of the initial crack the load was transferred rapidly to the bar. The beam failed at a maximum load of 315.98 kN and a maximum strain at the end of the splice of 19238.28 με.

Figure 57 depicts the strain of the concrete at the top surface (compression zone) against the applied load, the concrete strain at the location of the end of the splice was higher than the middle and this happened because the cracks initiated at the location of the splice end and were much wider than the cracks at the middle as can be seen in Figure 55.

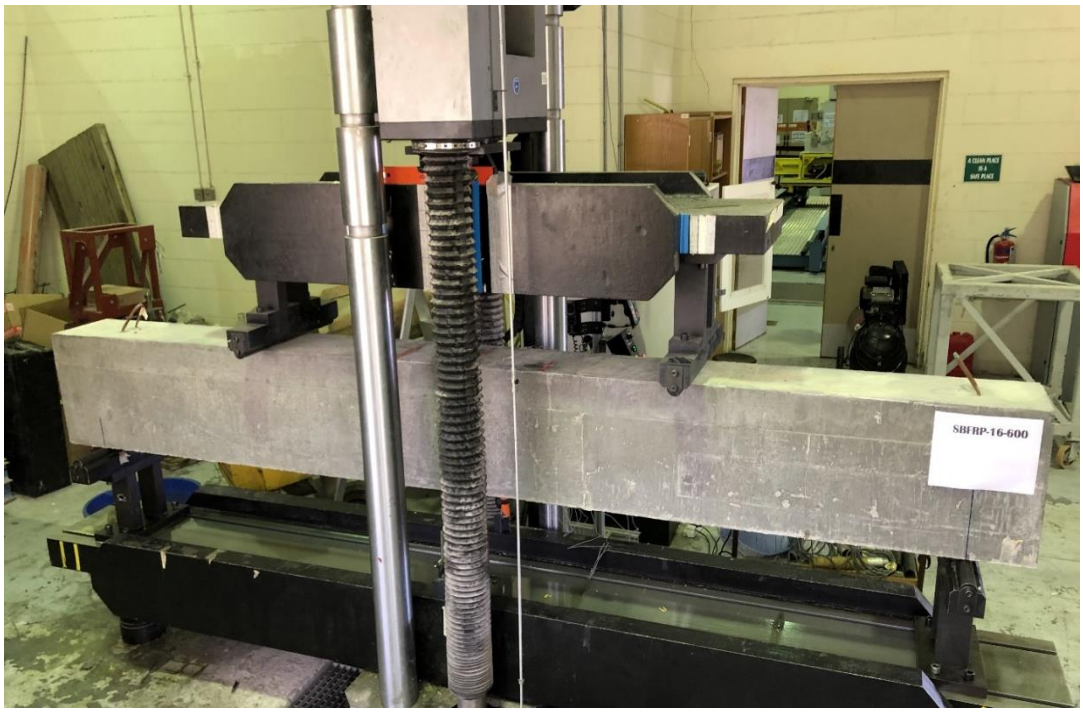

Figure 54: Beam 7 (SBFRP-16-600) testing setup

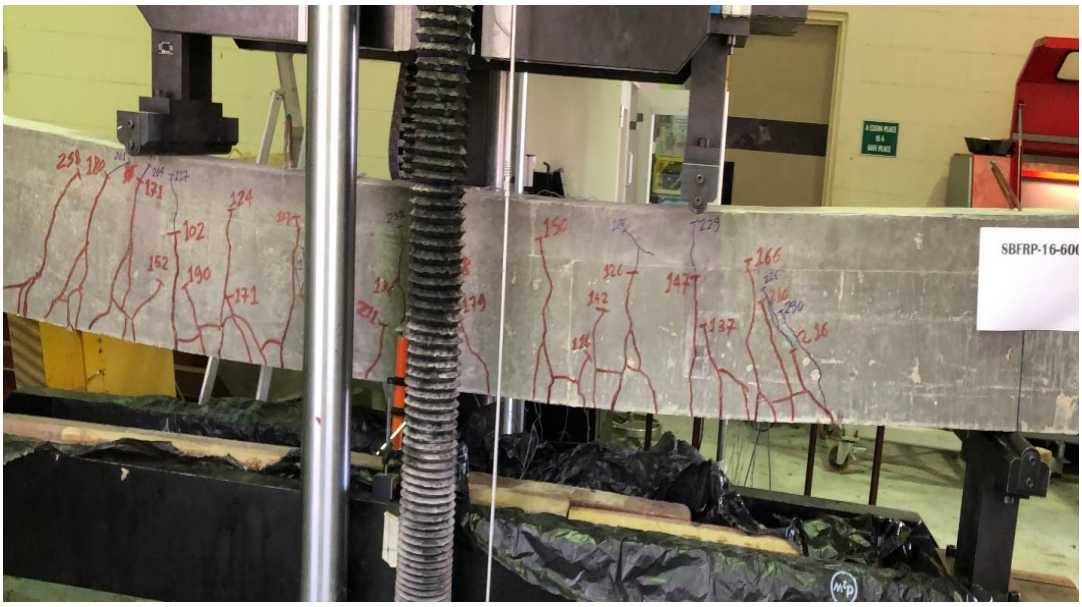

Figure 55: Cracking pattern of beam 7 (SBFRP-16-600)

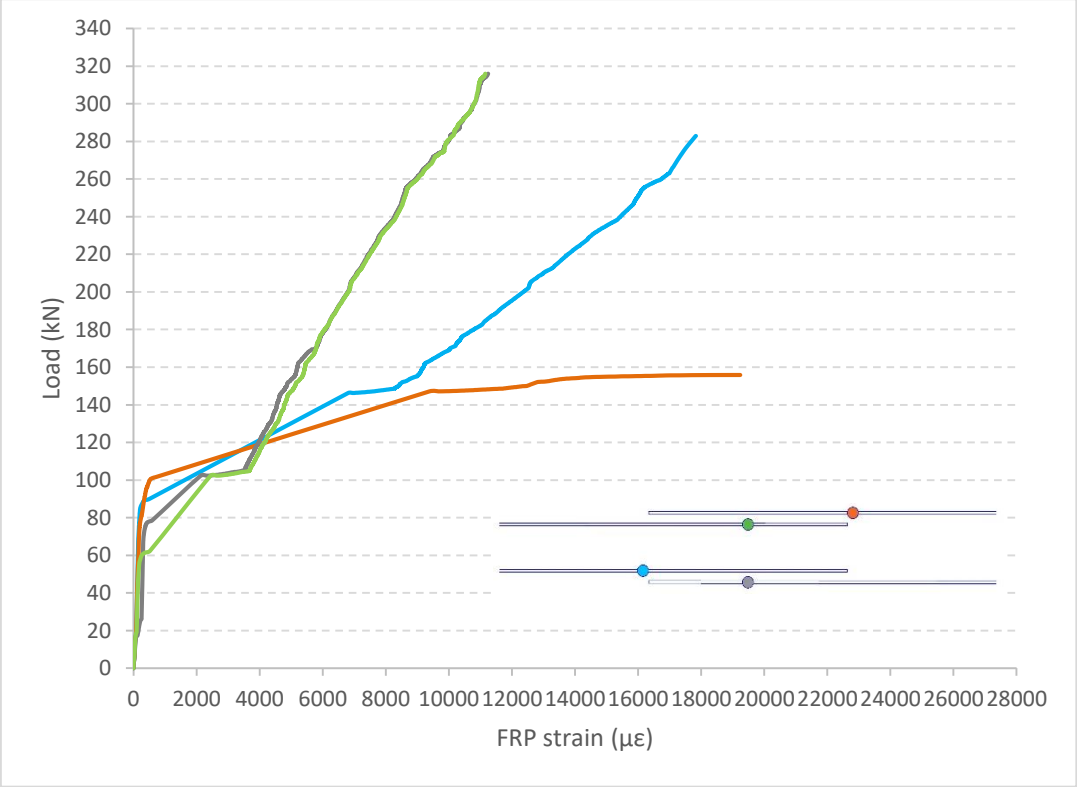

Figure 56: Variation of FRP strains of beam 7 with load along the SBFRP splice

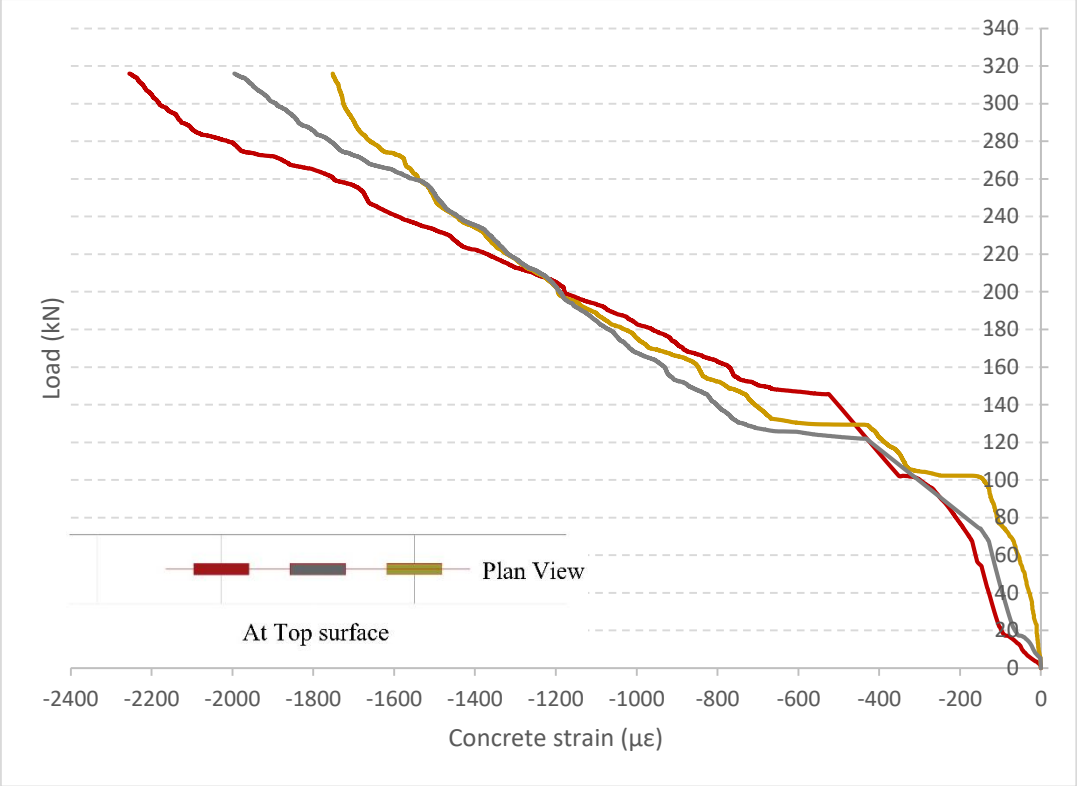

Figure 57: Concrete strains versus load in compression zone of beam 7

4.5.1.8 Beam 8 (SBFRP-16-900)

Beam specimen 8 (SBFRP-16-900) reinforced with 16 mm diameter sand-coated basalt FRP which has a lap splice of 900 mm. The specimen was tested in flexure as shown in Figure 58. The initial crack occurred at a load of 81 kN within the constant moment region near the right applied point load on the beam after the static load been applied gradually. More flexural cracks spread along the beams. All of the cracks were vertical ones and were initiated at the bottom and moved upward, at the same time the deflection of the beam was becoming more visible. With the increment of the applied load, the FRP bars have ruptured in the tension zone and beam 8 failed as illustrated in Figure 59.

Figure 60 indicates the measured strains along spliced FRP bars versus applied load. The strain values were very low at the beginning till the first crack occurred then a

massive increase in the strain values took place which indicates that upon the occurrence of the initial crack the load was transferred rapidly to the bar. The beam failed at a maximum load of 324.57 kN and a maximum strain at the end of the splice of 20837.32 με.

Figure 61 depicts the strain of the concrete at the top surface (compression zone) against the applied load, the concrete strain at the location of the end of the splice was higher than the middle and this happened because the cracks initiated at the location of the splice end and were much wider than the cracks at the middle as can be seen in Figure 59.

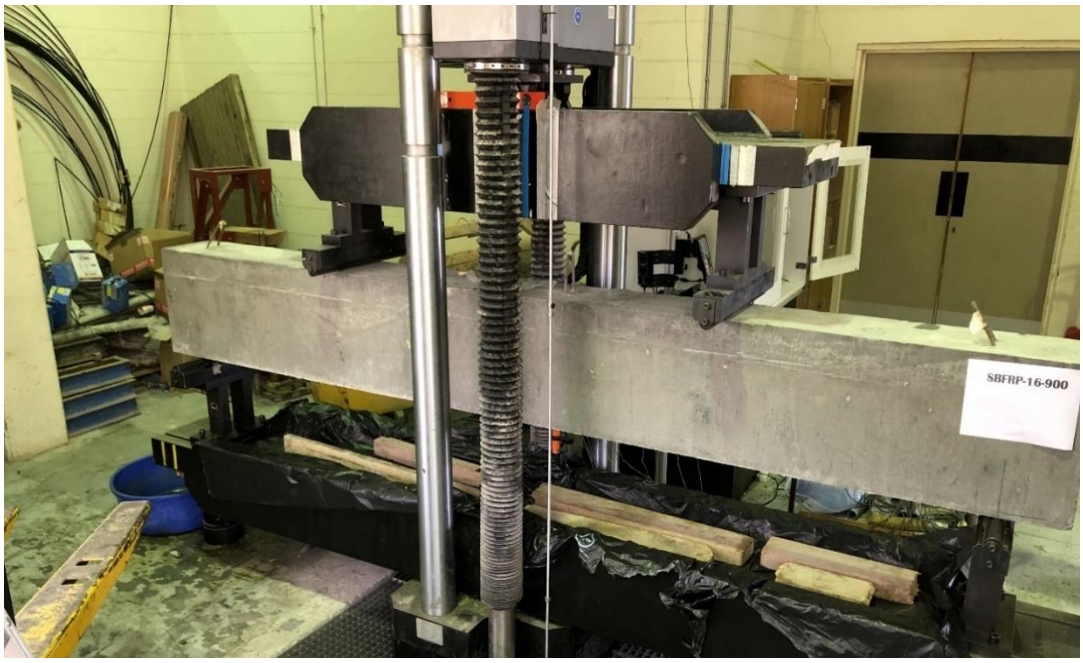

Figure 58: Beam 8 (SBFRP-16-900) testing setup

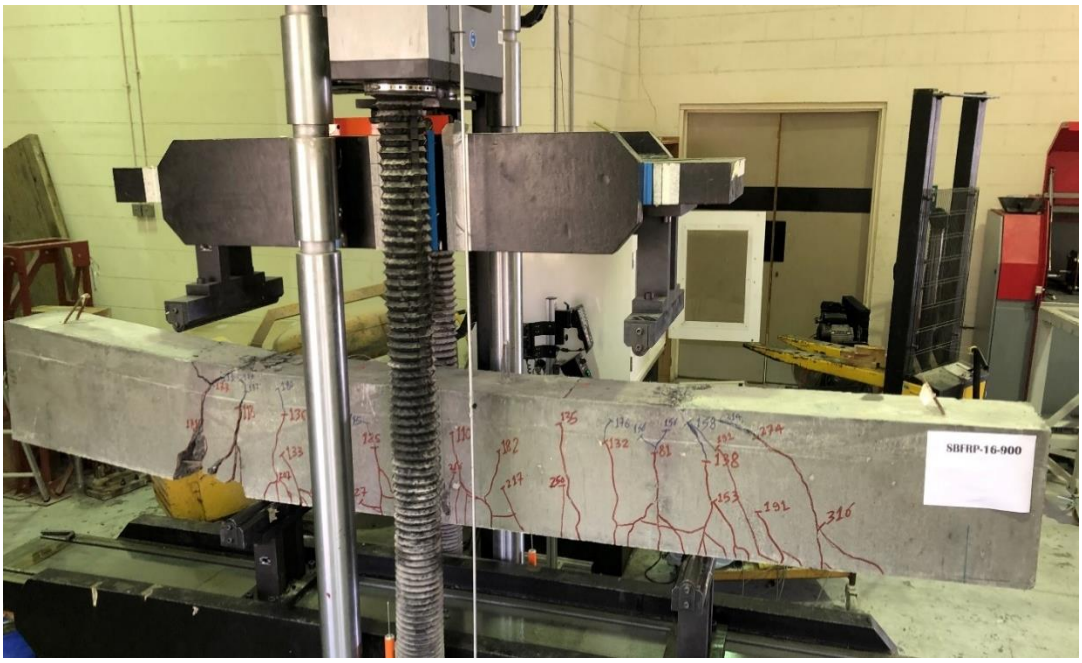

Figure 59: Cracking pattern of beam 8 (SBFRP-16-900)

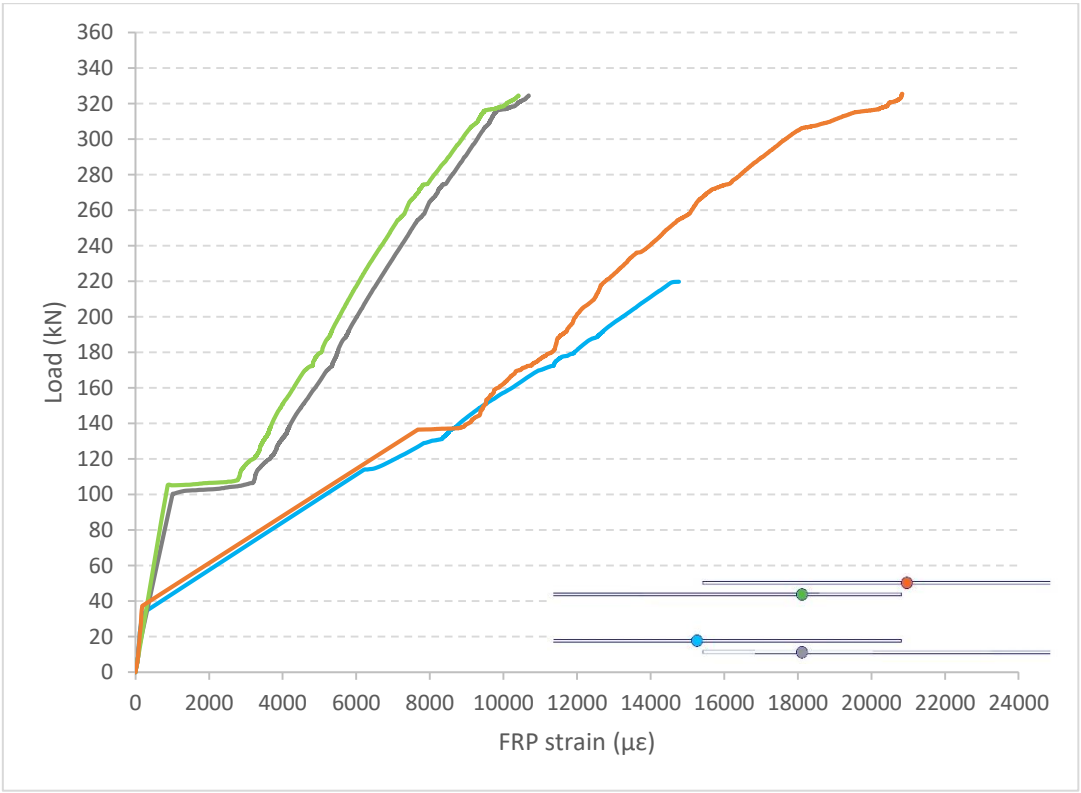

Figure 60: Variation of FRP strains of beam 8 with load along the SBFRP splice

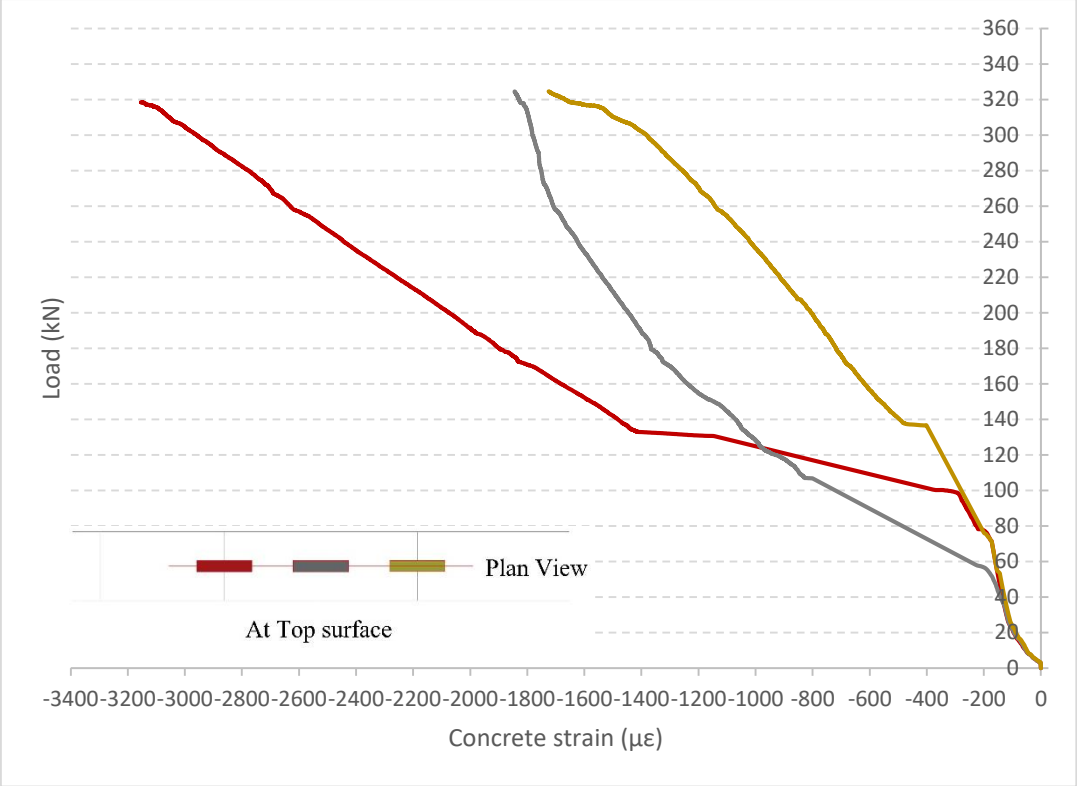

Figure 61: Concrete strains versus load in compression zone of beam 8

4.5.1.9 Beam 9 (SBFRP-16-1200)

Beam specimen 9 (SBFRP-16-1200) reinforced with 16 mm diameter sand-coated basalt FRP which has a lap splice of 1200 mm. The specimen was tested in flexure as shown in Figure 62. The initial crack occurred at a load of 123 kN within the constant moment region near the left applied point load on the beam after the static load been applied gradually. More flexural cracks spread along the beams. All of the cracks were vertical ones and were initiated at the bottom and moved upward, at the same time the deflection of the beam was becoming more visible. With the increment of the applied load, the FRP bars have ruptured in the tension zone and beam 9 failed as illustrated in Figures 63 and 64.

Figure 65 indicates the measured strains along spliced FRP bars versus applied load. The strain values were very low at the beginning till the first crack occurred then a

massive increase in the strain values took place which indicates that upon the occurrence of the initial crack the load was transferred rapidly to the bar. The beam failed at a maximum load of 367.19 kN and a maximum strain at the end of the splice of 25963.64 με.

Figure 66 depicts the strain of the concrete at the top surface (compression zone) against the applied load, the concrete strain at the location of the end of the splice was higher than the middle and this happened because the cracks initiated at the location of the splice end and were much wider than the cracks at the middle as can be seen in Figures 63 and 64.

Figure 62: Beam 9 (SBFRP-16-1200) testing setup

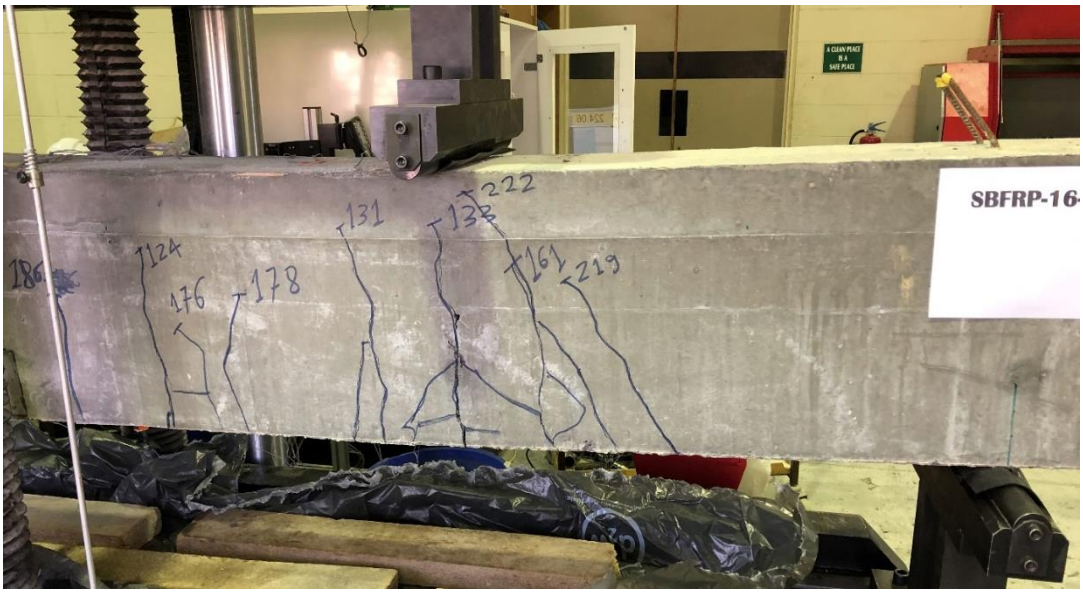

Figure 63: Cracking pattern of beam 9 (SBFRP-16-1200)

Figure 64: Cracking pattern of beam 9 (SBFRP-16-1200)

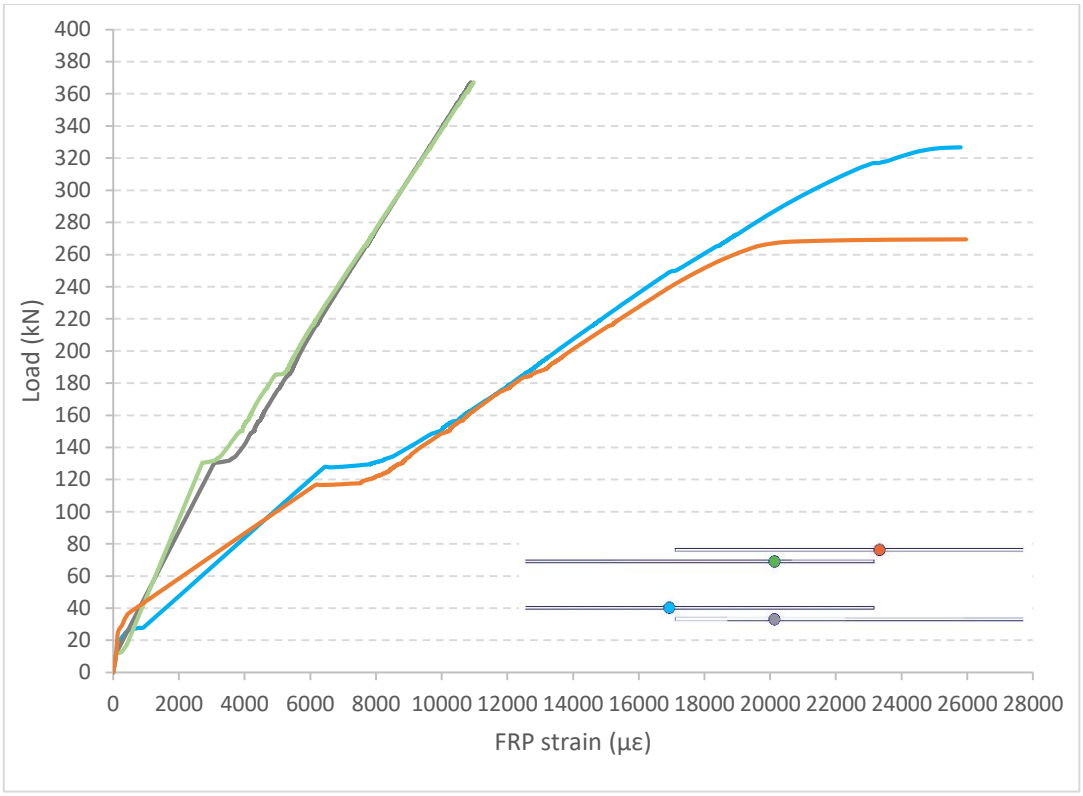

Figure 65: Variation of FRP strains of beam 9 with load along the SBFRP splice

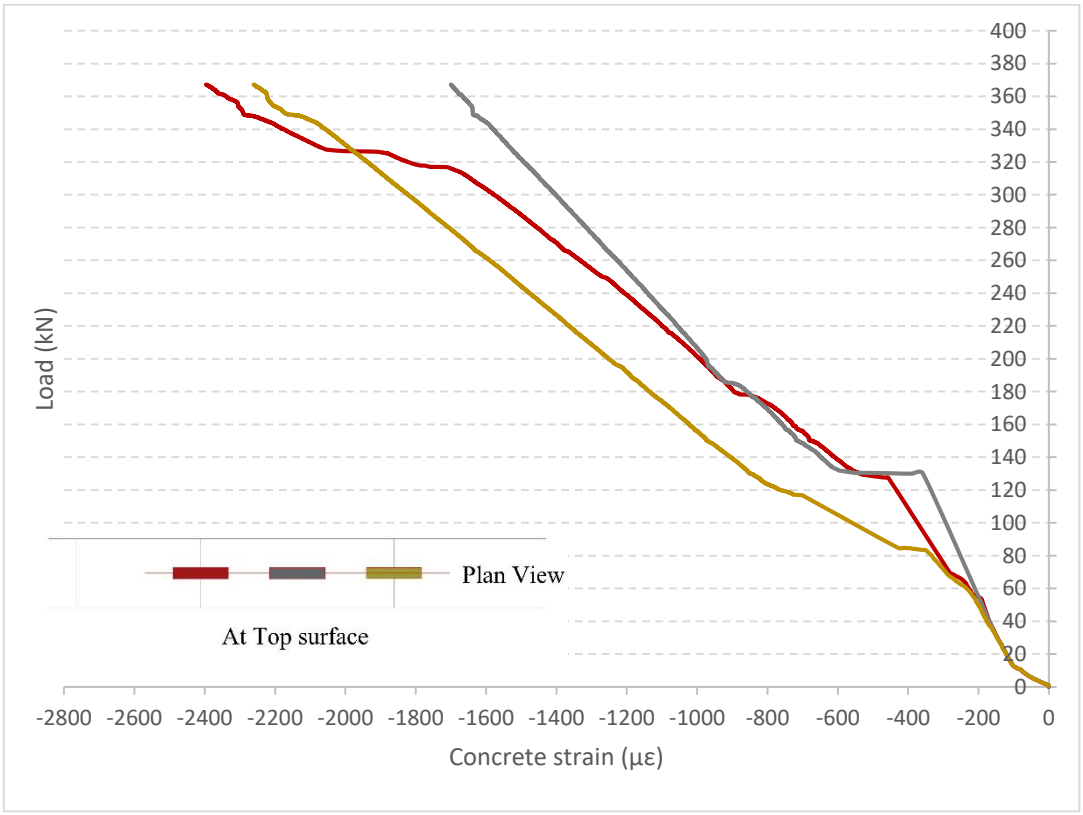

Figure 66: Concrete strains versus load in compression zone of beam 9

4.5.1.10 Beam 10 (HWBFRP-10-400)

Beam specimen 10 (HWBFRP-10-400) reinforced with 10 mm diameter helically wrapped basalt FRP which has a lap splice of 400 mm. The specimen was tested in flexure as shown in Figure 67. The initial crack occurred at a load of 145 kN within the constant moment region near the middle of the beam after the static load been applied gradually. More flexural cracks spread along the beams. All of the cracks were vertical ones and were initiated at the bottom and moved upward, at the same time the deflection of the beam was becoming more visible. As the load increased, the same initial crack started to become wider in addition to the formation of a second crack just next to it, then at the location of the first crack the concrete split at the tension zone which unveiled the FRP bars and made the overlap visible and beam 10 failed as illustrated in Figure 68.

Figure 69 indicates the measured strains along spliced FRP bars versus applied load. The strain values were very low at the beginning till the first crack occurred then a massive increase in the strain values took place which indicates that upon the occurrence of the initial crack the load was transferred rapidly to the bar. The beam failed at a maximum load of 145.19 kN and a maximum strain at the end of the splice of 10144.5 με.

Figure 70 depicts the strain of the concrete at the top surface (compression zone) against the applied load.

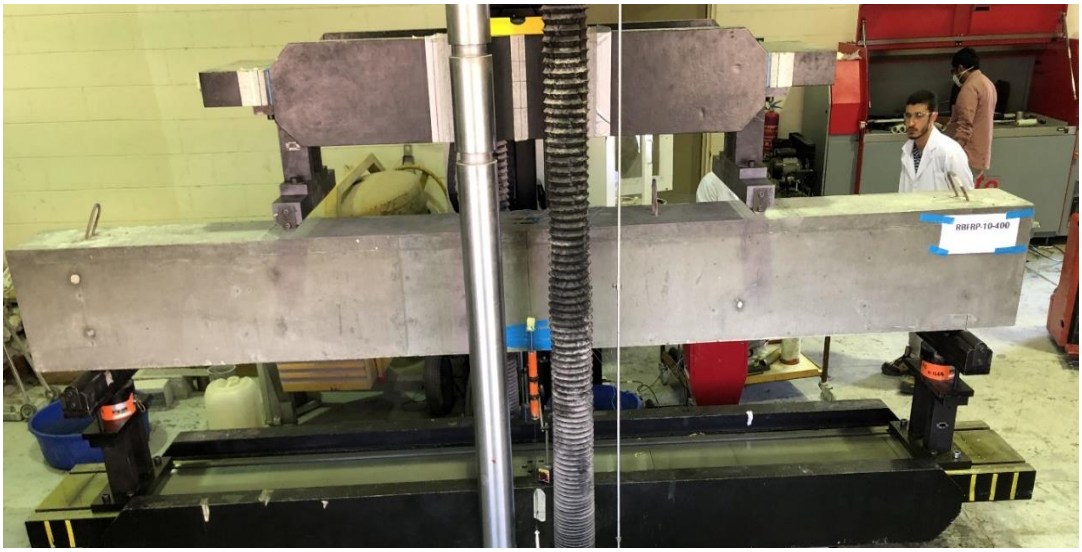

Figure 67: Beam 10 (HWBFRP-10-400) testing setup

Figure 68: Two cracks of beam 10 (HWBFRP-10-400)

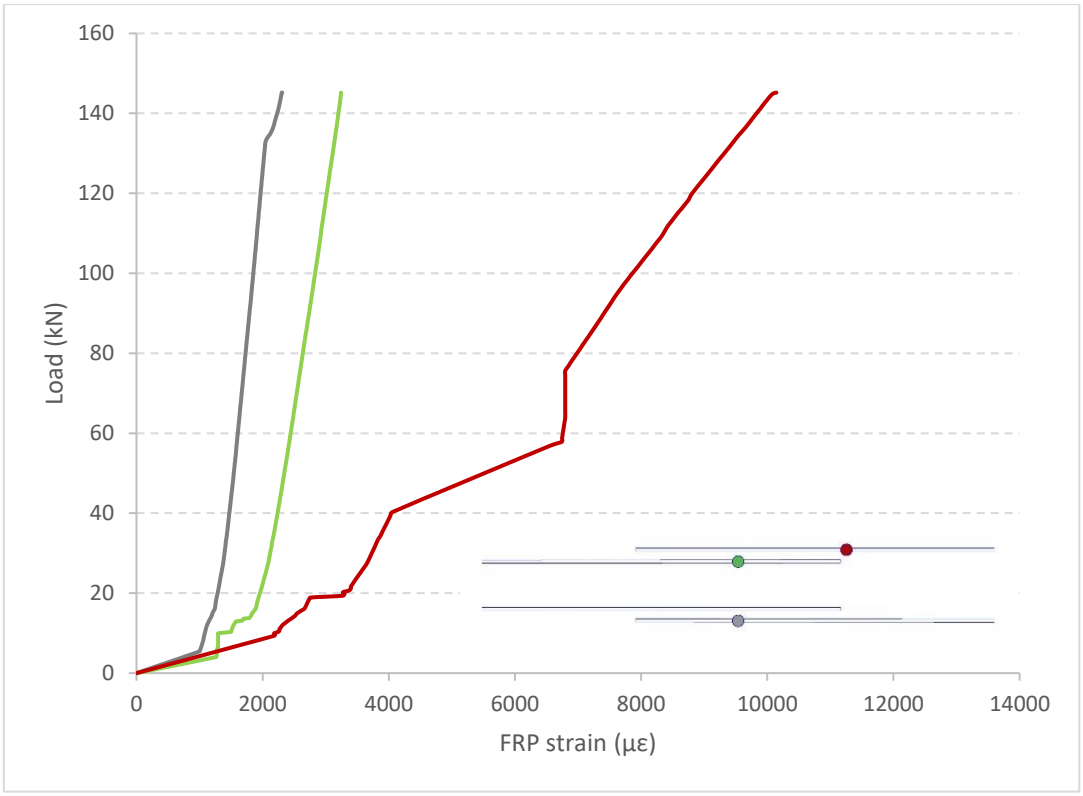

Figure 69: Variation of FRP strains of beam 10 with load along the SBFRP splice

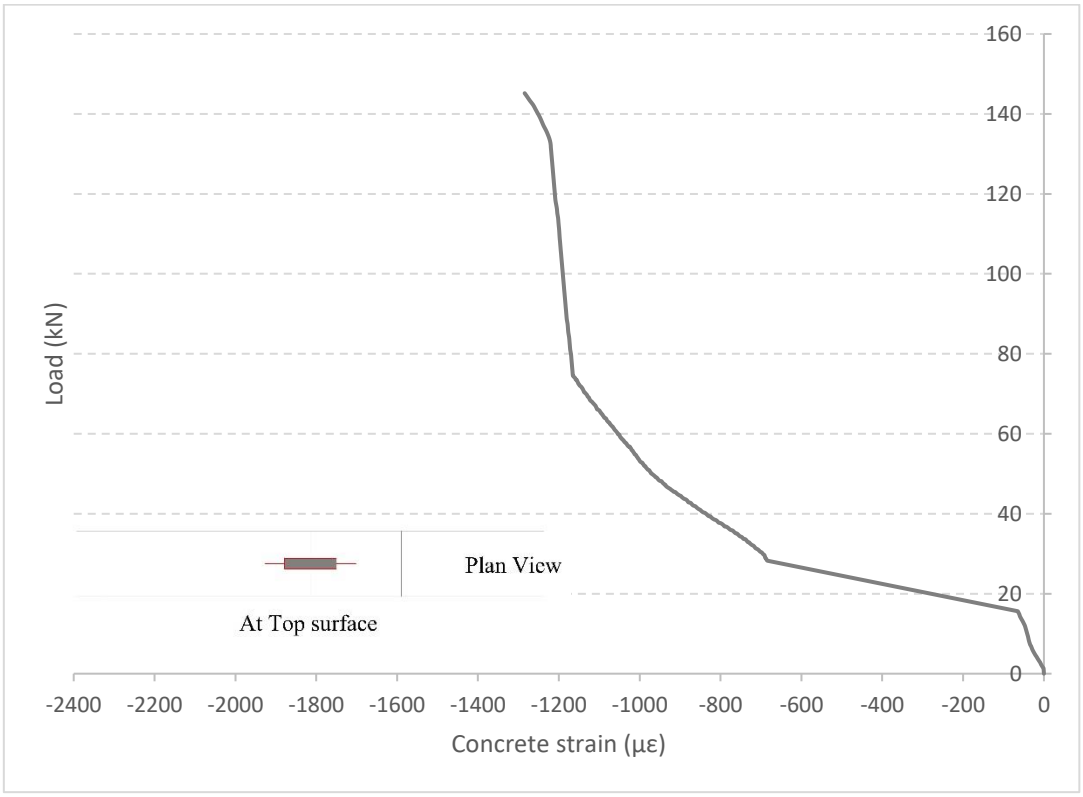

Figure 70: Concrete strain versus load in compression zone of beam 10

4.5.1.11 Beam 11 (HWBFRP-10-600)

Beam specimen 11 (HWBFRP-10-600) reinforced with 10 mm diameter helically wrapped basalt FRP which has a lap splice of 600 mm. The specimen was tested in flexure as shown in Figure 71. The initial crack occurred at a load of 140 kN within the constant moment region near the middle of the beam after the static load been applied gradually. More flexural cracks spread along the beams. All of the cracks were vertical ones and were initiated at the bottom and moved upward, at the same time the deflection of the beam was becoming more visible. As the load increased, the same initial crack started to become wider, then at the location of the first crack, the concrete split at the tension zone which unveiled the FRP bars and made the overlap visible and beam 11 failed as illustrated in Figure 72.

Figure 73 indicate the measured strains along spliced FRP bars versus applied load. Very low strains were recorded in the bars up to cracking that is marked by a sudden increase in the strain values. The load was transferred suddenly to the bar at the cracking. At loads below the failure, the results indicated that the strains changed slowly from the free end up to the middle of the splice but more rapidly at the loaded end. The beam failed at a maximum load of 145.6 kN and a maximum strain at the middle of the splice of 9883.254 με.

Figure 74 depicts the strain of the concrete at the top surface (compression zone) against the applied load.

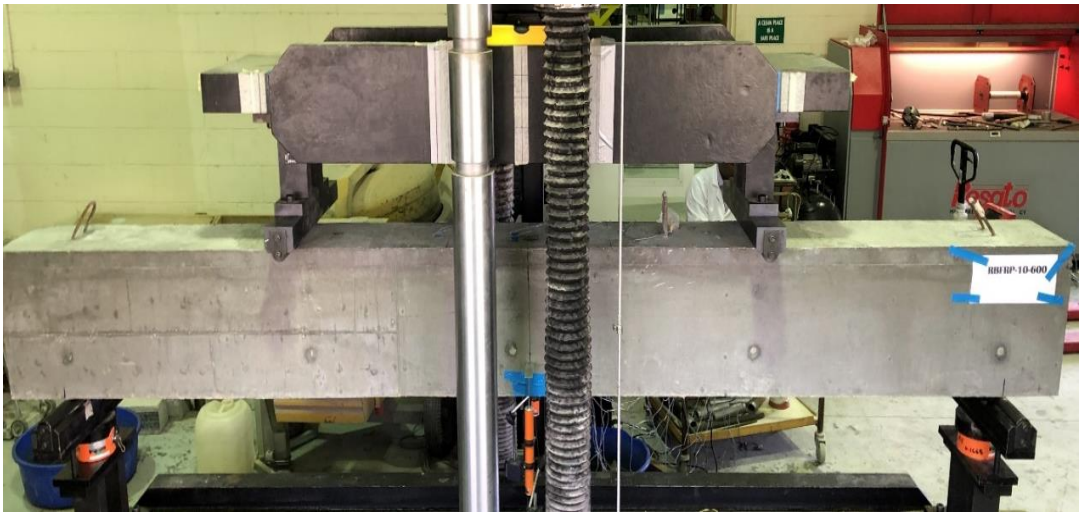

Figure 71: Beam 11 (HWBFRP-10-600) testing setup

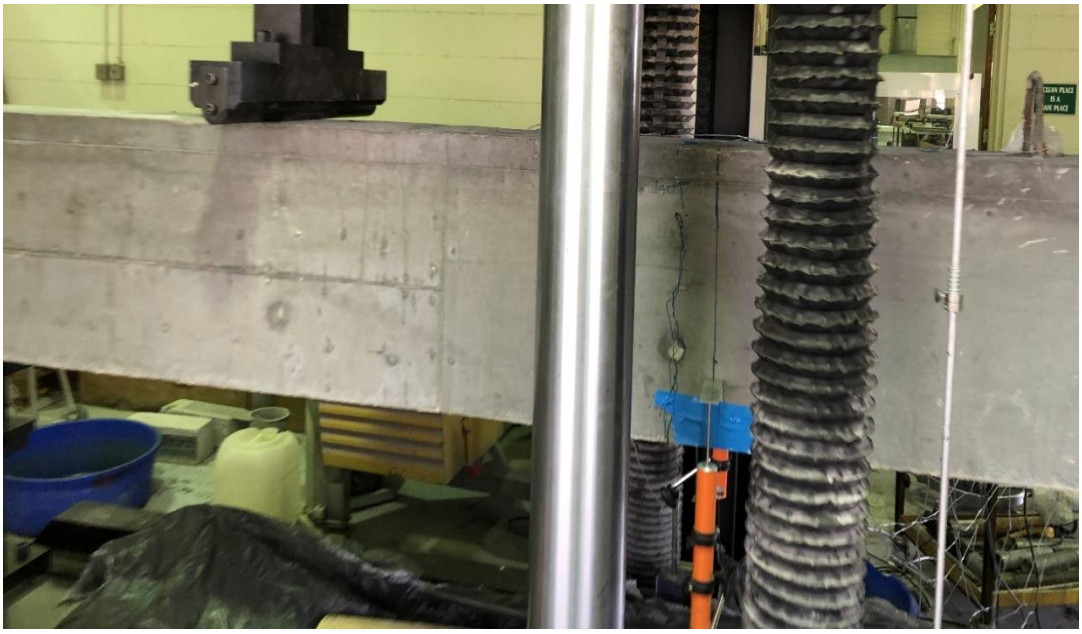

Figure 72: Failure of beam 11 (HWBFRP-10-600)

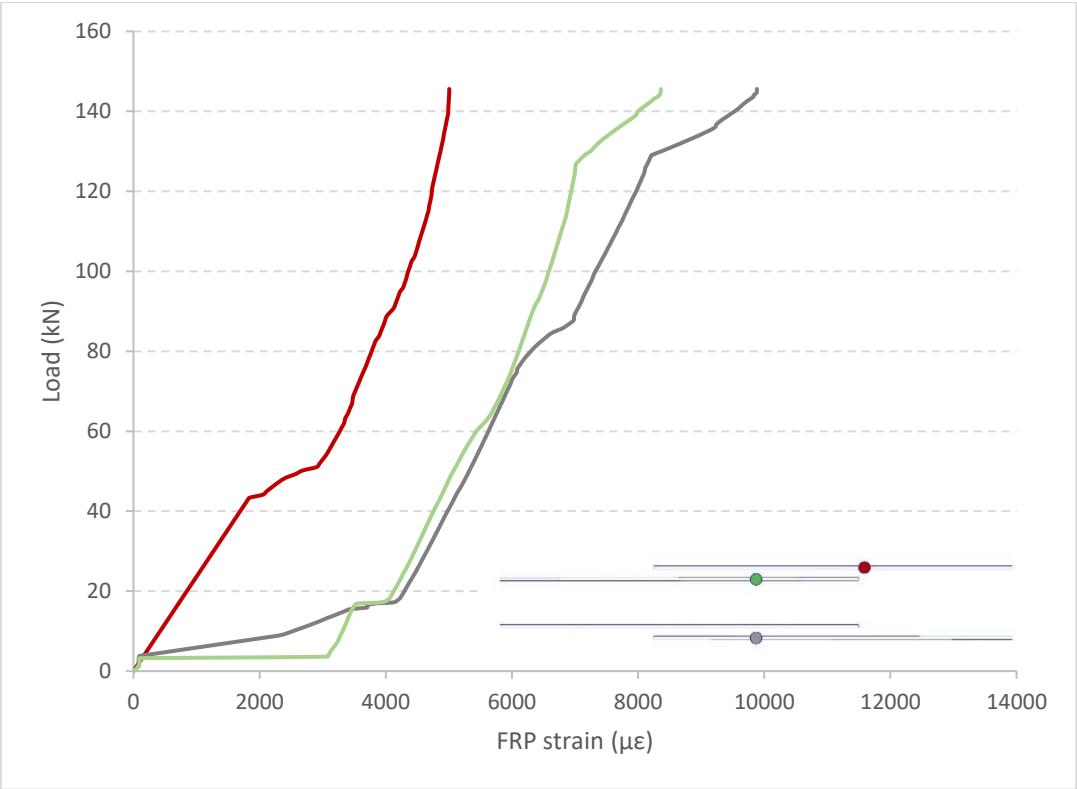

Figure 73: Variation of FRP strains of beam 11 with load along the SBFRP splice

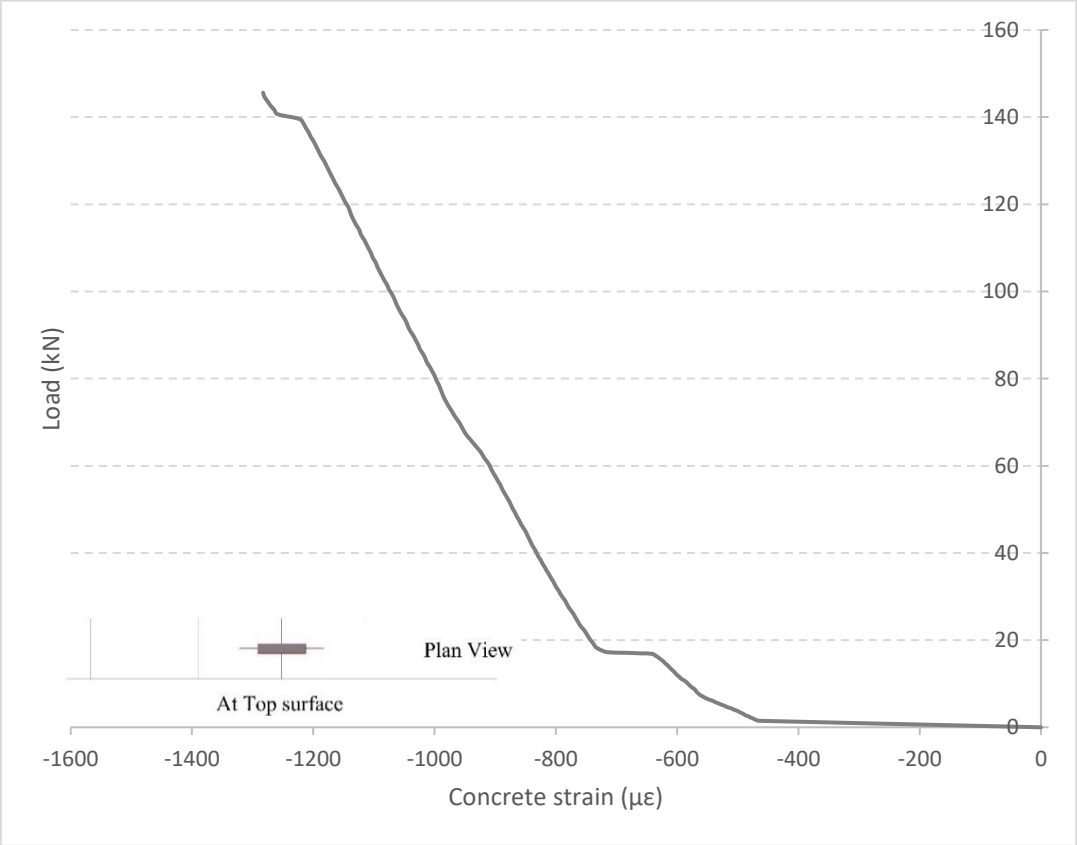

Figure 74: Concrete strain versus load in compression zone of beam 11

4.6 Modes of failure

The recorded modes of failure were two, splitting and FRP rupture failure. Splitting failure occurred in the beams which had a splice length smaller than the critical splice length, the rupture of FRP bars occurred mainly in the beams where an adequate splice length was provided. A typical splitting failure is shown in Figure 63(a). The marked lines in Figures 75 and 76 point to the end of the splice location in the beam. The splitting failure was observed when some transverse and longitudinal cracks was observed at the tension zone and the failure was followed by pulling the bar out as shown in Figure 77.

Figure 75: Splitting failure of concrete in the tension zone

Figure 76: Splitting failure of concrete in the tension zone

Figure 77: Splitting failure followed by slipping of the FRP bar

The observation of the FRP rupture was visual as shown in Figures 78 and 79 and confirmed it was confirmed by the strain recordings.

Figure 78: Typical rupture of FRP bars

Figure 79: Typical rupture of FRP bars

4.7 Comparison of the experimental results

4.7.1 Bar diameter

The bar diameter has an important role in possessing the beams to its ultimate capacity, this can be proved by comparing beams 2 (SBFRP-10-600) and 7 (SBFRP-16-600), both of the beams have the same splice length and bar's surface texture which leaves the bar diameter as the only variable. Beam 2 failed at a maximum load of 149.504 kN while beam 7 failed at a maximum load of 315.98 kN which means that the capacity of beam 7 is slightly higher than the double of the ultimate load capacity of beam 2. This leads us to the conclusion that increasing the bar diameter increases the ultimate load capacity of the beam while having the other testing parameters constant.

4.7.2 Splice length

The effect of the splice length on the beams can be studied by selecting any tested category of the 4 tested categories, for example category 1 which includes beams 1 (SBFRP-10-400), 2 (SBFRP-10-600) and 3 (SBFRP-10-850). Beams 1, 2 and 3 have an ultimate load capacity of 144.675, 149.504 and 170.592 kN, respectively. The illation of this point is that having a lengthier splice length gives the beam higher ultimate capacity. Also, comparing the cracks of the 3 beams, it can be noticed that the number of cracks and their severity is reduced as the splice length value gets higher. Additionally, the FRP bars maximum strain also increases as the length of the splice gets longer.

4.7.3 Surface texture

By comparing beams 1 (SBFRP-10-400) and 10 (HWBFRP-10-400) and comparing beams 2 (SBFRP-10-600) and Beam 11 (HWBFRP-10-600), we have the surface texture of sand-coated and helically wrapped bars as the sole variable. By comparing the first two beams we can see that beam 1 has a capacity of 144.675 kN while beam 10 has a capacity of 145.19 kN, the two capacities were very close however, Beam 2 had insufficient splice

length and a full bond was not developed, which draws a conclusion that the surface texture has a significant effect on the ultimate capacity of the beam. This conclusion can be supported by comparing the second two beams where beam 2 has a capacity of 149.504 while beam 11 has a capacity of 145.6 kN which means that the sand-coated-RC beams has a higher failure load than the helically wrapped RC beams, thus this conclusion is backed up. Moreover, the sand-coated bars exhibit a higher maximum strain than the helically wrapped bars.

4.8 Codes prediction of critical splice length

4.8.1 (CSA S806-12) (2012)

The splice length in the Canadian code for designing and construction of buildings using FRP reinforcement is given by:

$$l_s = (1.3)(1.15)\frac{k_1\, k_2\, k_3\, k_4\, k_5}{d_{cs}}\frac{f_F}{\sqrt{\mathrm{f'_c}}}A_{Fb} \qquad (13)$$

where l_d = development length in mm, A_{Fb} = FRP reinforcement's area (mm^2), f_F = FRP bar 's tensile strength of in MPa, k_1 = factor for bar location such that k_1= 1.3 for the horizontally placed reinforcement to allow additional 300 mm of more concrete to be casted in below the developmental region, and k_1 = 1 .0 for other conditions, k_2 = factor for density of concrete such that k_2= 1.3 for the low-density, k_2= 1.2 for the semi-low density, and k_2= 1.0 for the normal density, k_3 = bar size factor such that k_3 = 0.8 for $A_{Fb} < 300\ mm^2$ and = 1.0 for $A_{Fb} > 300\ mm^2$, k_4 = bar fiber factor such that k_4 =1.0 for CFRP and GFRP and k_4= 1.25 for AFRP, k_5 = bar surface profile factor such that k_5 = 1.0 for the braided surfaces, roughened surfaces, or the sand-coated surfaces, k_5= 1.05 for the surfaces that are ribbed or have a spiral pattern, and k_5= 1.8 for the indented surfaces, and d_{cs} = smaller for:

a) the length from the nearest concrete surface to centre of the bar being developed or

b) 2/3 of the bar spaces from centre to centre.

The term d_{cs} will not be used above $2.5d_b$, and $\sqrt{f'_c}$ will not be used above 5 MPa.

4.8.2 (CSA-S6-14) (2014)

The calculation of the splice length in the Canadian highway design code for FRP's is based on the following equation:

$$l_s = (1.3)(0.45)\frac{k_1\ k_4}{\left[d_{cs} + K_{tr}\frac{E_F}{E_c}\right]}\left[\frac{f_{Fu}}{f_{cr}}\right]A_{Fb} \tag{14}$$

$$K_{tr} = 0.45\frac{A_{tr}\ f_y}{10.5\ sn} \tag{15}$$

where $f_{cr} = 0.4\sqrt{f'_c}$ is concrete's cracking strength in MPa but less than 3.2 MPa, A_{tr} = area of the rebar stirrups in mm^2, f_y = yield strength of steel reinforcement bars in MPa. The term $\left[d_{cs} + K_{tr}\frac{E_F}{E_c}\right]$ will not be used above $2.5d_b$.

4.8.3 (ACI 440.1R-15) (2015)

The American code of the construction of structures reinforced with FRP bars suggests the following equation for evaluation the splice length:

$$l_d = \frac{\alpha\frac{f_{fr}}{0.083\sqrt{f'_c}} - 340}{13.6 + \frac{C}{d_b}}d_b \tag{16}$$

where α is the bar location modification factor, such that α = 1.5 when > 300 mm of fresh concrete is casted below the reinforcement bars, otherwise α = 1.0, and $C =$ min $\left(d_c, \frac{ctr-to-ctr\ spacing}{2}\right) \leq 3.5d_b$.

4.9 Assessment of the splice length based on the codes

The development length was estimated according to (CSA S806-12, CSA-S6-

14 and ACI 440.1R-15). Three diameters were used: 10, 12 and 16 mm for sand-coated BFRP bars and 10 mm for helically wrapped BFRP bars. The critical splice length based on the Canadian highway design code (CSA-S6-14) and the American code (ACI 440.1R-15) is almost like each other. The Canadian code for buildings (CSA S806-12) differs a lot from them. It can be seen that the larger the diameter the lengthier the required splice length, and sand-coated bars require longer splice than the helically wrapped bars however the three codes do not take into consideration the basalt bars also the helically wrapped texture, they only take into accounts the glass, carbon and aramid FRP bars also, the other surface texture such as: sand-coated and braided.

The following table summarizes the values of the critical splice length based on the codes:

Table 8: Summary of the critical splice length based on the recent codes

Type of the bar	10 mm diameter sand-coated BFRP bars	12 mm diameter sand-coated BFRP bars	16 mm diameter sand-coated BFRP bars	10 mm diameter helically wrapped BFRP bars
Splice Length (CSA S806-12) (mm) Eq. (13)	903.52 ≃ **905**	1061.87 ≃ **1100**	1335.41 ≃ **1340**	596.99 ≃ **600**
Splice Length (CSA-S6-14) (mm) Eq. (14)	690.53 ≃ **695**	811.55 ≃ **815**	1020.61 ≃ **1025**	434.53 ≃ **435**
Splice Length (ACI 440.1R-15) (mm) Eq. (16)	697.12 ≃ **700**	812.9 ≃ **815**	1006.17 ≃ **1010**	342.85 ≃ **345**

4.10 Experimental prediction of critical splice length

Figure 80 shows the results of the applied force versus the strain for three beams reinforced with 16 mm diameter sand-coated BFRP bars. Each solid line represents a splice length, the lowest strain is the 600 mm splice length while the highest strain refers to the 1200 mm splice length. The orange solid line reflects the 900 mm splice length. By applying the analysis of the ultimate strength, the theoretical values of load versus strain were drawn (dashed line). Since the strain of all the solid lines (experimental values) were very close to the dashed line (theoretical value), then the maximum strain in the spliced FRP bars can be predicted by applying ultimate strength analysis.

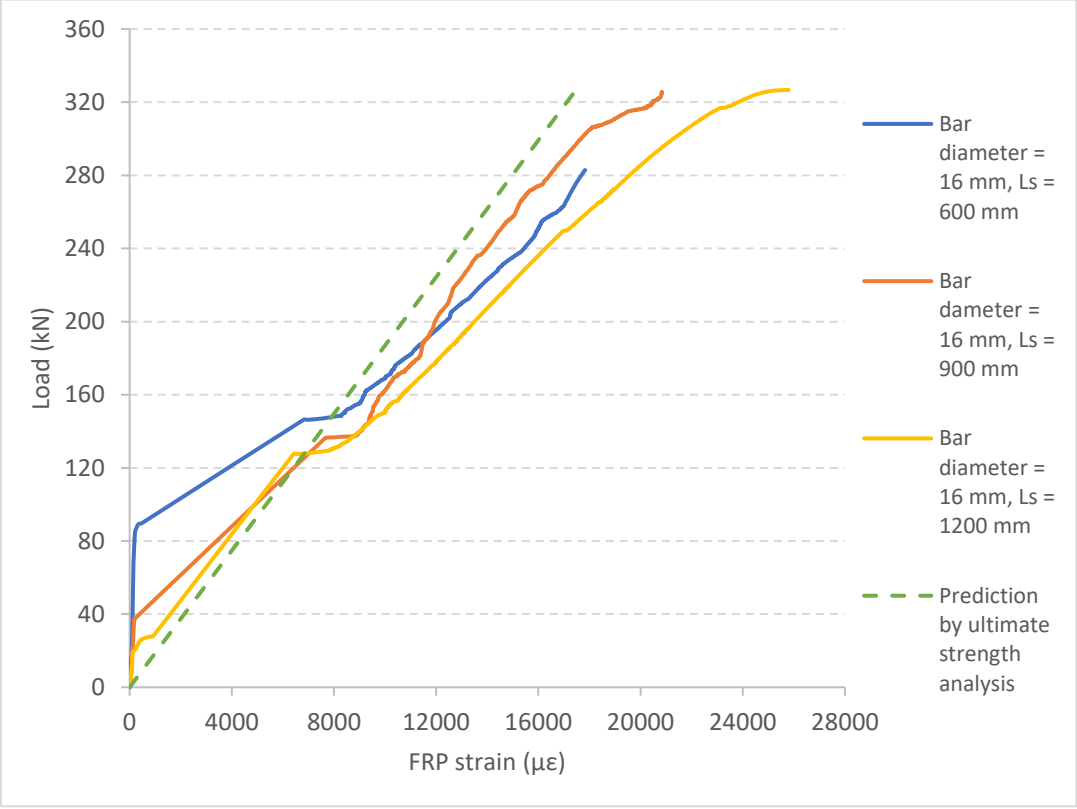

Figure 80: Prediction of strain at the end of splice length

Figures 81, 82 and 83 show the maximum strains at the ends of the spliced FRP bars versus splice length for the three categories of the san-coated basalt FRP bars; category

1 is 10 mm diameter bar, category 2 is 12 mm diameter bar, and category 3 is 16 mm diameter bars, respectively. The results confirmed that there is a direct linear relationship between the maximum strains at the ends of the spliced basalt bars and the splice length.

The continuous horizontal line in Figures 67, 68 and 69 indicates the maximum allowable strain. By linearly fitting the points of the test result, the sloped line was drawn which intersect two lines. The first line that the sloped line intersects is the dashed one and it represents the minimum allowable strain. The second line that the sloped line intersects with is solid and it depicts the maximum allowable strain. This means in order to predict the critical splice length at least one point is required, thus, one beam shall be tested.

Figure 84 expresses the prediction of critical splice length for the helically wrapped basalt FRP bars of 10 mm diameter but the value seems inaccurate compared to the theoretical one also from the strain values it is obvious that the tested beam had a problem in their big size which was designed based on a value of 1100 MPa for the tensile of the helically wrapped bars however, upon testing the bars inside our laboratory, the value was much less and approximately three quarters the provided value from the manufacturer.

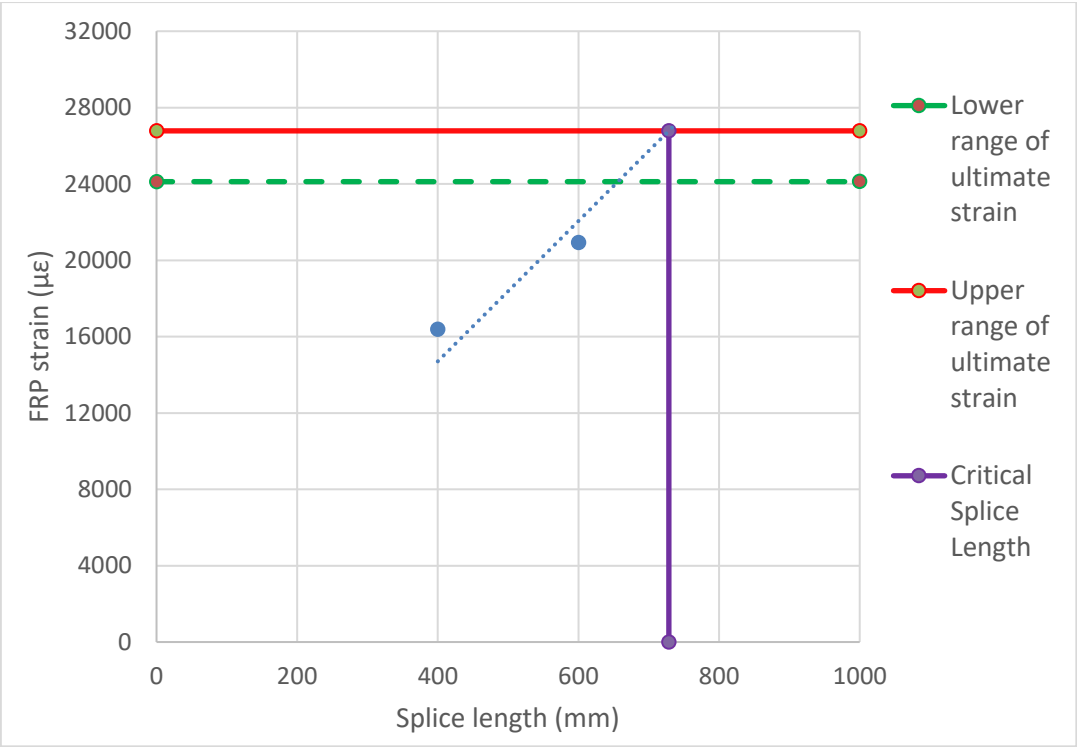

Figure 81: Typical strain variation versus splice length of bar diameter 10 mm sand-coated basalt FRP bars

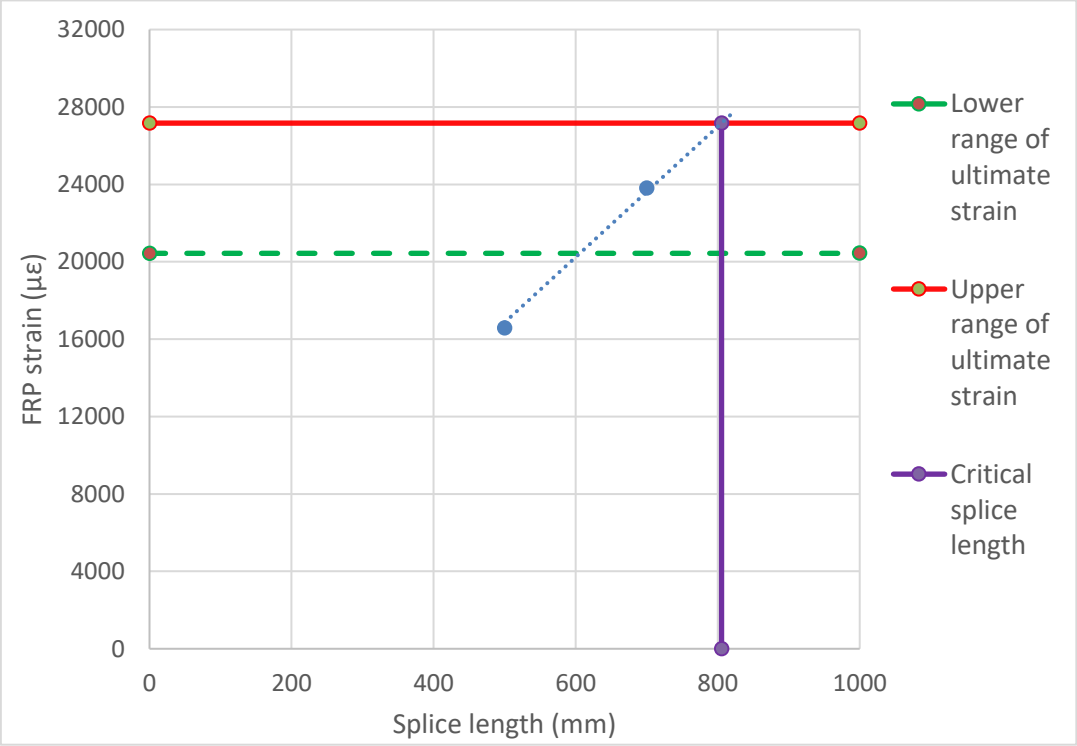

Figure 82: Typical strain variation versus splice length of bar diameter 12 mm sand-coated basalt FRP bars

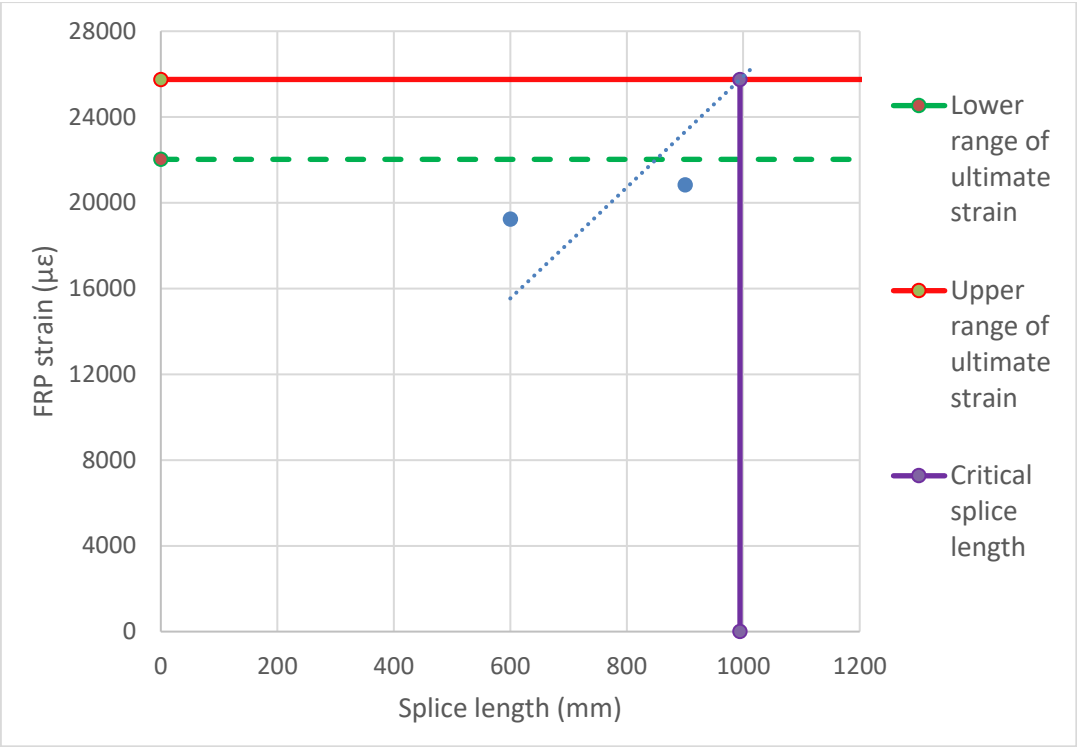

Figure 83: Typical strain variation versus splice length of bar diameter 16 mm sand-coated basalt FRP bars

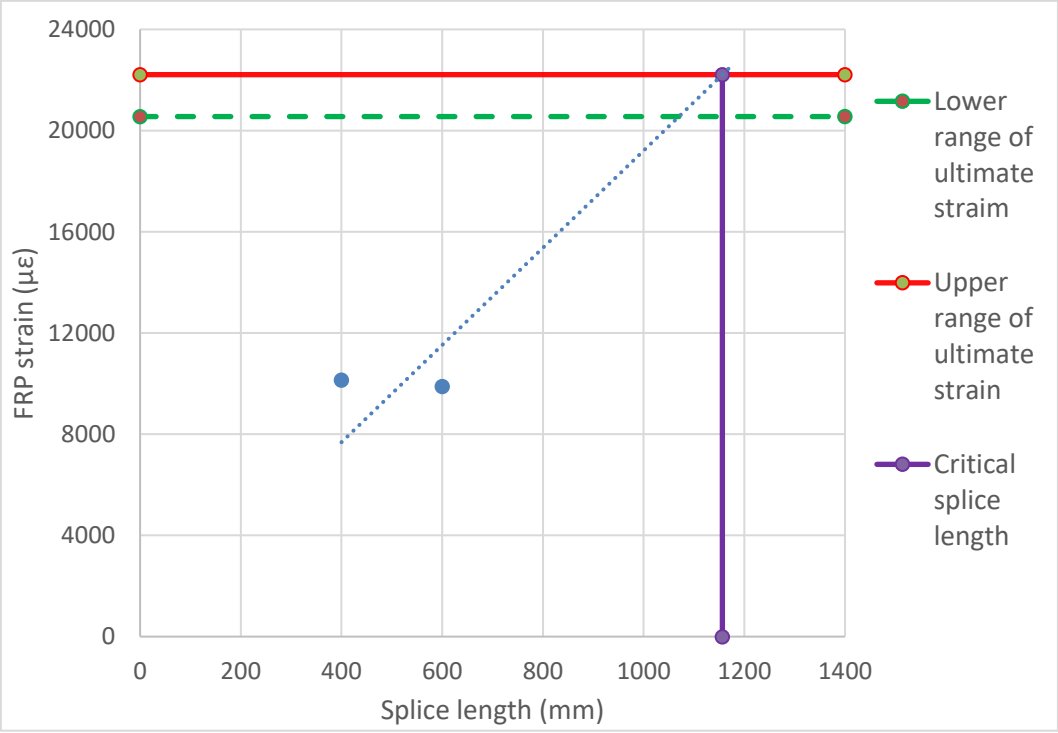

Figure 84: Typical strain variation versus splice length of bar diameter 10 mm helically wrapped basalt FRP bars

4.11 Comparison between current design guidelines (CSA S806-12, CSA-S6-14 and ACI 440.1R-15) and the experimental results

The relative relations between the required splice lengths and the critical splice lengths according to the test results are presented. The results indicate that applying the equations from the Canadian highway code (CSA-S6-14) or the American code for construction (ACI 440.1R-15) is almost enough but relying on the equation from the Canadian code for structures (CSA S806-12) is much better as it is conservative for all bar diameters and it is more than sufficient for all the tested diameters.

The following table depicts the comparison between the most recent Canadian and American guidelines and the experimental results:

Table 9: Comparison between design guidelines and the experimental results

Type of the bar	10 mm diameter sand-coated BFRP bars	12 mm diameter sand-coated BFRP bars	16 mm diameter sand-coated BFRP bars	10 mm diameter helically wrapped BFRP bars
Splice Length (CSA S806-12) (mm) Eq. (13)	903.52 ≃ **905**	1061.87 ≃ **1100**	1335.41 ≃ **1340**	596.99 ≃ **600**
Splice Length (CSA-S6-14) (mm) Eq. (14)	690.53 ≃ **695**	811.55 ≃ **815**	1020.61 ≃ **1025**	434.53 ≃ **435**
Splice Length (ACI 440.1R-15) (mm) Eq. (16)	697.12 ≃ **700**	812.9 ≃ **815**	1006.17 ≃ **1010**	342.85 ≃ **345**
Critical splice length Experimentally (mm)	728.62 ≃ 730	805.46 ≃ 810	994.47 ≃ 995	NA

Type of the bar	10 mm diameter sand-coated BFRP bars	12 mm diameter sand-coated BFRP bars	16 mm diameter sand-coated BFRP bars	10 mm diameter helically wrapped BFRP bars
Relative splice length: $\frac{l_s\ experimental}{l_s\ \text{CSA S806}-12}$	0.807	0.74	0.74	NA
Relative splice length: $\frac{l_s\ experimental}{l_s\ /\text{CSA}-\text{S6}-14}$	1.05	0.99	0.97	NA
Relative splice length: $\frac{l_s\ experimental}{l_s\ \text{ACI 440.1R}-15}$	1.04	0.99	0.985	NA

The three guidelines do not take into consideration the basalt fiber reinforced polymer. The results prove that the basalt can be treated as same as the CFRP and the GFRP using the CSA S806-12 thus, a value of 1 should be used for k_4, and the same value of k_4 should be used for CSA-S6-14 equation. Moreover, for the ACI440.1-15 the environmental reduction factor C_E should be 0.9 for the basalt and more research should be conducted.

4.12 Bond strength assessment

The transfer of the tensile force between the splice bars is controlled by the bond between them and the carrier is the concrete in this case. When the concrete splits around the spliced bar the bond between them fails. Two important factors play a huge role in the strength of this bond, and they are the concrete compression strength and the concrete tensile strength.

The bar chart expressed as Figure 85 shows how the bond strength of the spliced basalt

FRP bars in concrete is affected by the bar diameter and the splice length. The calculation of the bond strength between the FRP bar and the concrete within the spliced area is done by dividing the bar's tensile force over the surface area of the bar within the spliced region. The following equation was used to determine the bond strength while assuming that the distribution of the bond was uniform along the spliced length of the FRP bar.

$$\mu = \frac{d * f_s}{4 * l_s} \tag{17}$$

$$f_s = \frac{4 * M_a}{\pi * d^2 * jd} \tag{18}$$

Where:

$\mu = bond\ stress\ (MPa)$

$d = the\ diameter\ of\ FRP\ bar\ (mm)$

$f_s = developed\ stress\ in\ the\ bar\ (MPa)$

$l_s = splice\ length\ (mm)$

$M_a = Applied\ moment\ (kN.m)$

$jd = Resistant\ moment\ arm$

An inverse correlation was found between the bond stress and the splice length, as the later increases, the former decreases. The decrease in the bond strength attributes to several factors such the increase in the bar size which leads to increments in the frictional and mechanical interlock resistances along the embedment length, and the nonlinear distribution of the bond stress along the splice length. Similar behavior was

reported by (Achillides et al. 2004; Okelo and Yuan 2005; El Refai et al. 2014; Hossain et al. 2014; Tekle et al. 2016).

Additionally, there is a direct relationship between the bond stress and the FRP bar diameter. The critical bond stresses for the sand-coated BFRP bars of 10- and 16-mm diameters are 4.6 and 6.2 MPa, respectively. The high compressive strength concrete has affected the influence of bar diameter on the bond strength. The bond stress is calculated by dividing the maximum force (F_{max}) over the surface area of the bar ($\pi * d * l_s$), the increase in the bar diameter should decrease the overall outcome which is the bond strength however, the larger the diameter the higher the maximum force, and the increment in the force is higher than the increment in the surface area, which leads to an overall escalation in the bond strength.

Comparing the sand-coated bars to the helically wrapped bars shows that the sand-coated has higher bond strength and the difference between them increases as the bar diameter gets larger, this is because the surface roughness of the sand-coated improves the bond characteristics with the surrounding concrete, this observation was confirmed by Saleh et al. (2019) for the sand-coated and helically wrapped GFRP.

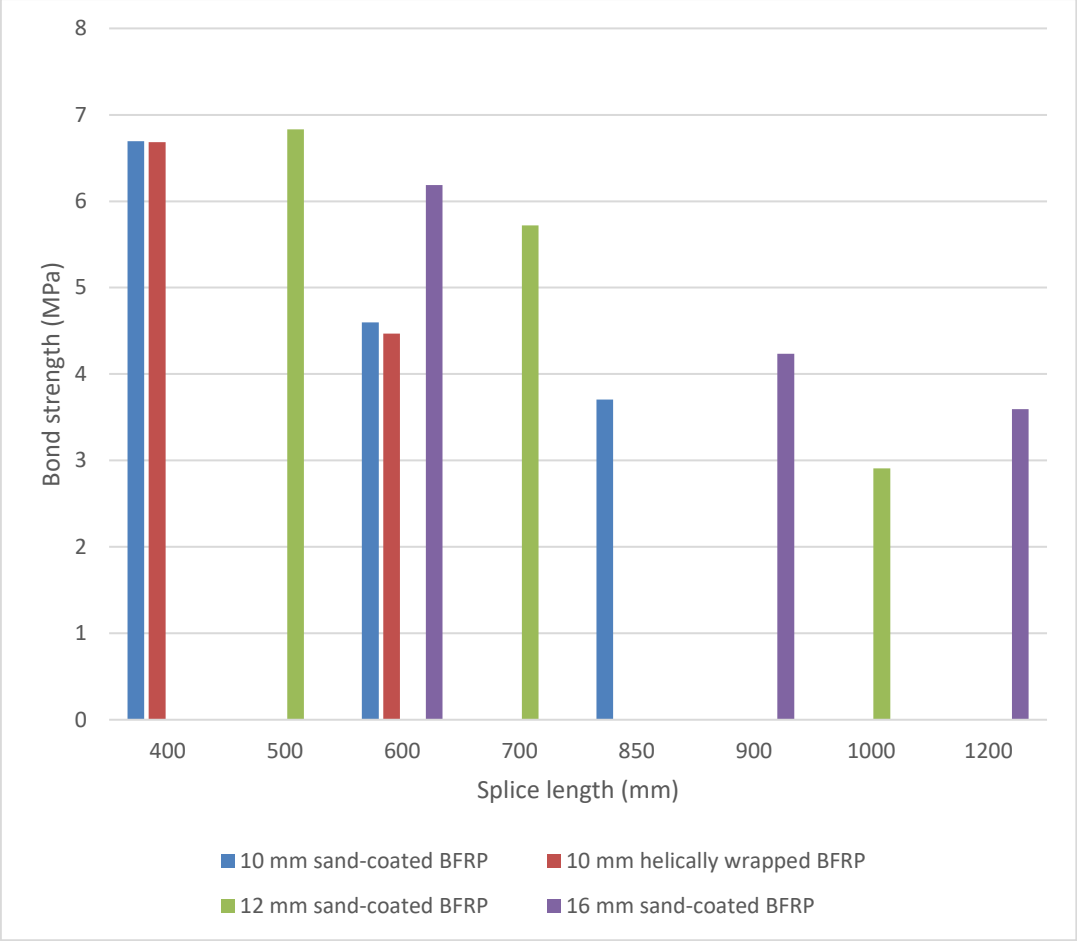

Figure 85: Average bond stress at failure versus splice length of the tested beams

4.13 Experimental and theoretical ultimate bending moments of the tested beams

In order to calculate the experimental bending moment, the failure mode must be determined to choose the correct analysis mode. The following part is an illustration of the failure mode and their analysis methods.

4.13.1 The Failure Modes

An FRP reinforced concrete has three major modes of flexural failures:

1. The balanced failure caused by the FRP rupture and concrete crushing.
2. The compression failure, which is caused by crushing of the concrete crushing as the FRP strain level remain lower than the ultimate strain).

3. The tension failure – caused by the FRP rupture that occurs prior to concrete crushing.

4.13.1.1 Balanced Failure

This mode of failure occurs when both the concrete and FRP attain their ultimate strains. The strain compatibility with one layer of FRP tension in a cross-section shown in Figure 86 can be used to determine the ratio of neutral axis to effective depth as shown below:

$$\frac{c_b}{d} = \frac{\varepsilon_{cu}}{\varepsilon_{cu} + \varepsilon_{Fu}} \tag{19}$$

where c_b = depth (mm) of neutral axis when there is a balanced failure, d = effective depth in mm, ε_{cu} = concrete compression's ultimate strain, and ε_{Fu} = FRP tension's ultimate strain. The distribution tension in the compression area of the concrete is nonlinear. Based on CSA A23.3-04, the stress distribution stress can be substituted by a block that has parameters α_1 and β_1 ; where α_1 = ratio of the concrete strength in the block to specific concrete strength, and β_1 = ratio of the block's depth to neutral axis's depth.

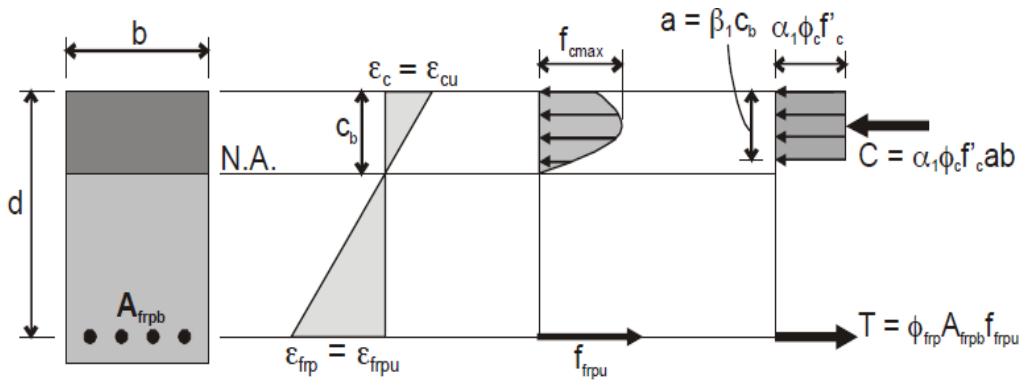

Figure 86: Balanced failure. From ISIS manual no. 3 (2007)

Based on equilibrium force in the cross section, the concrete's compression force is equal to the FRP bars' tension force, $C = T$. The compression stress resultant is calculated as:

$$C = \alpha_1 \, f'_c \, \beta_1 \, c_b \, b \tag{20}$$

and the tension stress resultant is calculated as:

$$T = \varepsilon_{Fu} \, E_F \, A_{Fb} \tag{21}$$

where C = nominal resultant force in the concrete (N), T = nominal inner force due to the FRP reinforcement's tension (N), $\alpha_1 = 0.85 - 0.0015 \, f'_c \geq 0.67$, $\beta_1 = 0.97 - 0.0025 \, f'_c \geq 0.67$, b = width of the compression plane in mm, A_{Fb} = Area of the reinforced FRP in mm^2, and E_F = FRP's young modulus of elasticity in MPa.

The balanced reinforcement ratio ρ_{Fb}, can be determined as shown in the following calculations:

$$\rho_{Fb} = \frac{A_{Fb}}{bd} = \alpha_1 \, \beta_1 \frac{f'_c}{f_{Fu}} \frac{\varepsilon_{cu}}{\varepsilon_{cu} + \varepsilon_{Fu}} \tag{22}$$

However, for ACI 440.1R-15 the balanced reinforcement ratio ρ_{Fb}, is determined from the following calculation:

$$\rho_{Fb} = 0.85 \, \beta_1 \frac{f'_c}{f_{Fu}} \frac{E_F \, \varepsilon_{cu}}{E_F \, \varepsilon_{cu} + f_{Fu}} \tag{23}$$

where $\beta_1 = 0.85 \; and \; for \; f'_c > 28 \; MPa \; it \; is \; reduced \; by \; a \; rate \; of \; 0.05 \; per \; each \; 7 \; MPa$, f_{Fu} is the ultimate FRP's tensile strength in MPa.

4.13.1.2 Compression Failure (Over-Reinforced Section)

Based on CSA A23.3-04, the concrete failure caused by crushing is deemed to occur when $\varepsilon_{cu} = 0.0035$ and the values of α_1 and β_1, are as defined above. The compression stress resultant is calculated as:

$$C = \alpha_1 \phi_c \, f'_c \, \beta_1 \, c \, b \tag{24}$$

where C = concrete's compressive stress in N, c = neutral axis' depth in mm, and $\phi_c = 0.65$ is the concrete's resistance. The FRP reinforcement's tensile force is calculated as shown below:

$$T = \phi_F \, A_{Fb} \, \varepsilon_F \, E_F \tag{25}$$

where T = inner force caused by FRP reinforcement's tension (N), $\phi_F = 0.75$ = concrete resistance factor of FRP reinforcement.

Forces inside the concrete and the reinforcement forces are determined through the iteration process that assumes the depth of neutral axis. If the equilibrium force is not attained, another depth value of the neutral axis is assumed. When there is equilibrium between C and T is as depicted in Figure 87, the ultimate bending moment resistance M_r, is determined as shown below:

$$M_r = C\left(d - \frac{\beta_1 \, c}{2}\right) = T\left(d - \frac{\beta_1 \, c}{2}\right) \tag{26}$$

For a rectangular section with one layer of reinforcement, $f_{FRP} = \varepsilon_F \, E_F$ can be calculated as:

$$f_{FRP} = \left(\sqrt{\frac{(E_F \, \varepsilon_{cu})^2}{4} + \frac{0.85 \, f'_c \, \beta_1}{\rho_F} E_F \, \varepsilon_{cu}} - 0.5 E_F \, \varepsilon_{cu}\right) \leq f_{Fu} \tag{27}$$

where $\beta_1 = 0.85 \; for \; f'_c \leq 28 \; MPa$

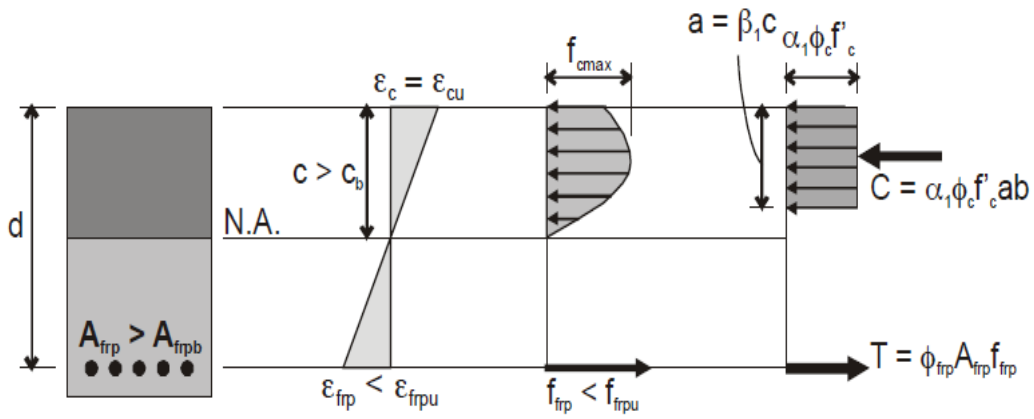

Figure 87: Compression failure. From ISIS manual no. 3 (2007)

4.13.1.3 Tension Failure (Under-Reinforced Section)

In an under-reinforced section, the strain at the bottom of the tensile reinforcement is similar to the ultimate reinforcement's tensile strain (Figure 88). The strain encountered at the top fiber in the concrete, ε_c, is determined using the strain compatibility; its value supposed to be lower than the ultimate strain of the compressed concrete, ε_{cu}. The failure in this case is resulting from FRP rupture. The FRP reinforcing bars' strain is determined as shown below:

$$\mathrm{E_{Fu}} = \frac{f_{Fu}}{\mathrm{E_F}} \tag{28}$$

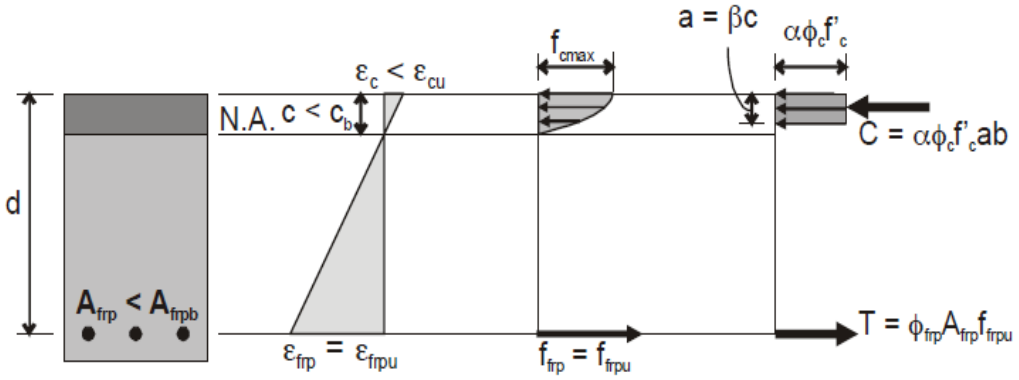

Figure 88: Tension failure. From ISIS manual no. 3 (2007)

The matching strain ε_c at the end of the compressive fiber should be lower than ε_{cu}. Therefore, the rectangular block might not be appropriate when it comes to describing the compressive stress distribution inside the concrete area. For the section that is under-reinforced, α and β are derived for the ε_c that varies up to 0.0035 because the coefficients α_1 and β_1, are valid only for $\varepsilon_c = \varepsilon_{cu}$. The parameters stress-block α and β are determined for the stain ε_c using Appendix B in the ISIS-M03-01 (2001) or by the following equations Collins and Mitchell (1997):

$$\beta = 2\left[1 - \frac{1}{\varepsilon_c}\left(\frac{\int_0^{\varepsilon_c} \frac{n_f\left(\frac{\varepsilon^2}{\varepsilon_p}\right)}{n_f - 1 + \left(\frac{\varepsilon}{\varepsilon_p}\right)^{n_f k}} d\varepsilon}{\int_0^{\varepsilon_c} \frac{n_f\left(\frac{\varepsilon}{\varepsilon_p}\right)}{n_f - 1 + \left(\frac{\varepsilon}{\varepsilon_p}\right)^{n_f k}} d\varepsilon}\right)\right] \tag{29}$$

$$\alpha = \frac{1}{\varepsilon_c \beta}\left[\int_0^{\varepsilon_c} \frac{n_f\left(\frac{\varepsilon}{\varepsilon_p}\right)}{n_f - 1 + \left(\frac{\varepsilon}{\varepsilon_p}\right)^{n_f k}} d\varepsilon\right] \tag{30}$$

$$n_f = 0.8 + \frac{f'_c}{17} \tag{31}$$

$$\varepsilon_p = \frac{\mathrm{f_c'}}{\mathrm{E_c}} \frac{n_f}{n_f - 1} \tag{32}$$

$$k = 0.67 + \frac{\mathrm{f_c'}}{62} \tag{33}$$

The ultimate compressive stress in the concrete, C, is determined as follows:

$$C = \alpha\ \phi_c\ \mathrm{f_c'}\ \beta\ \mathrm{c\ b} \tag{34}$$

where α and β are the stress-block factors for the concrete. The parameters of stress block α and β rely on the strain inside the concrete; when the strain stretches to 0.0035, the parameters are respectively identical to α_1 and β_1, in CSA A23.3-04.

The reinforcement's tensile force is determined as follows:

$$T = \phi_F\ \mathrm{A_{Fb}}\ \varepsilon_{\mathrm{Fu}}\ \mathrm{E_F} \tag{35}$$

In case there is an equilibrium between C and T, the section's bending moment of resistance is determined by:

$$M_r = C\left(d - \frac{\beta\ \mathrm{c}}{2}\right) = T\left(d - \frac{\beta\ \mathrm{c}}{2}\right) \tag{36}$$

For this kind of failure, the requirement for serviceability normally controls the design.

The summary of the three failure modes are shown in the following table:

Table 10: Summary of the FRP reinforced beams possible failure modes

	Tension	Balanced	Compression
Behavior	FRP rupture	FRP rupture and Concrete crushing	Concrete crushing
Desirability	Least desirable as the rupture is sudden and violent		Most desirable as it gives sufficient warning
Reinforcement ratio	$\rho_F < \rho_{Fb}$	$\rho_F = \rho_{Fb}$	$\rho_F > \rho_{Fb}$
Strain	$\varepsilon_F = \varepsilon_{Fu}$ $\varepsilon_c < \varepsilon_{cu}$	$\varepsilon_F = \varepsilon_{Fu}$ $\varepsilon_c = \varepsilon_{cu}$	$\varepsilon_F < \varepsilon_{Fu}$ $\varepsilon_c = \varepsilon_{cu}$

The mode of failure was tension failure therefore the concrete strain in the beams were less than the ultimate concrete strain, and the tension failure analysis was used.

The following table summarizes the results of the experimental and theoretical ultimate bending moments of the tested beams:

Table 11: Experimental and theoretical ultimate bending moments of the tested beams

Beam Identification	Mu (exp) (kN.m)	Mu (theory) (CSA-S806-12) (kN.m)	Mu (theory) (ACI-440.1-15) (kN.m)	Mean bond stress (MPa) Eq. (17)	Mode of failure
SBFRP-10-400	65.1	55	40	6.7	Splitting
SBFRP-10-600	67.3	55	40	4.6	Splitting
SBFRP-10-850	76.8	55	40	3.7	Rupture
SBFRP-12-500	99.28	78	56	6.8	Splitting
SBFRP-12-700	116.34	78	56	5.7	Splitting
SBFRP-12-1000	NA	78	56	2.9	Rupture

Beam Identification	Mu (exp) (kN.m)	Mu (theory) (CSA-S806-12) (kN.m)	Mu (theory) (ACI-440.1-15) (kN.m)	Mean bond stress (MPa) Eq. (17)	Mode of failure
SBFRP-16-600	142.19	126	93	6.2	Splitting
SBFRP-16-900	146.06	126	93	4.2	Splitting
SBFRP-16-1200	165.24	126	93	3.6	Rupture
HWBFRP-10-400	65.25	36	24	6.6	Rupture
HWBFRP-10-600	65.5	36	24	4.4	Rupture

By comparing the experimental result of the moments to the theoretical ones, it can be observed that the Canadian and American codes underestimate the capacity of the beam when designing it, which means that they give a safe value for the design. Also, it can be noticed that the CSA-S806-12 gives a better accuracy than the ACI-440.1-15.

CHAPTER 5: SUMMARY, CONCLUSION, AND FUTURE WORK

5.1 Summary

A total of 11 spliced beams tests were conducted to investigate the behavior of both sand-coated and helically wrapped basalt fiber reinforced polymer (BFRP) rebar splices cast within high strength concrete. The beams were designed to fit similar dimensions (3900 mm span x 300 mm width x 450 mm depth) and to be controlled by tension failure. The splice length varied depending on the used bottom reinforcement bars size. Three bar sizes were used: 10, 12- and 16-mm bar diameters. The compressive strength of the concrete was obtained by compression strength testing for concrete cylinders in our laboratory. The tensile strength of the bars was obtained through tensile testing of specimens of used bars.

5.2 Conclusion

An illation was drawn from the test results and it is summarized in the following points:

1. To predict the strain at the end of the splice, the ultimate strength analysis can be used.
2. The critical splice length can be predicted by performing at least one beam test as the strain at the end of splice is proportional to the splice length.
3. The experimental prediction of the splice length is approximately the same as using either the ACI440.1R-15 or CSA-S6-14 equations. However, it is preferable and more conservative to use CSA-S806-12 equation.
4. The splice length for the basalt can be calculated by the equations provided by the Canadian codes by treating it as carbon fiber reinforced polymer (CFRP) and glass fiber reinforced polymer (GFRP) therefore, using a value of 1 for the factor k_4. Also, for the American code an environmental reduction factor C_E of 0.9 should be used for the basalt fiber reinforced polymer (BFRP).

5. The surface texture influences the critical splice length as the tensile strength differ; the required splice length for helically wrapped bars is much less than the sand coated bars.
6. The concrete tensile strength is an essential factor in enhancing the bond strength of splices. Thus, the compression strength of concrete is taken into consideration in evaluating the bond strength.
7. The bond strength increases as the diameter of the reinforcement bars increases, while it decreases as the splice length increases.
8. The bond strength of the sand-coated BFRP bars is higher than the bond strength of the helically wrapped BFRP bars.
9. The load capacity of the beams reinforced with sand coated BFRP bars is higher than the load capacity of the beams reinforced with helically wrapped BFRP bars while having the same splice length.

5.3 Future work

The behavior of the spliced bar is still not well known, that's why a more research is needed. Some the areas of the future researches are:

1. Study the bond behavior of spliced BFRP bars without transverse reinforcement in beams and slabs.
2. Study the influence of casting position on the spliced length.
3. Research needs to be conducted to determine the effect of longitudinal bar spacing.

REFERENCES

[1] Achillides, Z., Pilakoutas, K., & Waldron, P. (1997). Bond Behaviour of FRP Bars to Concrete. *NONMETALLIC FRP REINFORCEMENT FOR CONCRETE STRUCTURES*, *2*, 341–348

[2] Achillides, Z., & Pilakoutas, K. (2004). Bond Behavior of Fiber Reinforced Polymer Bars under Direct Pullout Conditions. *Journal of Composites for Construction*, *8*(2), 173–181. doi: 10.1061/(asce)1090-0268(2004)8:2(173)

[3] ACI (American Concrete Institute). (2015). "Guide for the design and construction of structural concrete reinforced with FRP bars." ACI 440.1R-15, Farmington Hills, MI.

[4] Aly, R. (2005). *Experimental and analytical studies on bond behaviour of tensile lap spliced FRP reinforcing bars in concrete* (Ph.D. Thesis). University of Sherbrooke, Sherbrooke (Quebec), Canada.

[5] Aly, R. (2006). Tensile Lap Splicing of FRP Reinforcing Bars in Concrete. *ACI Structural Journal*, *103*(6), 857–864. doi: 10.14359/18239

[6] Aly, R. (2007). Stress along tensile lap-spliced fibre reinforced polymer reinforcing bars in concrete. *Canadian Journal of Civil Engineering*, *34*(9), 1149–1158. doi: 10.1139/l07-046

[7] Bakis, C., Uppuluri, V., Nanni, A., & Boothby, T. (1998). Analysis of bonding mechanisms of smooth and lugged FRP rods embedded in concrete. *Composites Science and Technology*, *58*(8), 1307–1319. doi: 10.1016/s0266-3538(98)00016-5

[8] Benmokrane, B., Tighiouart, B., & Chaallal, O. (1996). Bond Strength and Load Distribution of Composite GFRP Reinforcing Bars in Concrete. *ACI Materials Journal*, *93*(3), 246–253. doi: 10.14359/9810

[9] Brzev S., Pao J. (2006). Reinforced Concrete Design A Practical Approach. Pearson Prentice Hall, Toronto.

[10] Canbay, E., & Frosch, R. J. (2005). Bond Strength of Lap-Spliced Bars. *ACI Structural Journal*, *102*(4), 605–614. doi: 10.14359/14565

[11] CAN/CSA-S6-14, "Canadian Highway Bridge Design Code," Canadian Standards Association, Rexdale, Ontario, Canada, 2014.

[12] CAN/CSA, S806-12: Design and Construction of Building Components with Fiber-Reinforced Polymers, Canadian Standards Association, Canada, 2012.

[13] Chaallal, O., Benmokrane, B., & Masmoudi, R. (1992). An Innovative Glass fibre Composite Rebar for Concrete Structures. *Advanced Composite Materials in Bridges and Structures*, 169–177.

[14] Choi, D.-U., Chun, S.-C., & Ha, S.-S. (2012). Bond strength of glass fibre-reinforced polymer bars in unconfined concrete. *Engineering Structures*, *34*, 303–313. doi: 10.1016/j.engstruct.2011.08.033

[15] Cosenza, E., Manfredi, G., & Realfonzo, R. (1995). Analytical Modeling of Bond between FRP Reinforcing Bars and Concrete. *Proceedings Non-Metallic (FRP) Reinforcement for Concrete Structures*, 164–171.

[16] Cosenza, E., Manfredi, G., & Realfonzo, R. (2002). Development Length of FRP Straight Bars. *Composites*, *33*(Part B), 493–504. doi: 10.1016/s1359-8368(02)00051-3

[17] Ehsani, M. R., Saadatmanesh, H., & Tao, S. (1996). Design Recommendations for Bond of GFRP Rebars to Concrete. *Journal of Structural Engineering*, *122*(3), 247–254. doi: 10.1061/(asce)0733-9445(1996)122:3(247)

[18] El Refai, A. E., Ammar, M.-A., & Masmoudi, R. (2015). Bond Performance of Basalt Fiber-Reinforced Polymer Bars to Concrete. *Journal of Composites for Construction*, *19*(3), 04014050. doi: 10.1061/(asce)cc.1943-5614.0000487

[19] Esfahani, M., & Rangan, B. (2000). Influence of transverse reinforcement on bond strength of tensile splices. *Cement and Concrete Composites*, *22*(3), 159–163. doi: 10.1016/s0958-9465(00)00005-6

[20] Esfahani, M. R., Rakhshanimehr, M., & Mousavi, S. R. (2013). Bond Strength of Lap-Spliced GFRP Bars in Concrete Beams. *Journal of Composites for Construction*, *17*(3), 314–323. doi: 10.1061/(asce)cc.1943-5614.0000359

[21] Ferguson, P. M., Turpin, R. D., & Thompson, J. N. (1954). Minimum Bar Spacing as a Function of Bond and Shear Strength. *ACI Journal Proceedings*, *50*(6), 869–888. doi: 10.14359/11798

[22] Hamad, B. S., & Mansour, M. Y. (1996). Bond Strength of Noncontact Tension Lap Splices. *ACI Structural Journal*, *93*(3), 316–326. doi: 10.14359/9691

[23] Hamad, B. S., & Najjar, S. (2002). Evaluation of the role of transverse reinforcement in confining tension lap splices in high strength concrete. *Materials and Structures*, *35*(4), 219–228. doi: 10.1007/bf02533083

[24] Harajli, M., & Abouniaj, M. (2010). Bond Performance of GFRP Bars in Tension: Experimental Evaluation and Assessment of ACI 440 Guidelines. *Journal of Composites for Construction*, *14*(6), 659–668. doi: 10.1061/(asce)cc.1943-5614.0000139

[25] Harajli, M., & Salloukh, K. (1997). Effect of Fibers on Development/Splice Strength of Reinforcing Bars in Tension. *ACI Materials Journal*, *94*(4), 317–324. doi: 10.14359/315

[26] Harris, K. A., Porter, M. L., & Busel, J. P. (2003). FRP Materials and Concrete – Research Needs. *ACI Concrete International*, *25*(10), 69–74.

[27] Hattori, A., Kawasaki, K., Miyagawa, T., & Fuji, M. (1997). Bond Behaviour of Carbon Fibre Strand and Aramid Fibre Deformed Bar. *Proceedings of the Third*

International Symposium on Non-Metallic (FRP) Reinforcement for Concrete Structures, *2*, 349–356.

[28] Hossain, K. M. A., Ametrano, D., & Lachemi, M. (2014). Bond Strength of Standard and High-Modulus GFRP Bars in High-Strength Concrete. *Journal of Materials in Civil Engineering*, *26*(3), 449–456. doi: 10.1061/(asce)mt.1943-5533.0000758

[29] Hossain, K., Ametrano, D., & Lachemi, M. (2017). Bond strength of GFRP bars in ultra-high strength concrete using RILEM beam tests. *Journal of Building Engineering*, *10*, 69–79. doi: 10.1016/j.jobe.2017.02.005

[30] ISIS Canada, Reinforcing Concrete Structures with Fiber Reinforced Polymers. Design Manual N8 3 Version 2, Canada ISIS Canada Corporation, Manitoba, 2007.

[31] Japan Society of Civil Engineers (1997). Recommendation for design and construction of concrete structures using continuous fiber reinforcing materials. Concrete Engineering Series 23; Tokyo, Japan Society of Civil Engineers.

[32] Köroğlu, M. A. (2018). Artificial neural network for predicting the flexural bond strength of FRP bars in concrete. *Science and Engineering of Composite Materials*, *26*(1), 12–29. doi: 10.1515/secm-2017-0155

[33] Larralde, J., & Silva-Rodriguez, R. (1993). Bond and Slip of FRP Rebars in Concrete. *Journal of Materials in Civil Engineering*, *5*(1), 30–40. doi: 10.1061/(asce)0899-1561(1993)5:1(30)

[34] Lutz, L. A., Mirza, S. A., & Gosain, N. K. (1993). Changes to and Applications of Development and Lap Splice Length Provisions for Bars in Tension (ACI 318-89). *ACI Structural Journal*, *90*(4), 393–406. doi: 10.14359/3980

[35] MacGregor J.G., Wight J.K. (2005). Reinforced Concrete Mechanics and Design Fourth Edition. Pearson Prentice Hall, New Jersey.

[36] Mains, R. M. (1951). Measurement of the Distribution of Tensile and Bond Stresses Along Reinforcing Bars. *ACI Journal Proceedings*, *48*(11), 225–252. doi: 10.14359/11882

[37] Mesbah, H. & Benmokrane, B., (2002). Evaluation of Bond Properties of FRP Rods in Concrete. Technical Report, submitted to *International Round Robin Test for FRP Reinforcement*, ConFibreCrete TMR Network, Department of Civil Engineering, University of Sheffield, Sheffield, UK, December, 53.

[38] Newhook, J., Ghali, A., & Tadros, G. (2002). Concrete Flexure Members Reinforced with Fibre Reinforced Polymer: Design for Cracking and Deformation. *Canadian Journal of Civil Engineering*, *29*, 125–134.

[39] Okelo, R., & Yuan, R. L. (2005). Bond Strength of Fiber Reinforced Polymer Rebars in Normal Strength Concrete. *Journal of Composites for Construction*, *9*(3), 203–213. doi: 10.1061/(asce)1090-0268(2005)9:3(203)

[40] Plizzari, G. A., Marchina, E., & Giuriani, E. (1996). Experimental study of splitting and flexural cracks in a RC beam with overlapped splices. *Materials and Structures*, *29*(1), 19–27. doi: 10.1007/bf02486003

[41] Rezansoff, T., Zhang, S., & Sparling, B. (1997). Influence of different stirrup configurations on lap splices in beams. *Canadian Journal of Civil Engineering*, *24*(1), 106–114. doi: 10.1139/cjce-24-1-106

[42] Sakurada, T., Morohashi, N., Nishihara, H., Tabata, T., & Tanaka, R. (1995). A Study On The Bond Splitting Strength Of All Lapped Splices At The Same Section With Large-Diameter Bars. *Journal of Structural and Construction Engineering (Transactions of AIJ)*, *60*(478), 153–162. doi: 10.3130/aijs.60.153_2

[43] Saleh, N., Ashour, A., & Sheehan, T. (2019). Bond between glass fibre reinforced polymer bars and high - strength concrete. *Structures*, *22*, 139–153. doi: 10.1016/j.istruc.2019.08.003

[44] Şener, S., Baant, Z. P., & Becq-Giraudon, E. (1999). Size Effect on Failure of Bond Splices of Steel Bars in Concrete Beams. *Journal of Structural Engineering*, *125*(6), 653–660. doi: 10.1061/(asce)0733-9445(1999)125:6(653)

[45] Tabata, T., Nishihara, H., Morohashi, N., & Sakurada, T. (1998). Bond Splitting Strength of Lap Splices Put Main Bars in the Direction of Beam Depth. *Transactions of the Japan Concrete Institute*, *20*, 253–260.

[46] Taly, N., & Hota, G. (2001). Bond Behaviour of FRP Reinforcing Bars-the State-of-the-Art. *46th International SAMPE Symposium*, 1784–1796.

[47] Tekle, B. H., Khennane, A., & Kayali, O. (2016). Bond Properties of Sand-Coated GFRP Bars with Fly Ash–Based Geopolymer Concrete. *Journal of Composites for Construction*, *20*(5), 1–13. doi: 10.1061/(asce)cc.1943-5614.0000685

[48] Tepfers, R. (1980). Bond stress along lapped reinforcing bars. *Magazine of Concrete Research*, *32*(112), 135–142. doi: 10.1680/macr.1980.32.112.135

[49] Tepfers, R. (1982). Lapped Tensile Reinforcement Splices. *ASCE Journal of the Structural Division*, 108(ST1), 283-301.

[50] Tepfers, R. (1998). Bond Between FRP-Bars and Concrete. *Chalmers University of Technology (Building Technology)*.

[51] Thompson, M. A., Jirsa, J. O., Breen, J. E., & Meinheit, D. F. (1979). Behavior of Multiple Lap Splices in Wide Sections. *ACI Journal Proceedings*, *76*(2), 227–248. doi: 10.14359/6945

[52] Tighiouart, B., Benmokrane, B., & Gao, D. (1998). Investigation of bond in concrete member with fibre reinforced polymer (FRP) bars. *Construction and Building Materials*, *12*(8), 453–462. doi: 10.1016/s0950-0618(98)00027-0

[53] Tighiouart, B. (1997). *Bond of Fibre Reinforced Plastic (FRP) Reinforcing Bars Embedded in Concrete* (Ph.D. Thesis). University of Sherbrooke, Sherbrooke (Quebec), Canada.

[54] Tighiouart, B., Benmokrane, B., & Mukhopadhyaya, P. (1999). Bond strength of glass FRP rebar splices in beams under static loading. *Construction and Building Materials*, *13*(7), 383–392. doi: 10.1016/s0950-0618(99)00037-9

[55] Zemour, N., Asadian, A., Ahmed, E. A., Khayat, K. H., & Benmokrane, B. (2018). Experimental study on the bond behavior of GFRP bars in normal and self-consolidating concrete. *Construction and Building Materials*, *189*, 869–881. doi: 10.1016/j.conbuildmat.2018.09.045